EXPERIMENTAL STUDY OF A
COLD FLOW RADIAL TURBINE

EXPERIMENTAL STUDY OF A

COLD FLOW RADIAL TURBINE

by

Robert Richardson Marshall, B.Eng

A Thesis

Submitted to the School of Graduate Studies

in Partial Fulfilment of the Requirements

for the Degree

Master of Engineering

McMaster University

August 1977

MASTER OF ENGINEERING (1977).   McMASTER UNIVERSITY
(Mechanical Engineering   Hamilton, Ontario

TITLE: Experimental Study of a Cold Flow Radial
                    Turbine

AUTHOR: Robert Richardson Marshall, B.Eng,
                                          McMaster University

SUPERVISORS: Dr. J. H. T. Wade and Dr. D. S. Weaver

NUMBER OF PAGES: xiii, 95

ABSTRACT

The experimental study of an inward radial flow turbine is described in this report. Preliminary tests of the turbine by United Aircraft of Canada Ltd. indicated that the isentropic efficiency was some 50% below the design target of 80% efficiency. In an effort to locate problem areas in the turbine design, the unit's response is examined under four different load conditions at speeds ranging from 10,000 to 75,000 RPM and pressure ratios from 1.2 to 2.4. The results of these tests are presented using a series of non-dimensional parameters typically employed in turbine and compressor design. From these parameters it is evident that the poor response of the unit is due to the high degree of exit swirl introduced into the primary diffuser by the "exducerless" turbine blades.

The response characteristics of the unit are examined in the light of the experimental results, and explanations of various phenomena are offered.

iii

ACKNOWLEDGMENTS

TABLE OF CONTENTS

LIST OF FIGURES

FIGURES IN APPENDICES

x

NOMENCLATURE

Upper Case

Co'	Isentropic spouting velocity
E	Energy
EMF	Electromotive force
°F	Degrees Farenheit
H	Adiabatic head equivalent velocity
Hg	Mercury
Hp	Horsepower
Hz	Hertz
I	Moment of inertia
IFR	Inward flow radial
J	Joule equivalent
KE	Kinetic energy
M	Moment or torque
M	Mass
N	Rotational speed
P	Pressure
PE	Potential energy
P.R.	Pressure ratio
Pr	Rotameter pressure
R	Specific gas constant
°R	Degrees Rankine
RPM	Revolutions per minute
Sg	Specific gravity
T	Temperature
U	Internal energy

U_T	Blade tip velocity
V	Velocity
V_a	Absolute gas velocity
V_c	Calibrated volumetric airflow
V_{eq}	Equivalent volumetric airflow
V_r	Relative gas velocity

Lower Case

c_p	Specific heat at constant pressure
g	Acceleration due to gravity
h	Specific enthalpy
m	Mass flow
mm	Millimetre
mv	Millivolt
m.w.	Molecular weight
p.s.i.a.	Pounds force per square inch absolute
p.s.i.g.	Pound force per square inch gage
r	Radius
t	Time
v	Specific volume
vs	Versus
w	Work

Subscripts

abs	Absolute
atm	Atmospheric
o	Total or stagnation
s	Isentropic

Superscripts

o   Degrees

"   Inch

Greek

α Angular acceleration

Δ Difference

η Efficiency

π Constant ≈ 3.1415926536

σ Standard deviation

θ Angle

Ω Ohm

γ ratio of specific heats

CHAPTER 1

INTRODUCTION

For many years, gas turbines have been the object of intense research, both in the industrial and the academic worlds. Efficiencies of these machines have been increased to the point where what was once a non-functioning concept is now an economically feasible prime-mover. The form of this machine has also assumed many aspects. The once popular configuration of radial compression matched with axial flow turbine has been almost totally replaced by the axial compression, axial turbine design. Radial compression, radial flow gas turbines are virtually non-existent, limited to applications where low weight and reduced size overcome the heat transfer problems encountered in such a design [1]. However, radial flow turbines themselves are often used as so-called "cold-flow" devices; that is a supply of compressed gas (such as air) is used to provide rotational energy to the turbine blades. Small high-speed milling machines, aircraft air-conditioning units, and some cryogenic coolers are powered in this manner. Generally speaking though, the radial flow turbine is limited to very specific applications, and as a developmental unit is not usually made available for research at a University considering the facilities required.

Thus it was considered most fortunate that the

author's senior supervisor, Dr. J. H. T. Wade, received
an invitation from Pratt & Whitney Aircraft of Canada Ltd.,
(Longueil, Quebec) to test a cold-flow radial turbine
of relatively new design. A description of the design
and purpose of this turbine was offered by Mr. Ü. Okapuu,
Chief of Turbine Research at P&WACL in his initial letter
to Dr. Wade [2].

"The turbine in question is shown in the attached

sketch. It was designed to run with its axis

vertical, exhausting upwards. Its application

was intended to be the drive of various fatigue

test specimens in our spin pits, which were to

be hung below the turbine at the end of a long

and flexible spindle, to assure a stable rotation

about the C.G. of the specimen and the absence of

critical speeds. This manner of spin testing is

routine and causes no problems other than the fact

that for minimum power requirements the spin test

portion of the pit has to be evacuated, causing a

pressure difference between the turbine and the

specimen, necessitating sealing.

Our spin pits are mainly used for fatigue testing

of rotor discs. These tests consist of cyclic speed

changes of the specimens; acceleration to some

specified maximum speed followed immediately by a

deceleration to a specified minimum speed, then

acceleration again, etc. Since the number of cycles

required ranges into tens of thousands, some specimens take months of continuous cycling to complete the program. This is a long time to wait for data, particularly if you are trying to solve a development problem. Shorter cycling times clearly would reduce the total lapsed time. The turbines commercially available (Barbour-Stockwell practically dominates the market) come in various sizes, the larger sizes producing more torque, but having a lower allowable maximum speed, for stress reasons. The resulting locus of torque-max. speed pairs offered, sets a limit to the cycling frequency of any given test specimen. It was this torque-max. speed problem that prompted us to attempt the design of the radial spin pit drive turbine in which I am trying to interest you. The radial blades, and the low diameter solid hub permit far higher tip speeds than the Pelton-wheel type, supersonic inlet commercial turbine rotors. The not inconsiderable expertise we had acquired in the design of radial turbines suggested to us that total-total efficiencies in the high 70's could be expected for the given design point conditions, compared to the 13% to 35% (depending on size) for the equivalent commercial turbines. This translates into a saving of compressed air, which also may be significant with many pits in simultaneous operation. The problem of low braking torque was solved by the provision of two stator nozzles,

one for acceleration, the other for braking. The main disadvantage of the conventional radial turbine rotor, its high manufacturing cost, was circumvented by the elimination of the "exducer" portion of the rotor blades, resulting in each blade lying entirely in the plane of the drawing (i.e., the "meridional" plane, formed by the turbine axis and one radial line). As rotor speed increases, therefore, the absolute rotor exit flow angle increases as well, making a rather long annular diffuser desirable.

The present design thus differs from the standard 90° IFR turbine, with which we have considerable experience, on two counts: the double nozzle and the meridional-bladed rotor. The rotor did not undergo the customary aerodynamic analysis, due to the limited budget for this project, but our broad design rules suggested that its performance would be adequate. It did undergo a proper stress analysis, however, and was found quite acceptable for its mission. Each side of the nozzle received vanes of the proper shape, but the aerodynamic interaction between the (alternating) active and passive chambers was recognized to be an unknown."

Preliminary tests conducted on this turbine by Pratt & Whitney of Canada Ltd. showed a total to total primary stream efficiency of about 30%, a figure much below

the design target of 80%. The possible explanations con-
sidered by the designers were:

1) The experimental configuration is misleading, and
losses external to the turbine itself exist. This
also could imply that the actual measurements may
be in error for a number of reasons.

2) The novel design features introduce unexpected
losses into the system which are responsible for
the low efficiency. The double nozzle, exducer-
less rotor, and the large exit swirl in the diffuser
may all contribute to this low efficiency.

3) The existing design rules which have proven valid
on larger IFR turbines are incapable of being
extrapolated to the small size of the present design.
Reynolds numbers, ratios of wetted wall area to flow
area, etc. may all affect the turbine performance
far more strongly than previously anticipated.

It was proposed that the turbine be tested exhaus-
tively to see if any of these three explanations is valid.

This study, then, comprises two phases. The initial
phase is concerned with the design and construction of the
test facilities, while the second phase consists of experi-
mentation and analysis of results in order to try to identify
problem areas of the turbine design.

CHAPTER 2

LITERATURE SURVEY

In the Proceedings of the Institution of Mechanical Engineers [3], Wallace outlined the theoretical performance of inward flow radial (IFR) turbines. Using simple isentropic flow theory, he derived sixteen isentropic equations which specified the rotor configuration and turbine performance at the design point. He then carried out a theoretical analysis of flow conditions in the rotor passage, and developed a criterion for blade spacing. The effects of part-load conditions on the IFR turbine were also examined. Communications to the I.Mech.E. regarding the paper, and the author's replies to these letters were also listed.

Dadone and Pandolfi [4] have compared the theoretical evaluation of off-design characteristics, as presented by Pandolfi [5] in an earlier paper, with experimental results for an IFR turbine. They tested the turbine at various expansion ratios and equivalent speeds. In all cases the experimental results were found to be in good agreement with Pandolfi's previous original analysis [5].

Benson [6] reviewed methods for determining loss coefficients in IFR turbines. He examined nozzle losses and

rotor losses, including incidence coefficients, fluid
friction coefficients, coefficients for friction losses
in rotor passages, clearance coefficients and disc friction.
He also reviewed test data and compared the loss relations
with experimental values.

Okapuu and Calvert [7, 8] described the design of
a high-temperature, high-work IFR Turbine. This turbine had
blades and nozzles which were cooled with air from the
primary stream to reduce thermal stresses and creep problems.
The papers discussed the aerodynamic and mechanical designs,
and included results of aerodynamic, structural, and thermal
analyses. The rotor fabrication, and a casting development
program was also reviewed. The rig used for turbine testing
was described in detail by the authors.

In his discussion of radial turbines, Kovats [9]
pointed out the importance of having symmetrical flow to
the impellers. He also discussed turbine losses including
the frictional loss due to fluid flow through the machine,
leakage losses which reduced the flowrate (and hence volu-
metric efficiency), and mechanical losses due to friction.

Scheel [10] discussed a study of blade erosion made
by the General Electric Company. He indicated that erosion
of blade tips was in part due to the condensation of the
working fluid (caused by rapid expansion) flowing counter-
currently against the centripetal gas flow and interfering
with the blades.

CHAPTER 3

EXPERIMENTAL APPARATUS

The experimental facilities are composed of equip-
ment supplied by Pratt & Whitney of Canada Ltd. and equipment
designed and built at McMaster. The former consists
of the actual turbine hardware including the oil damper,
shroud, drive spindle, load disc and the turbine itself.
Also supplied were numerous spare parts such as bearings,
and various total temperature probes, pressure probes, etc.
The equipment designed at McMaster included primary sub-
systems such as air, hydraulic, and vacuum as well as
secondary subsystems such as pressure and temperature read-
out equipment. Figure 1 shows a photograph of the experi-
mental facilities.

3.1 Turbine Hardware

The turbine (see Figure 2 for labels) is an inward
radial flow design with a 3 1/4 inch diameter blade section
(a) machined from a forged Waspaloy (PWA 1007 or CPW 203)
bar. These blades lack the traditional exhaust plane
diffuser (termed "exducer") to reduce manufacturing
costs.   Air is supplied to the blades by either of
a twin ring of nozzles (h) one situated above the other.
The lower nozzle is used for acceleration while the upper
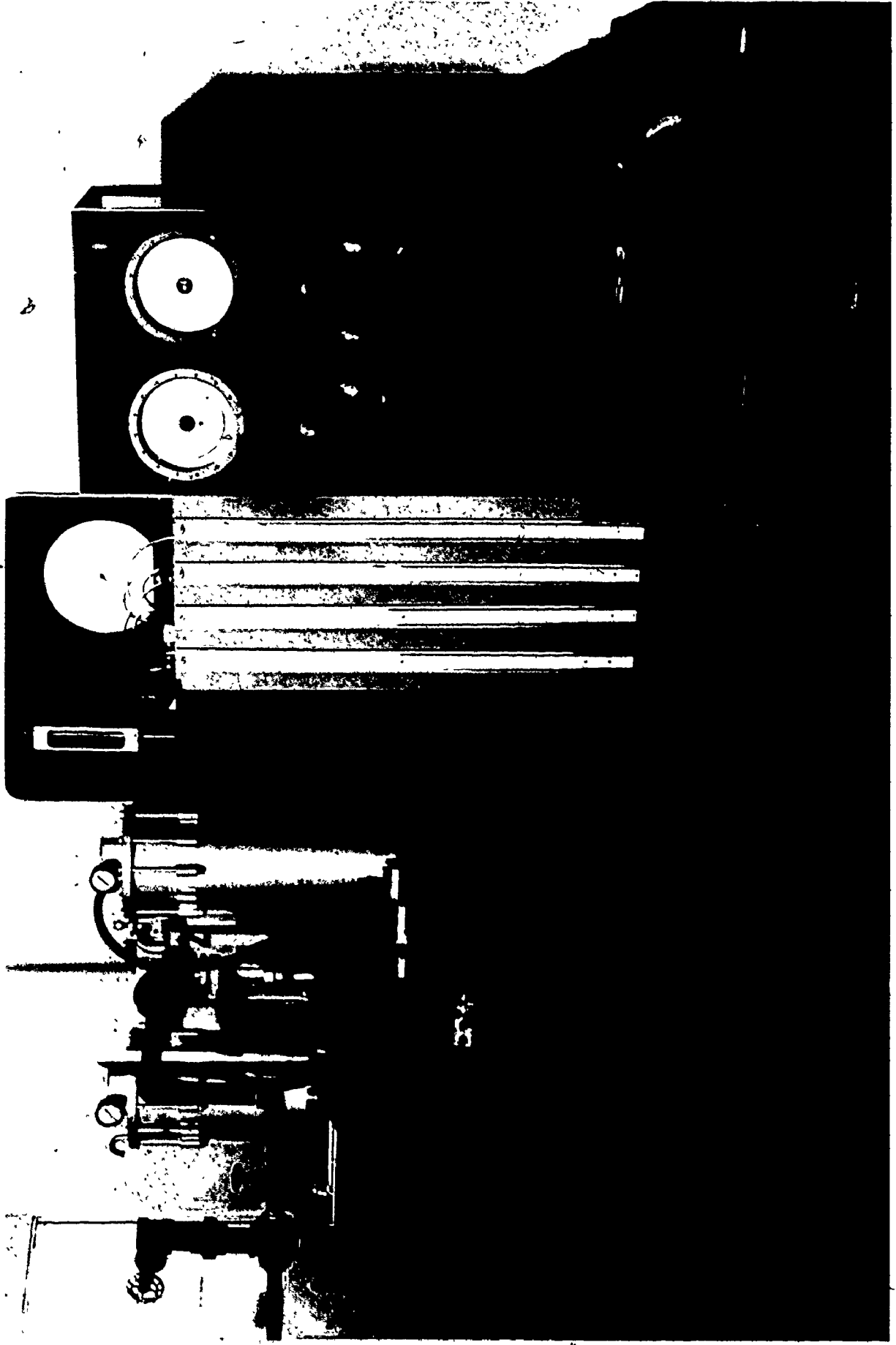
Figure 1 Experimental Facilities .

a. ROTOR

b. UPPER BEARING

c. SPACING COLLAR

d. LOWER BEARING

e. MAGNETIC PICKUP DISC

f. COLLAR

g. SEALING PLATE

h. NOZZLE RING

i. HOUSING

j. QUICK DISCONNECT COUPLING

k. OIL DAMPER
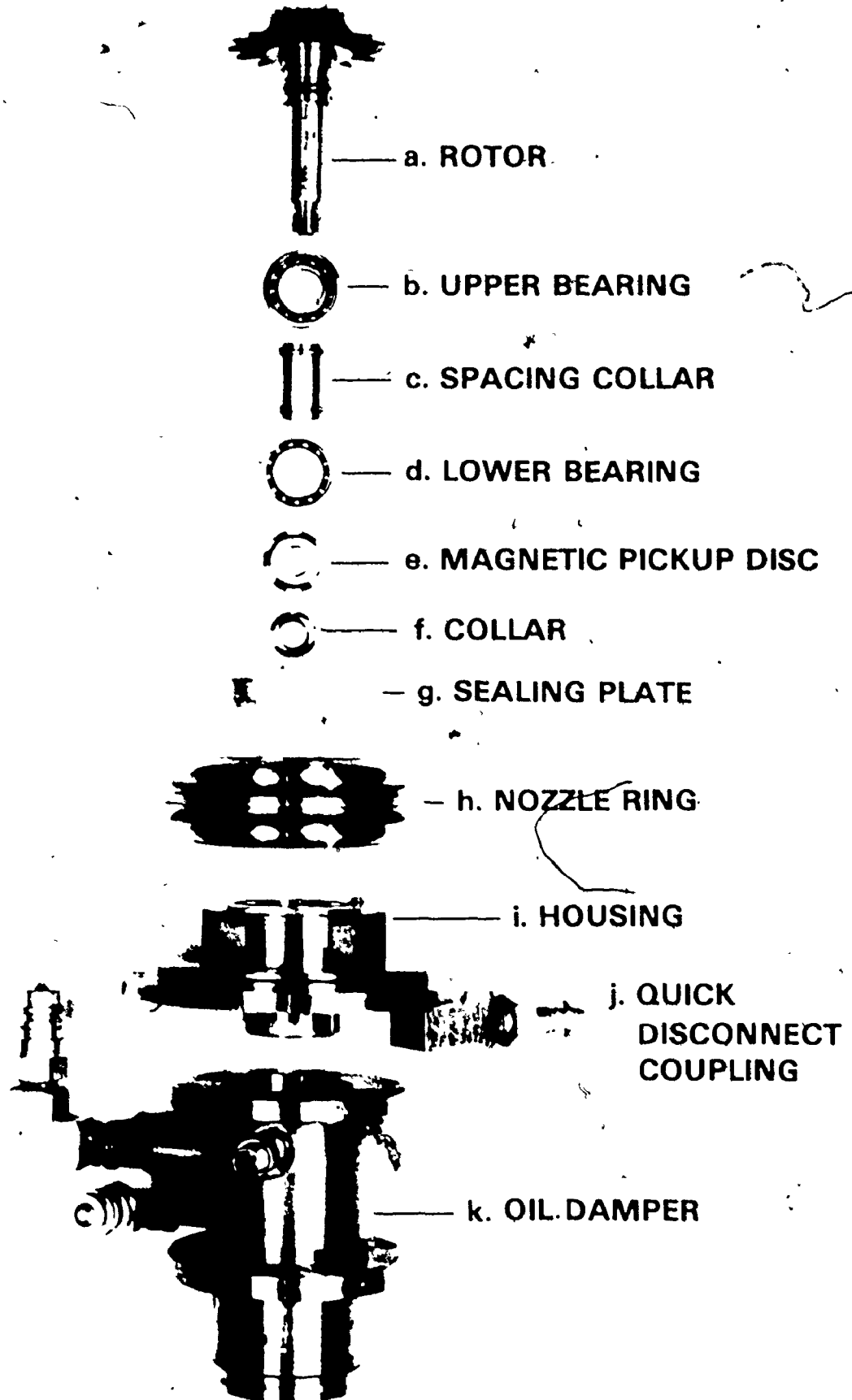
Figure 2 Exploded View of the Turbine

nozzle provides deceleration. The rotor is mounted in the turbine housing by two bearings (b, d) separated by a spacing collar (c). Bearing temperatures are monitored through copper/constantan thermocouples which touch the outer ring of each bearing. Above the upper bearing is an aluminum sealing plate (g) through which oil is supplied to both sets of bearings. Oil enters the turbine body through a quick disconnect coupling (j) located on the underside of the housing (i). A locking collar (f) ensures the vertical location of the blade section while also securing a magnetic pick-up disc (e) for speed monitoring. Figure 3 shows the turbine hardware (without body and shroud) as assembled.

The turbine is composed of three plenum chambers formed by welding AISI 1020 plate steel rings in a cannister of the same material. The lower two chambers seal with the upper and lower nozzle ring of the turbine. The aluminum shroud is bolted to the upper plenum ring of the turbine body. This shroud forms the upper face of the blade passage and the outer portion of the annular diffuser. The diffuser centrebody is machined integrally with the body cap. Air is exhausted from the turbine through the resulting annular diffuser to the upper plenum chamber. Figure 4 shows a sectioned view of the body and shroud. Air from the upper plenum chamber flows to the atmosphere through a conical type diffuser (Figure 5).

The drive spindle is a steel shaft fabricated from AMS 6415. It has a threaded upper end, a flare with a flat

e. OIL SCAVENGE CONNECTOR

a. BLADES

b. NOZZLE RING

c. HOUSING

d. LUBRICATING OIL SUPPLY CONNECTOR

g. MAGNETIC PICKUP SENSOR

f. OIL DAMPER CONNECTOR
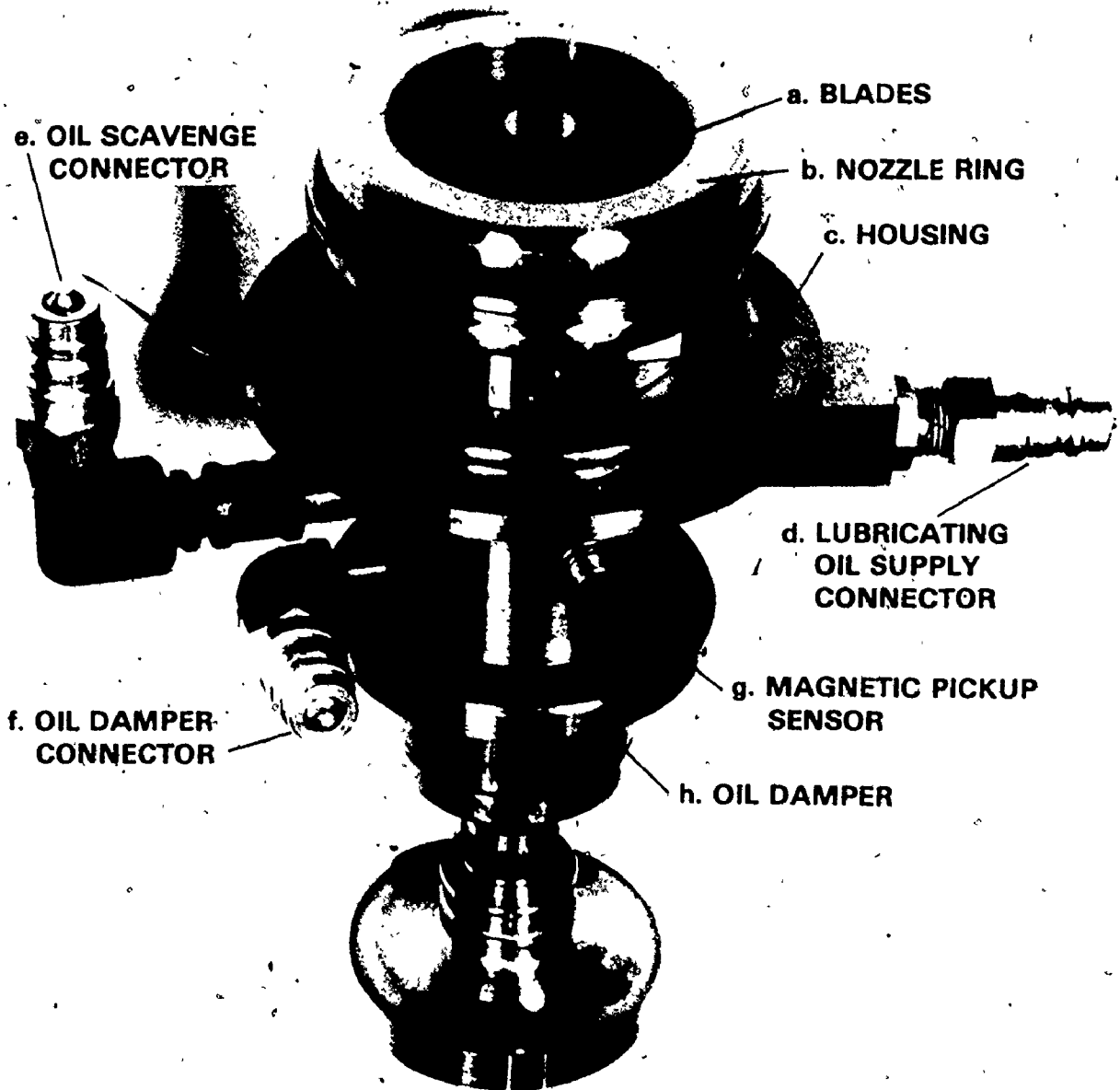
h. OIL DAMPER

Figure 3   Turbine Hardware as Assembled

EXHAUST PLENUM

SHROUD

INLET PLENUM
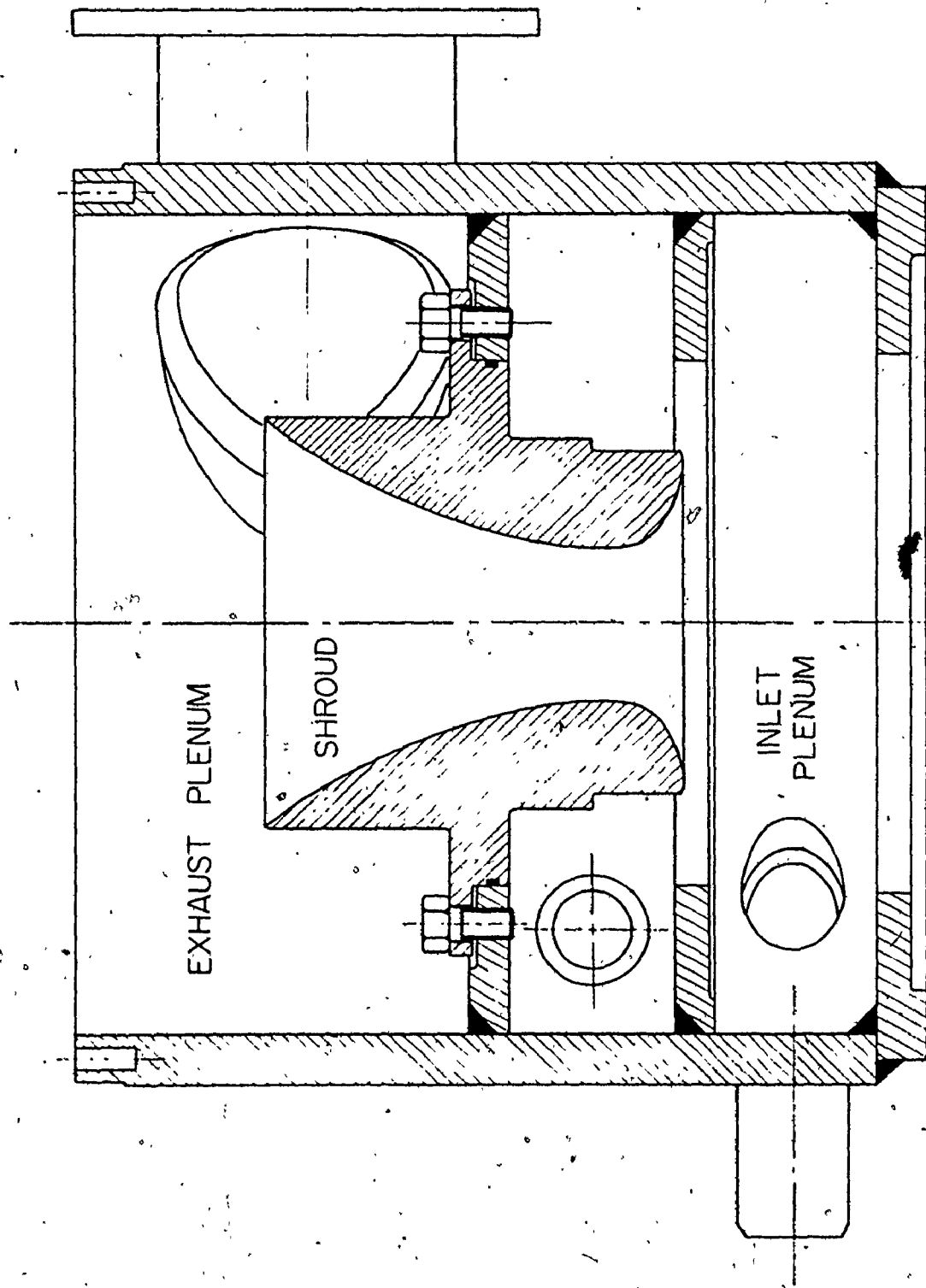
Figure 4 Sectioned View of Body and Shroud

$2\Theta = 19°$
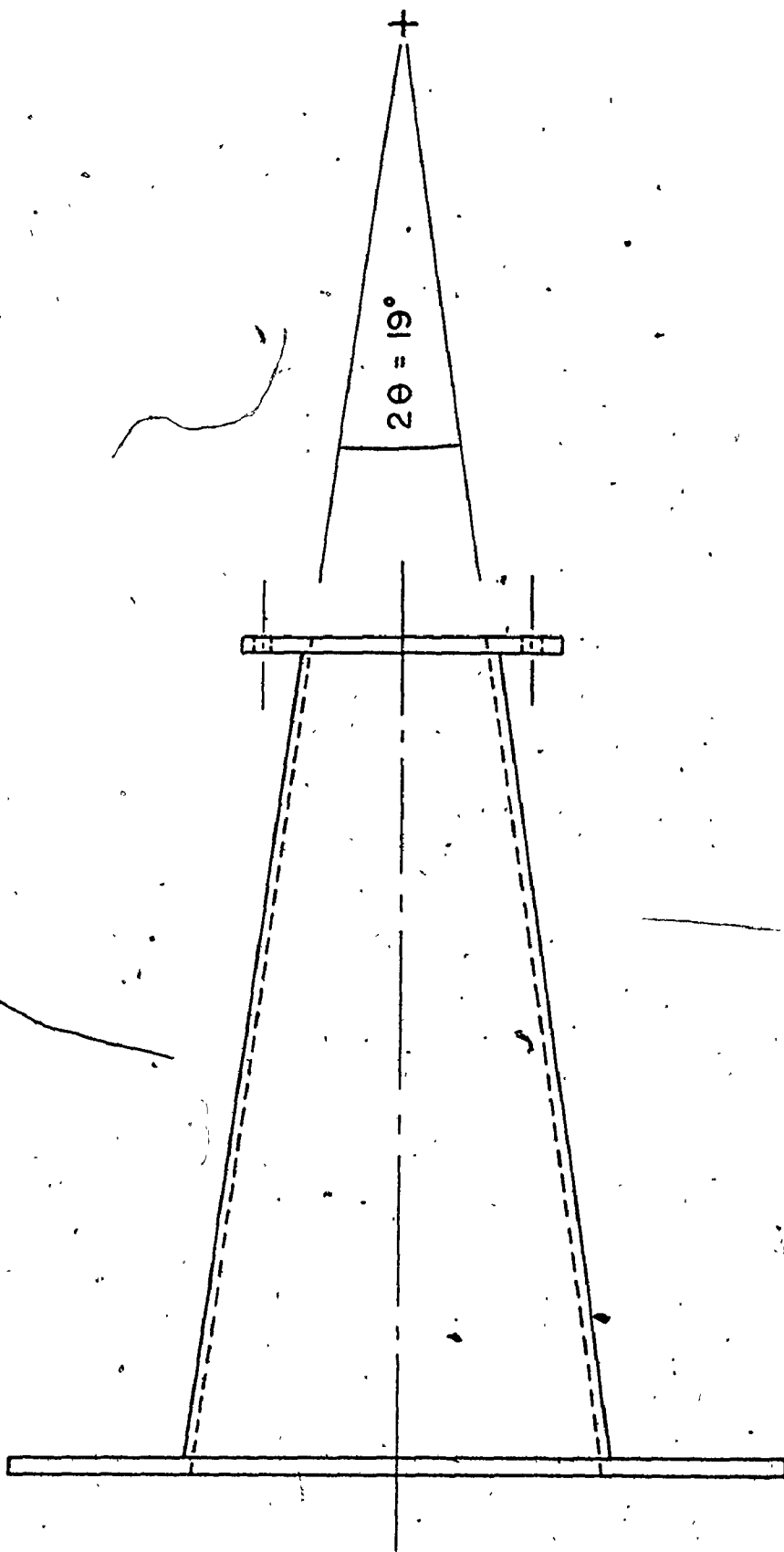
Figure 5   Conical Diffuser

upper surface to interface with the oil damper, and a notched
lower end to which the load disc is attached.

The load disc is a Pratt & Whitney Aircraft PT6
gas turbine drive rotor with the "fir-tree" blade attach-
ment points removed to reduce stress concentrations. The
stress analysis of this disc indicates that the maximum
safe rotational speed is approximately 80,000 RPM. Figure
6 illustrates the load disc and the drive spindle.

3.2 Spin Pit

It was decided to utilize one of the existing floor-
to-ceiling service accesses to house the spin pit for the
turbine. Accordingly, two mild steel plates were cut to
cover the access, one for below the floor and one for above
it. The plates were bolted together at the corners, forming
a between floors containment some eight inches in height.
A nine inch diameter hole cut in the upper plate permitted
the cannister containing the load disc to reside in the "pit".
Eight 3/8 inch diameter holes, drilled and tapped into the
upper plate permit the lid of the vacuum containment to be
secured in place (Figure 7).

The turbine and oil damper assembly bolts on top of
the vacuum containment lid. This provides easy access to
the unit for service but leaves the operator relatively
unprotected should the turbine shatter. In the
interests of safety, an auxilliary shield was installed which
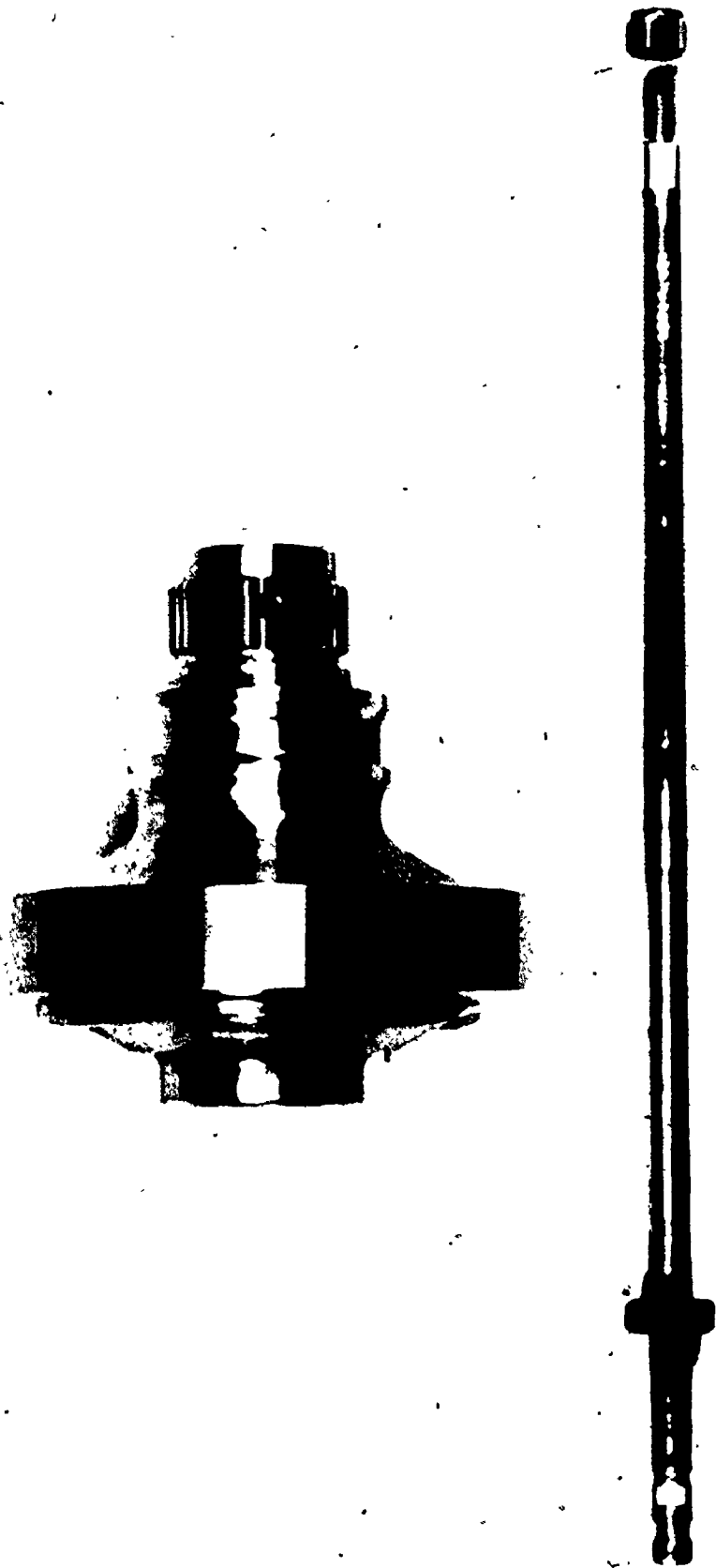
Figure 6 Load Disc and Drive Spindle

LOAD DISC CANNISTER

GAS INLET

FLOOR PLATES
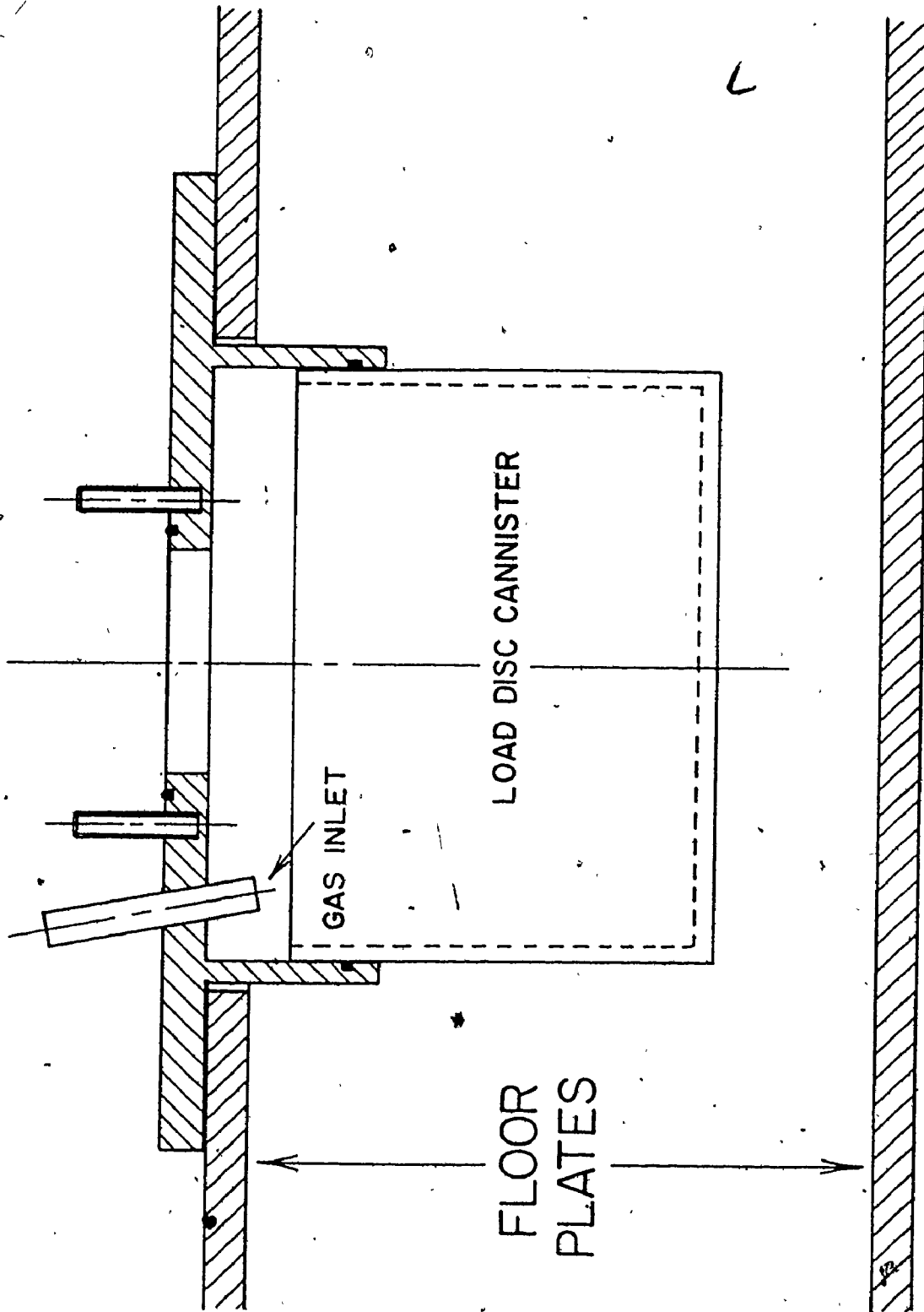
Figure 7   Cross Section of the Spin Pit

surrounds the entire turbine assembly. This shield was
constructed of 1/4 inch thick mild steel piping, some
fourteen inches in diameter and twenty one inches high. The
pipe was sectioned vertically into two pieces and drilled to
accommodate the turbine air inlet and outlet lines. Access
holes for various sensor leads and other attachments were.
machined through the walls of the pipe at various locations.
The shield was held together by steel strapping and capped
with a 1/4 inch plate steel lid. Figure 8 illustrates the
containment shield.

3.3 Ancilliary Systems

Three ancilliary systems - air, oil, and vacuum -
were required for running the turbine experiments. Figure
9 shows a schematic of the air flow system. This system
supplied clean "shop air" at approximately 100 p.s.i.g. to
the turbine. Figure 10 shows a schematic of the oil flow
system. This system provided lubricating oil to the rotor
bearings and oil damper. The vacuum system, shown schematically
in Figure 11 allowed a partial vacuum to be supplied to the
load disc cannister.

3.4 Measurement System

As with most experimental apparatus, the measurement
systems for the spin pit testing underwent continual modi-
fication as new tests were devised. The following sections
give a brief description of each system as it evolved.
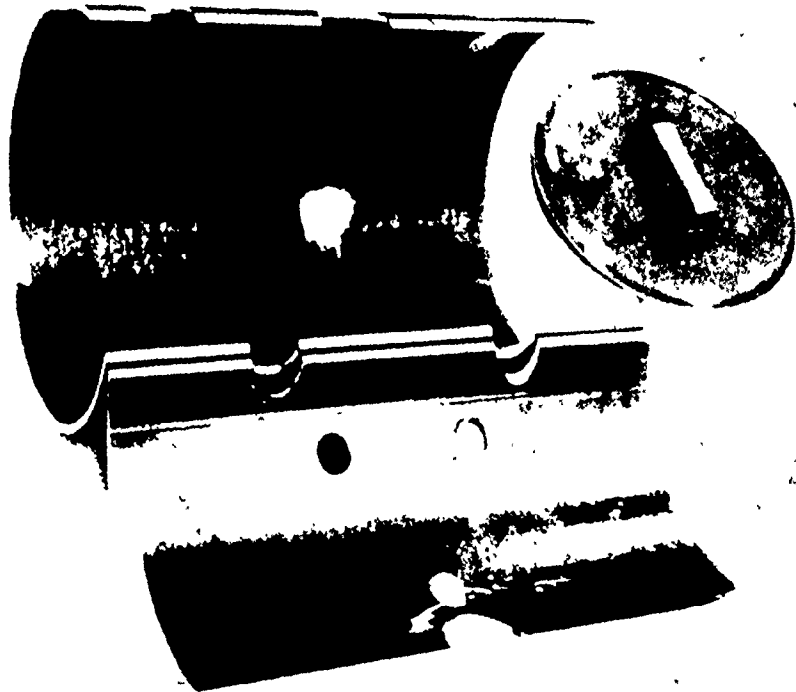
a. EXPLODED
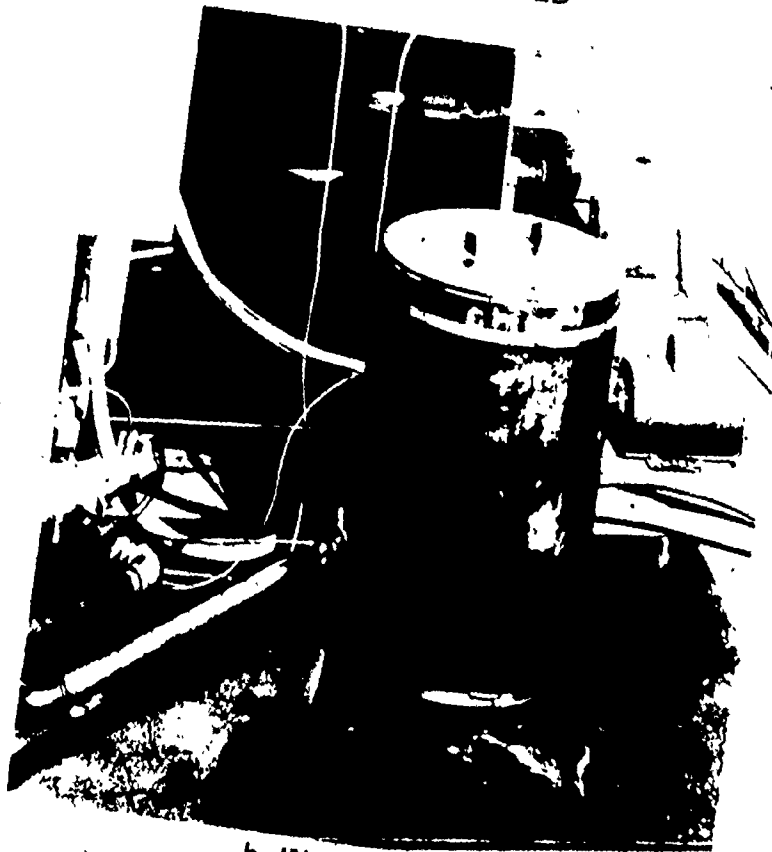
b. IN SITU

Figure 8 Turbine Containment Shield

LEGEND

D	AIR DRIER
F	FILTER
P	PRESSURE GAGE
R	ROTAMETER
T	TURBINE
V	VALVE
VS	SOLENOID VALVE

AIR PRESSURE TO SOLENOID
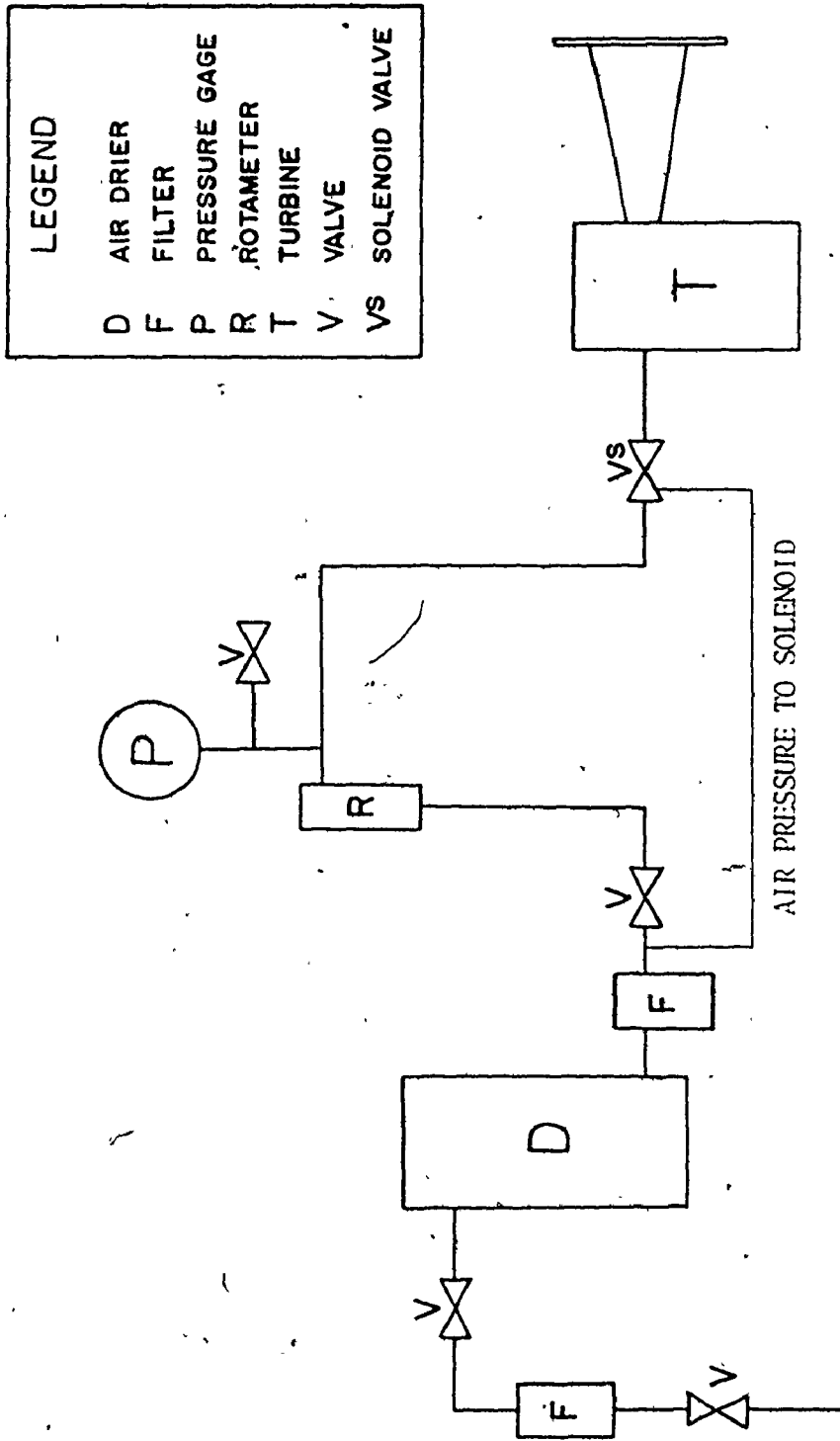
Figure 9   Schematic of the Air Flow System
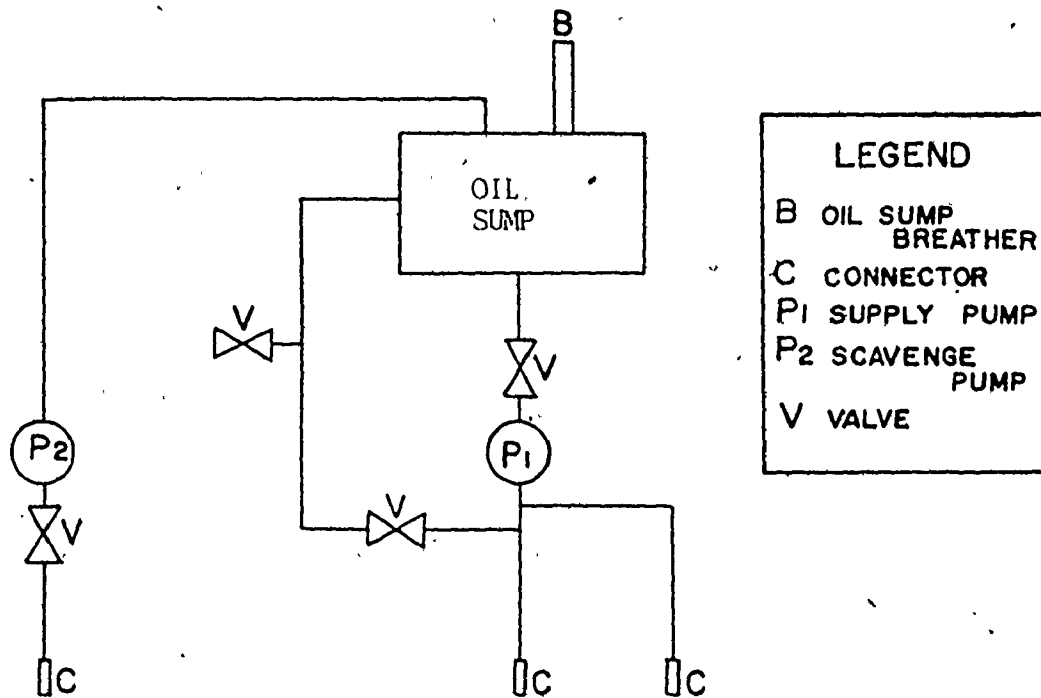
Figure 10 Schematic of the Oil Flow System
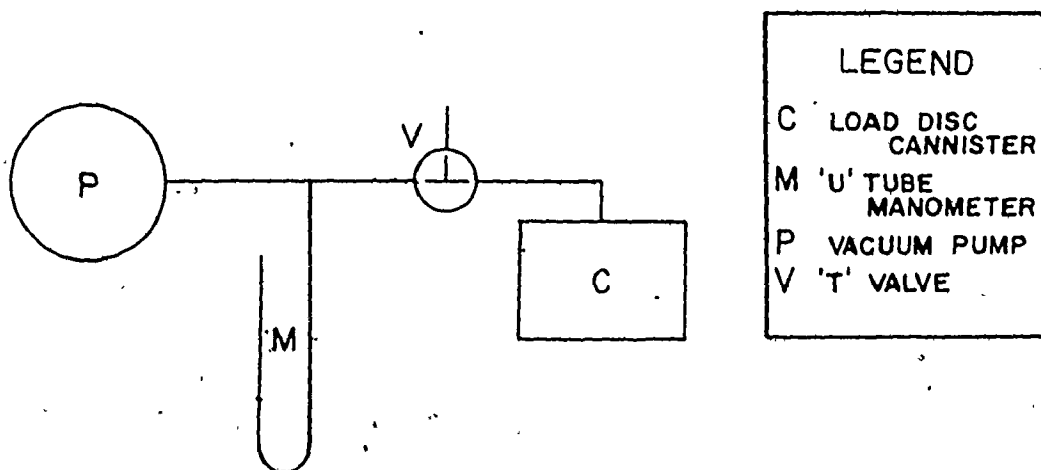
Figure 11 Schematic of the Vacuum System

3.4.1 Rotational Speed

The rotational speed of the turbine was measured by a magnetic pick-up which received six pulses per revolution of the turbine blades. This pick-up was located immediately above the upper seal of the oil damper. The pick-up signals were fed through a shielded, co-axial cable to an electronic pulse shaping unit [11]. The schematic for this unit is shown in Figure 12.

From the pulse shaper, the signal was split into two cables connected in parallel. One cable led to a frequency counter* and the other to the overspeed trip unit**. Due to the nature of the pick-up, a display of X Hz on the frequency counter was equivalent to 10X RPM. The overspeed trip unit was a device designed to provide turbine shut-down capability in any of the four following situations:

1. an overspeed condition occurs

2. the turbine speed is below 300 RPM

3. the speed signal is disconnected

4. a power failure occurs

The unit was on loan from Pratt & Whitney Aircraft of Canada Ltd.

---

* Hewlett-Packard 5300B Measuring System with 5308A 75 MHz Timer/Counter

** P&WACL Model OS-1-X-5467
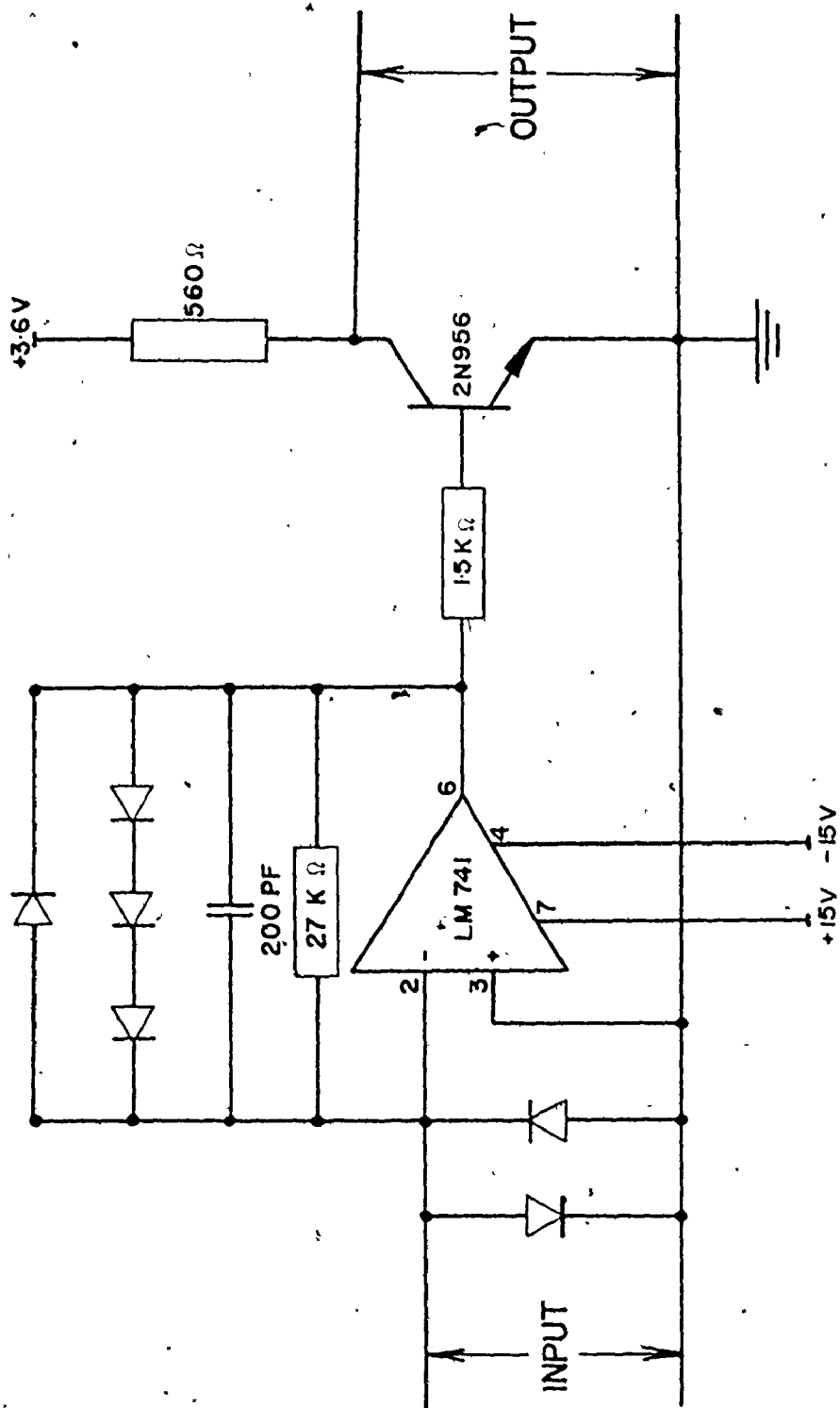
ALL DIODE : IN 659

Figure 12   Schematic of the Electronic Pulse-shaping Unit

3.4.2 Mass Flow

As mentioned in section 3.3, a rotameter * was an integral part of the air supply system. This rotameter was used to measure the mass flow of air to the turbine.

Since the scavenge pump was noted to draw air as well as oil from the turbine system during preliminary tests, a rotameter ** was connected to the oil breather on the sump. This rotameter measured the leakage air mass flow-rate.

3.4.3 Bearing Temperature

A Ceramo type copper/constantan grounded thermocouple was positioned against each of the upper and lower bearings. The differential EMF between the bearing temperature and an ice junction was displayed on a chart recorder.*** This EMF was used to calculate the bearing temperature.

3.4.4 Air Flow Temperature

The air temperatures before and after the turbine were measured with copper/constantan thermocouples encased in total temperature probes as supplied by Pratt & Whitney of Canada (Figure 13(a)). The EMF between the probes and an

---

*   . Brooks AR-MET Model 12-3623-1118 Magnetic Follower Type

**   Brooks Model 1307-12B

***   Rikadenki Model B-28L
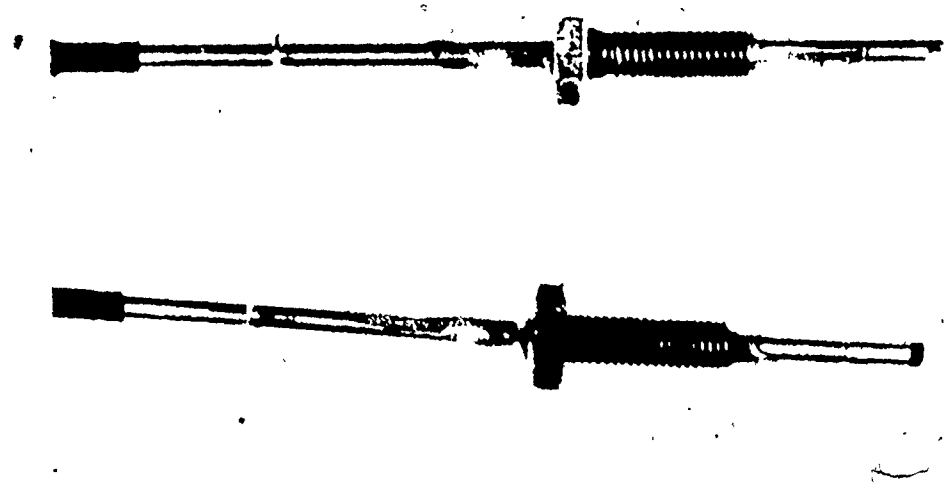
(a) Probes as epoxied in housing attachment bolts

Thermocouple Junction
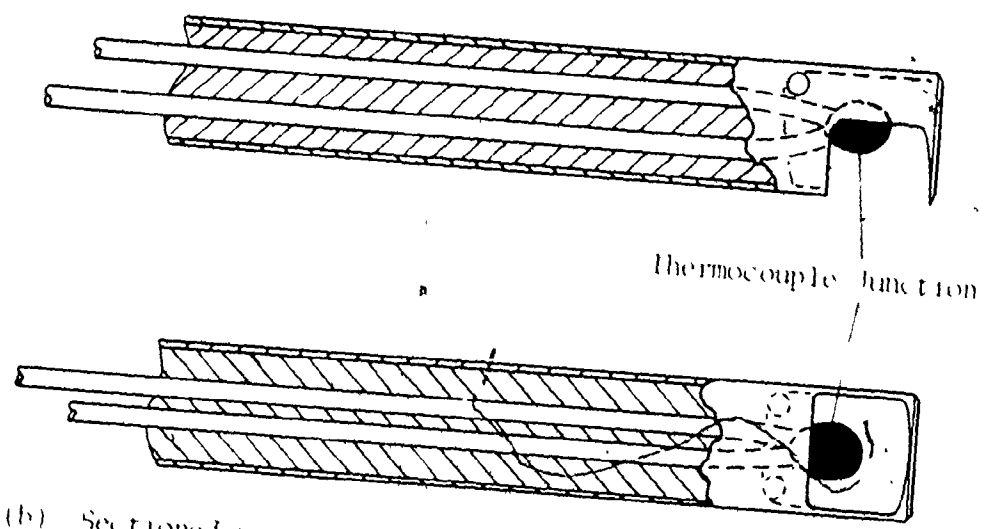
(b) Sectioned view

Figure 15 Total Temperature Probes

ice junction was measured using a precision potentiometer*
and the resultant reading used to calculate the airstream
temperature.

The initial (i.e., upstream of the turbine) air
temperatures for all the experiments performed were measured
from a single probe located in the reducing section immediately
upstream of the turbine body. All final (i.e., downstream
from the turbine) temperatures were measured by a probe
immediately downstream of the annular diffuser located in
the turbine shroud.

When the results of the initial tests were presented
to Pratt & Whitney of Canada, recommendation was made
that all temperature measurements be taken in triplicate.
It was further recommended that the final temperature probes
be located in the plenum into which the annular diffuser
exhausts. This ensured a more proper mixing of the flow, and
reduced the possibility of swirl affecting the measurements.
Prior to these recommendations, plans had been made to move
the single initial temperature probe to the inlet plenum
by drilling through the centre of a body attachment bolt and
passing the probe through it (Figure 13(b)).

The three relocated inlet probes were epoxied into
body attachment bolts which were spaced at 120° intervals
around the inlet plenum. The three relocated final temperature

---

* Rubicon Portable Precision Potentiometer Type 2745

probes were placed at 120° intervals around the exhaust plenum and sealed with Swagelok fittings (Figure 14). Through a series of knife switches the EMF's between these probes and the ice point were passed to the potentiometer. Experimentation using these probes was interrupted during the first test due to failure of the upper bearing.

3.4.5 Pressure

The air pressure immediately downstream of the rotameter was measured with a temperature compensated pressure gage*. The gage was connected to the main air lines by a 1/4 inch copper tubing sealed with a Swagelok fitting.

The initial pressures for the first three experiments were measured by a single probe in the 1 inch diameter line immediately upstream of the turbine body housing. The probe was connected to another temperature compensated gage**.

When the results of the first experiments were presented to Pratt & Whitney of Canada, it was recommended that a series of pressure probes be installed in the annular diffuser immediately downstream of the turbine blade section. These probes would permit an examination of the flow as it emerged from the blades. Accordingly, three pressure probes were

---

* Heise Model 40830
** Wallace and Tiernan Model FA145

PRESSURE PROBE
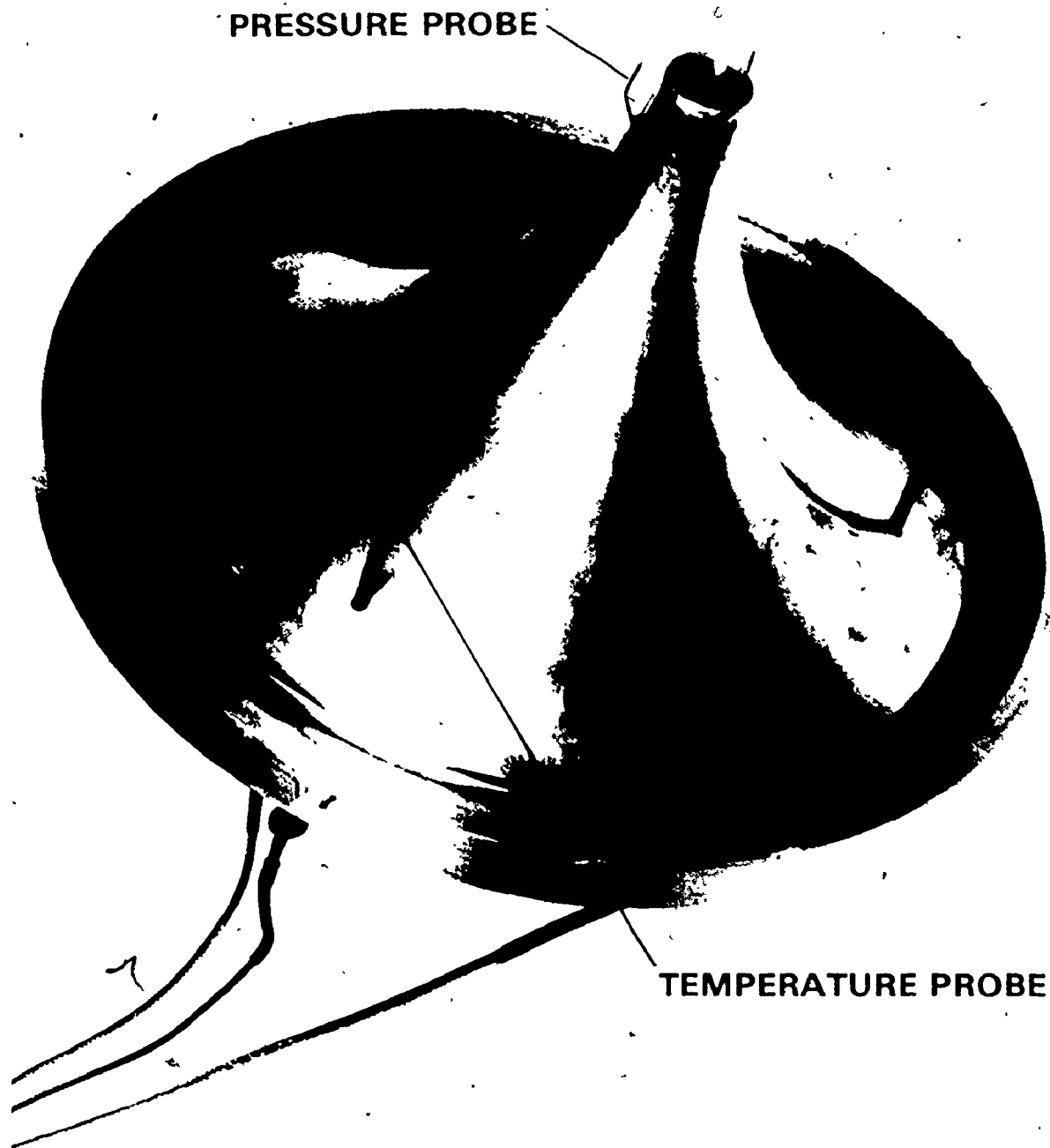
TEMPERATURE PROBE

Figure 14. Annular Diffuser Centerbody Showing Relocated
Temperature and Pressure Probes

installed at a distance of 0.1 inch downstream of the turbine blades. These probes were spaced at 120° intervals in the annular diffuser, and located radially at 0.1 inch, 0.2 inch and 0.3 inch from the centrebody surface (Figure 14). Experimentation using these probes was also interrupted during the first test due to failure of the upper bearing.

Atmospheric pressure was measured with a mercury column barometer*.

3.5 . Turbine Blade Clearance

The clearance between the turbine blades and the backface and shroud was set with feeler gages to 0.006 inch. This represented a total gap of 12% of the blade width at the tip and 3.4% of the width at the hub.

---

* Wallace and Tiernan Model FA135.

CHAPTER 4

EXPERIMENTAL PROCEDURE

4.1 . Introduction

As mentioned in Chapter 1, the initial tests
performed on the turbine at Pratt & Whitney of Canada, showed
that the isentropic efficiency of the unit was much lower
than the design target of 80%. The isentropic efficiency
was expected to be a better measure of the turbine's per-
formance than the mechanical efficiency, since the former
was computed from the gas path power using thermodynamic
relations alone, while the latter was found by comparing
the energy available to the turbine thermodynamically with
the power absorbed by the unit mechanically.

Since the only variables in the isentropic efficiency
equation (A6) were temperature and pressure, the sole
factor affecting the uncertainty of this efficiency was the
accuracy to which these quantities were measurable. There
were two main sources of error in the temperature measure-
ments: conduction error, which could be estimated very
accurately, and the inherent thermocouple manufacturing error,
which could be reduced by the use of multiple probe systems.
The pressure errors could also be reduced by using multiple
probes in zones of low pressure fluctuation. By comparison,
the mechanical efficiency (equation (A18)) required pressure

and temperature measurements as well as an estimate of the frictional drag on the system, and a precise measurement of the mass flowrate. For this reason, the isentropic efficiency was the criterion used to judge the performance of the turbine. A derivation of both the isentropic and mechanical efficiencies was performed and is shown in Appendix D.

In an effort to locate problem areas in the turbine design, the unit's response was examined under several load conditions. The design of a braking device to provide the turbine with variable loads presented a considerable problem in itself. Commercially available devices such as electrical generators or eddy-current dynamometers had to be rejected because of the severe stress levels imposed upon them at the high speeds attained by the turbine. It was finally decided to use aerodynamic loading on a disc which could be spun at high speeds and still remain within acceptable stress limits. Load variation could then be affected by changing the density of the drag medium.

Pressures in the load cannister were maintained at approximately atmospheric for all cases except the first test in which the drag gas employed was air at about 1/30 atmosphere. The other gases used included air (m.w. = 28.8), sulfur hexafluoride (m.w. = 146.1) and carbon dioxide (m.w. = 44.0).

Each experiment was performed in the same manner in order to yield results that were both internally consistent and reproducable. At the start of every test, the turbine

was spun at a relatively low (10,000-20,000 RPM) speed
to permit temperature stability. The speed was then increased
to the maximum value to be tested by opening the main control
valve. The bearing temperatures stopped increasing and
remained at a fixed value when steady state was achieved.
At this point the required temperatures, pressures and mass
flows were measured. The driving pressure was then fractionally
reduced by closing the control valve, and the procedure repeated.
Careful adjustment of the supply oil pressure using the
feedback loop control valve allowed the bearing temperatures
to be controlled.

For the first experiment, the load disc was spun in
a partial vacuum. Test results were taken at speeds ranging
from 18,000 to 74,000 RPM. In the second experiment, the
load disc was spun in air at atmospheric pressure. Results
were measured for speeds ranging from 43,000 to 74,000 RPM.
The turbine was then shut down, and the oil allowed to cool
while adjustments were made to the oil damper housing
connections. The test was recommenced, and values recorded
in the 19,000 to 36,000 RPM range. In this way, the
turbine's sensitivity to bearing drag could be examined,
since the viscous loads at the bearings were higher
for the cooler oil. Sulfur hexafluoride was used in
the third experiment to provide drag on the load disc.
Test results were recorded from speeds of 20,000 RPM to
50,000 RPM at approximately 5,000 RPM increments. The
final experiment was performed with the load disc rotating

in carbon dioxide at atmospheric pressure. The results were obtained at 5,000 RPM increments between 5,000 and 60,000 RPM.

4.2   Temperature Measurements

When the turbine achieved a steady state condition, three to six inlet and outlet temperature measurements were recorded. The left-hand setting of the single knife-switch connected the potentiometer to the air inlet and ice-point thermocouples. Similarly, the switch's right-hand setting connected to the outlet thermocouple (Figure 15). The thermoelectric potential with reference to the ice-bath was then measured by balancing the potentiometer. Conversion of EMF to temperature was done using the National Bureau of Standards values.

The six relocated temperature probes were connected to the potentiometer and the ice-point thermocouples by three knife switches (Figure 16). The EMF between the ice bath and the first two inlet probes was measured using the first switch. With the other switches in the open (knives vertical) positions, the potentiometer was connected to the first thermocouple through the left-hand setting of the first switch. Similarly, the right-hand setting connects the potentiometer to the second probe. The second switch controlled the third inlet and first outlet probes (left and right settings respectively) and the third switch the remaining two outlet probes. It was essential that two switches remained
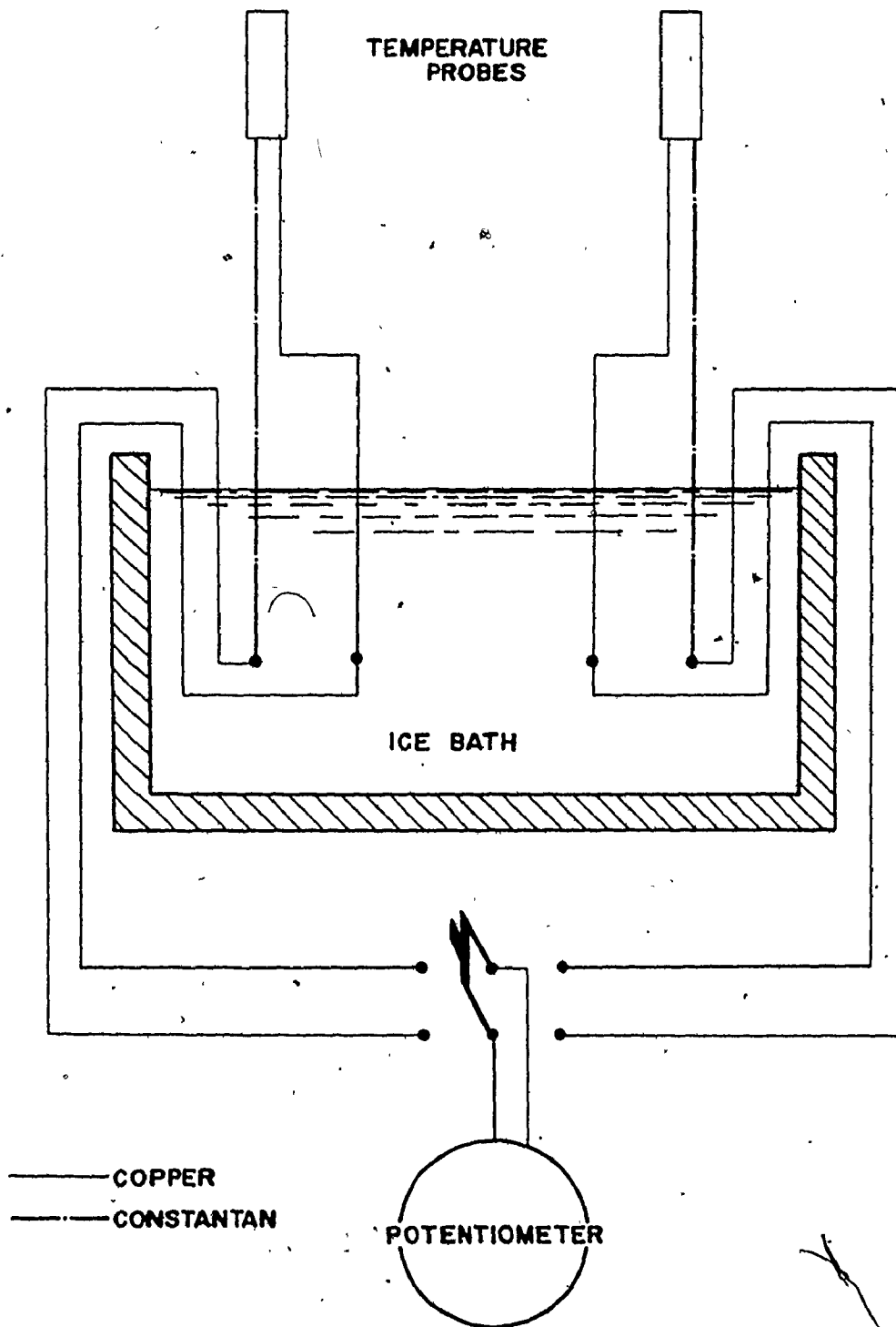
Figure 15   Schematic of the Temperature Measurement System

PROBES

ICE BATH

POTENTIOMETER

——————— COPPER

——·——·—— CONSTANTAN
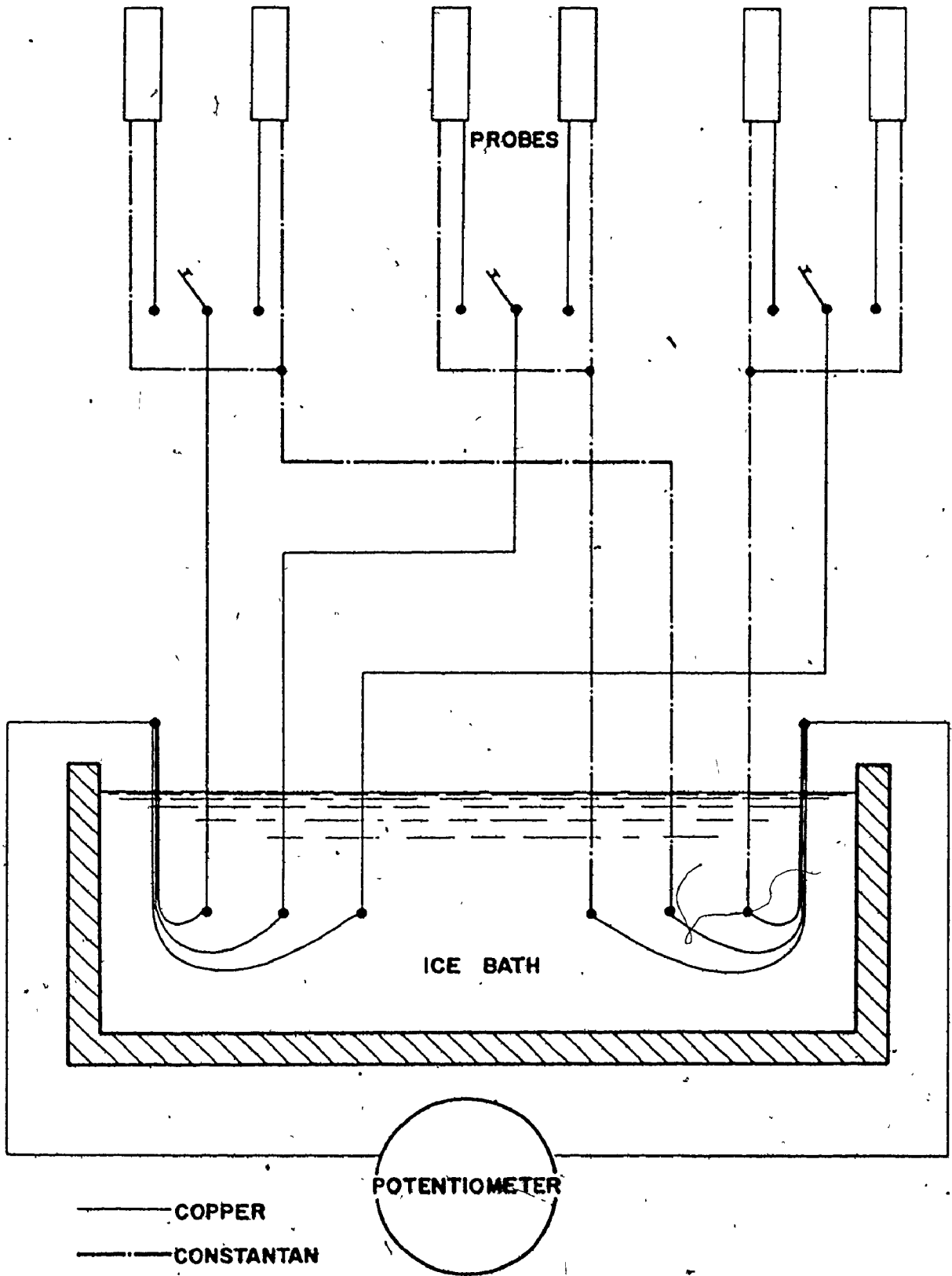
Figure 16   Schematic of the Re-designed
Temperature Measurement System

,inoperative while any one switch was employed.

The bearing temperatures were recorded on the chart recorder. With the scale set to 10 millivolts per·inch, the EMF resulting between the bearing and ice-bath thermocouples were read directly from the chart.

4.3   Pressure Measurements

Measurements of air pressure at various stages of the turbine and air delivery system were recorded with each set of inlet and outlet temperatures. Immediately downstream of the supply air rotameter, the air pressure was measured with a static probe connected to a pressure gage. For the first three experiments, the inlet pressure immediately upstream of the turbine body housing was measured with a static pressure tap connected to a temperature compensated pressure gage. In the fourth experiment, the inlet plenum pressure ·was also recorded with a static probe connected to another temperature compensated pressure gage.

Since the isentropic efficiency of the system (Appendix D) was that which occurred between upstream and environmental conditions, the final (downstream) pressures were all considered to be atmospheric. The ambient pressure was measured with a mercury column barometer.

The relocated pressure probes which span the annular diffuser immediately downstream of the turbine were connected with Tygon tubing to water-filled "U" tube manometers from which the pressure was read directly. ·

4.4 Mass Flow Measurements

As mentioned in Chapter 3, the flowrate of supply air was measured with a rotameter integral to the air delivery system. Since this rotameter was calibrated at $70^{\circ}F$ and 100 p.s.i.g., a correction had to be made·for the actual conditions of the gas whose flowrate was required. According to Bennett [12], the rotameter has been calibrated in terms of the equivalent air flow volume, V_{eq}, at 14.7 p.s.i.a. and $70^{\circ}F$ for a specified temperature, pressure, and specific gravity (condition 1). If the rotameter was employed at conditions (2) other than the original specifications, then a correction factor had to be applied.

$$\text{Correction Factor} = \sqrt{\frac{Sg_1 \; T_1 \; P_2}{Sg_2 \; T_2 \; P_1}} \tag{1}$$

where T = absolute temperature

P = pressure, p.s.i.a.

Sg = fluid specific gravity

= 1.0 for air

Thus

$$V_{eq} = V_c \times (\text{correction factor})$$

where V_c = calibrated flow reading

To convert this equivalent air flow to metered gas flow, the following relationshion [13] has been used:

$$V_{eq} = \frac{M(\frac{RT}{P})}{Sg_2} \left(\sqrt{\frac{Sg_2 \; T_2 \; P_1}{Sg_1 \; T_1 \; P_2}} \right) \tag{2}$$

where M = Mass flowrate in lbm/min.

R = Specific gas constant

Thus

$$M = \frac{V_{eq}\, Sg_2}{(\frac{53.3 \times 530}{14.7 \times 144}) \sqrt{\frac{Sg_2 \times T_2 \times 14.7}{1.0 \times 530 \times P_2}}} \tag{3}$$

for air flow with $Sg_1 = Sg_2 = 1.0$ and $P_1 = 100$ p.s.i.g.

$$M = \frac{V_c \sqrt{\frac{P_2}{100 + P_{atm}}}}{13.34 \times 60 \sqrt{\frac{T_2}{P_2}(\frac{14.7}{530})}} \tag{4}$$

where P_{atm} = Atmospheric pressure

M = Mass flowrate in lbm/sec.

This simplified to yield

$$M = 7.502 \times 10^{-3}\; \frac{V_c \sqrt{\frac{P_2}{100 + P_{atm}}}}{\sqrt{\frac{T_2}{P_2}}} \tag{5}$$

The leakage airflow rate was also measured with a rotameter.

CHAPTER 5

ANALYSIS AND DISCUSSION
OF EXPERIMENTAL RESULTS

5.1   General Observations

As shown in Figure 17, the values of isentropic
efficiency at given speeds for the load disc spun in vacuum
are moderately scattered ($\pm$ 5% η) above 25,000 RPM, and
increasingly scattered at lower speeds (up to 12% η). This
low speed scatter is generally considered the result of
temperature fluctuations.

With the load disc in atmospheric pressure air, slightly
less scatter ($\pm$ 3.5% η) is observed in the isentropic effic-
iency values (Figure 18). A discontinuity in the curve occurs
where the turbine was shut down, and cooled. The observed
turbine efficiency increases due to the resulting higher
viscous loads imposed on the rotor by the bearings.

The scatter in isentropic efficiency with the load
disc in SF_6, shown in Figure 19, is also low ($\pm$ 3.5% η). At
speeds of approximately 15,000 RPM, the design target
efficiency of 80% is reached.

In the final test with the load disc in CO_2, the
greatest amount of scatter ($\pm$ 6% η) is observed in the
isentropic efficiency values (Figure 20). This may in part
be due to varying loads at the upper bearing which was near-
ing the end of its serviceable lifetime.
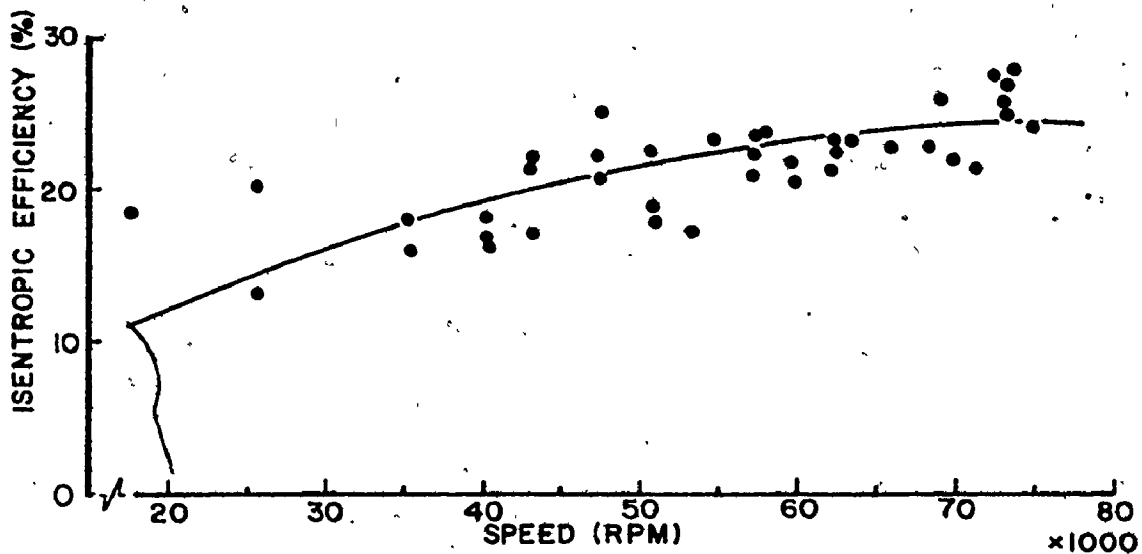
Figure 17 Graph of Isentropic Efficiency vs.
RPM for Load Disc in a Partial Vacuum
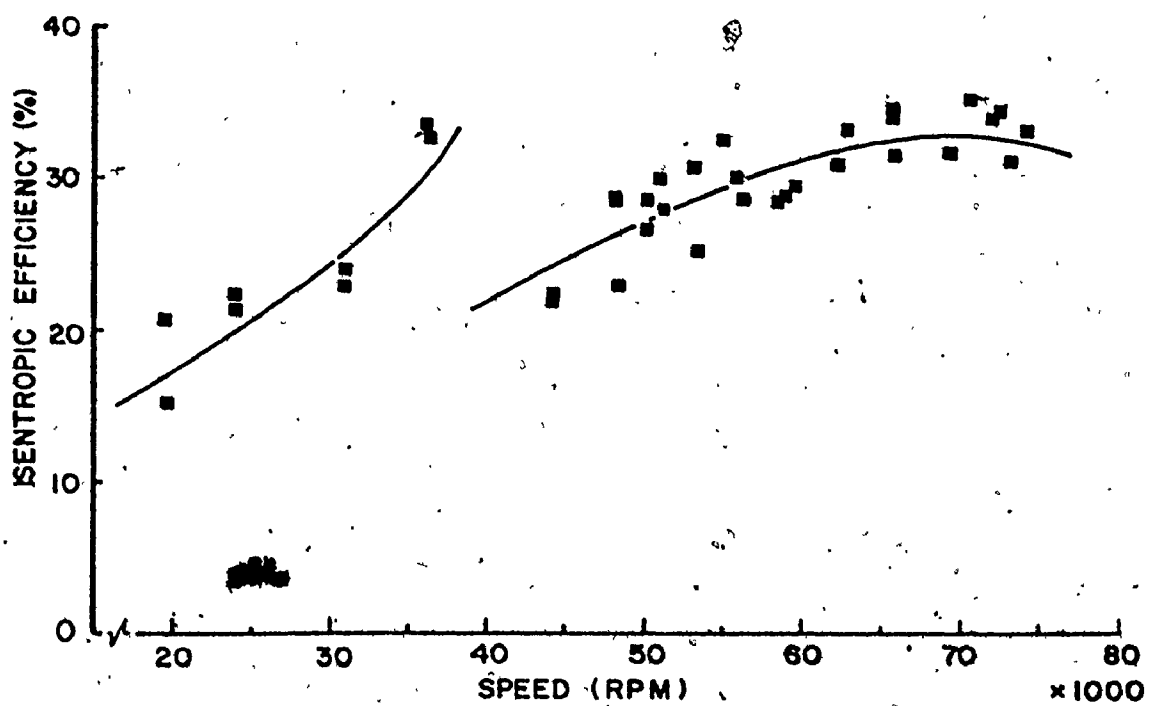
Figure 18 Graph of Isentropic Efficiency vs. RPM
for Load Disc in Air
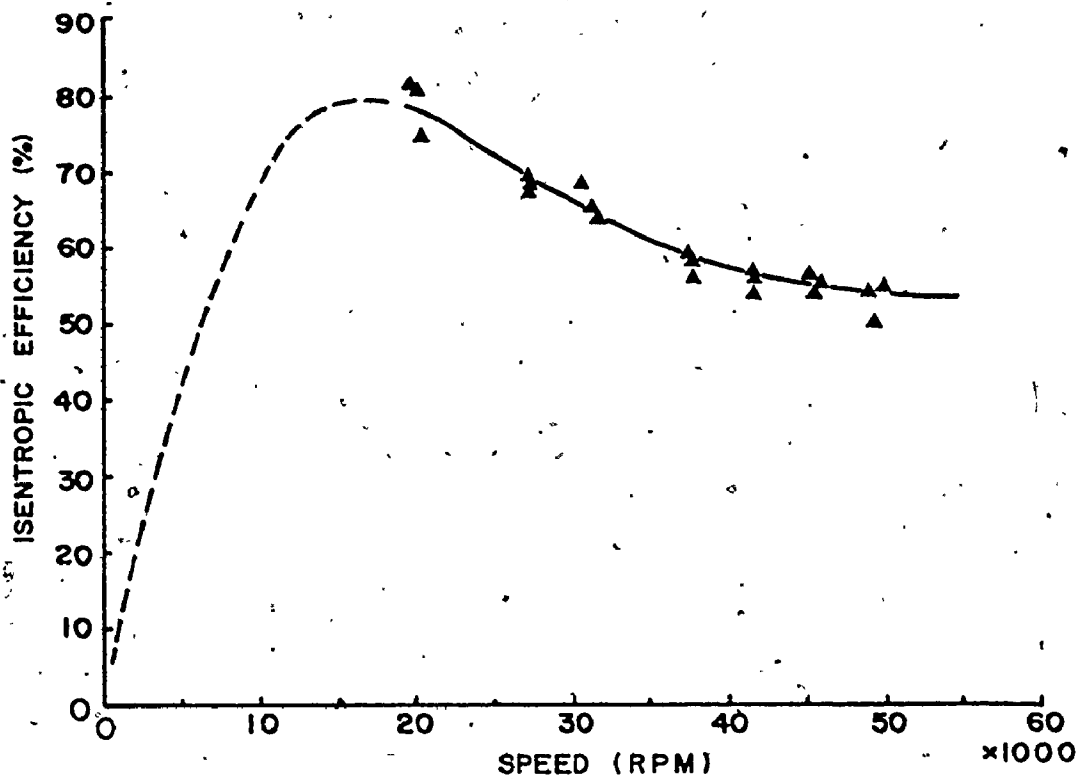
Figure 19 Graph of Isentropic Efficiency vs.
RPM for Load Disc in Sulfur Hexafluoride
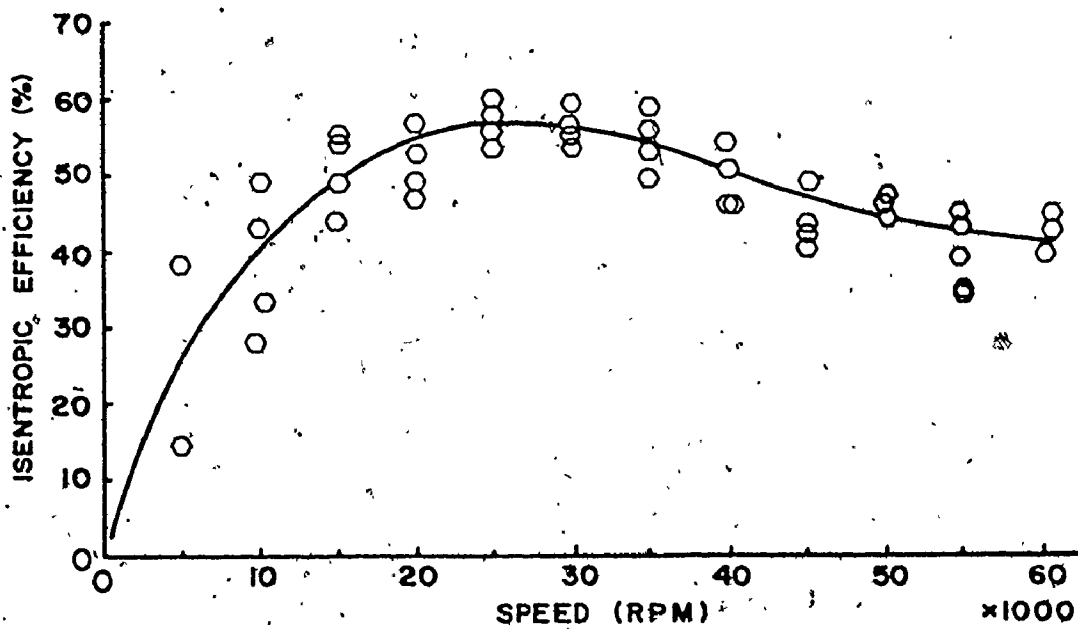
Figure 20 Graph of Isentropic Efficiency vs RPM
for Load Disc in Carbon Dioxide

It was noted that the air inlet temperature increased
with increasing turbine speed. A plot of this temperature
against mass flowrate (Figure 21) showed that the trend
increased monatonically. This indicated that relative
to the turbine requirements, the system's air reservoir
was small, and the compressor was supplying the turbine more
or less directly. Support for this argument was given experi-
mentally in terms of supply line pressures. Upstream of the
turbine, the line pressure dropped appreciably at high mass
flowrates, and fluctuated moderately as the compressor
worked to restore the pressure.

Both inlet plenum pressure and mass flowrate increased
with increasing turbine speed. There were small fluctuations
in plenum pressure at high speeds due to the previously
mentioned compressor problem. These fluctuations were
accompanied by associated changes in RPM. There was little
scatter in the mass flow data (see Appendix F, Figures A12-A15).

Qualitatively speaking, scatter in the experimental
results was observed to increase with decreasing turbine speed
in all the tests performed. This phenomenon was reflected
most strongly in the calculated values of isentropic
efficiency.

5.2 Analysis and Discussion

The presentation of data in this section is carried
out using parameters customarily employed at Pratt & Whitney
of Canada in turbine and compressor design. In this way it
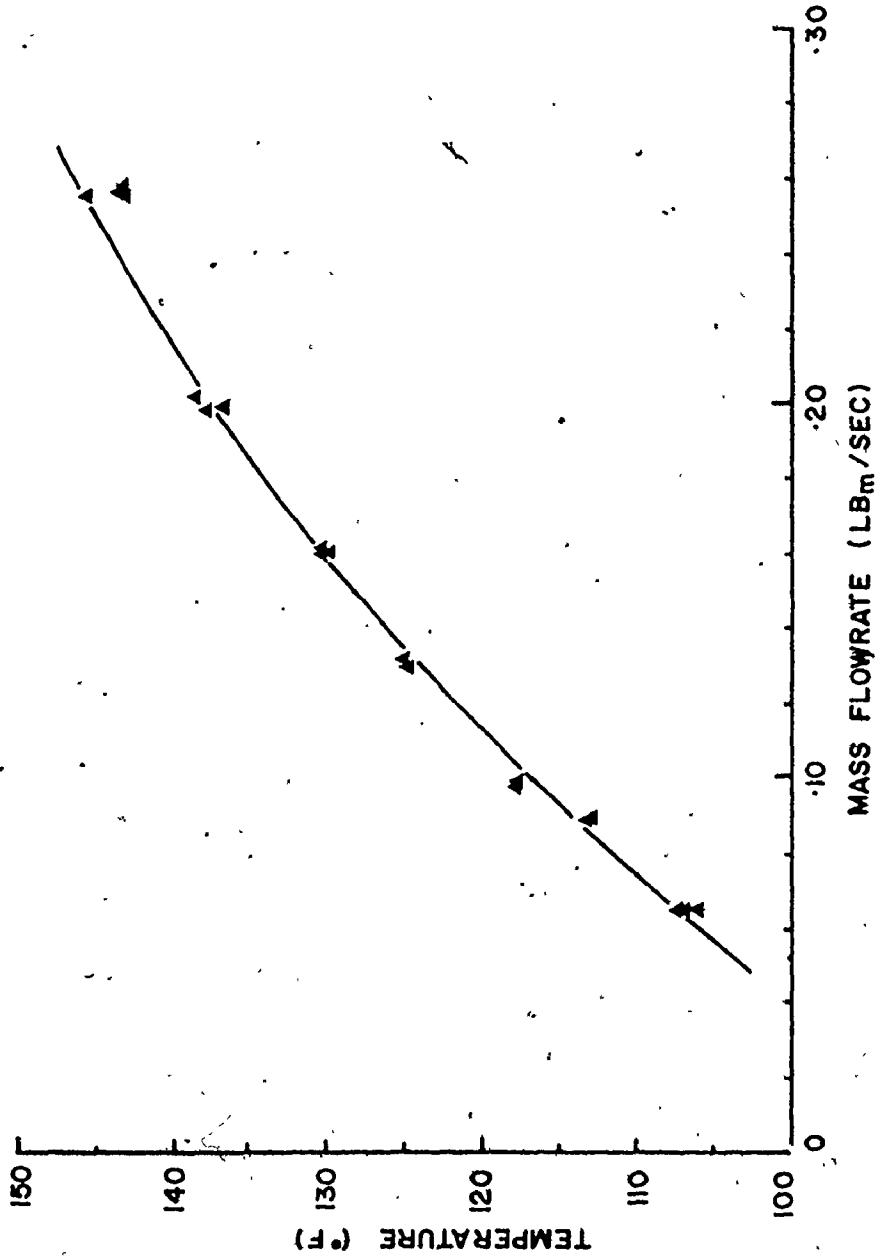
Figure 21 Graph of Temperature vs Mass Flow

is felt that the results of this analysis will be most easily incorporated into the existing body of knowledge on the performance of this turbine. The following terms are used: P.R, pressure ratio, is the ratio of the turbine inlet plenum pressure to the atmospheric pressure; η is the isentropic efficiency measured between the conditions immediately upstream of the turbine and atmospheric conditions, calculated from: (see Appendix D)

$$\eta = \frac{(T_{inlet} - T_{outlet})/T_{inlet}}{1 - (\frac{1}{P.R.})^{\frac{\gamma-1}{\gamma}}} \quad ; \qquad (A6)$$

$N/\sqrt{T_0}$ is the ratio of turbine speed to the inlet temperature ($^\circ$R), and gives values of speed normalized to remove any temperature effects; U_T/C_0' is the ratio of turbine blade tip speed to the isentropic spouting velocity, calculated from

$$U_T/C_0' = \sqrt{\frac{.0143\ N}{12,025\ T_0[1 - (\frac{1}{P.R.})^{\frac{\gamma-1}{\gamma}}]}} \quad ; \qquad (6)$$

Figure 22 shows a plot of pressure ratio against $N\sqrt{T_0}$. This graph provides an indication of turbine response for given pressure inputs. It can be seen that for increasing loads, greater pressure ratios are required to achieve the same speed. This is the expected response for an IRF
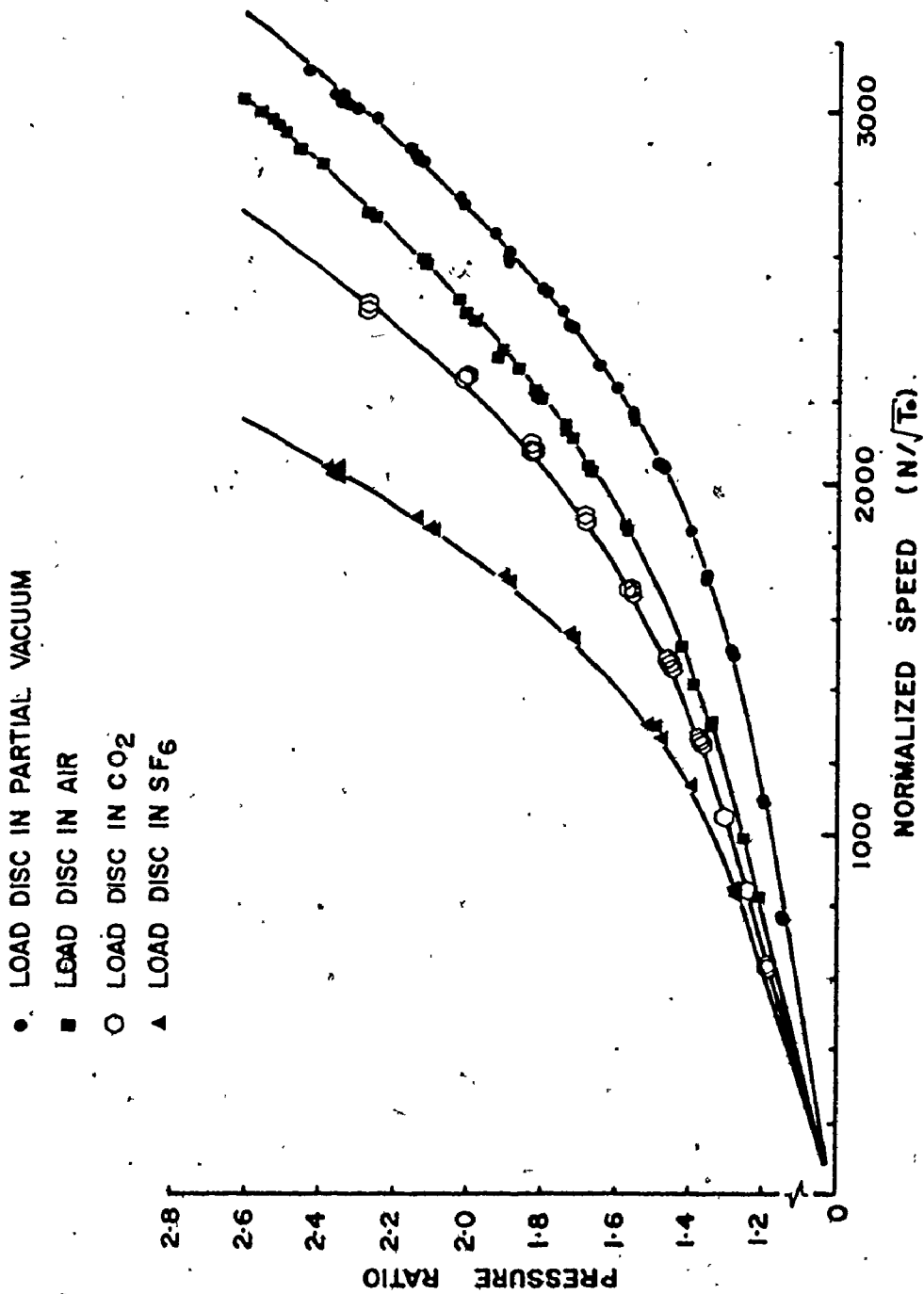
Figure 22 Graph of Pressure Ratio vs. Normalized Speed

turbine. However, a comparison of the design specifications (Appendix A) with these experimental results indicates that the pressure ratio falls far below the specified P.R. = 4.29 at the design point of $N/\sqrt{T_0} = 3242$ (i.e., 75,000 RPM).

For the sake of clarity, the data shown on the graphs in the rest of this chapter are limited to the mean of each pertinent set of observations.

Figure 23 shows lines of constant pressure ratio on a graph of η against U_T/C_0'. For IFR turbines in general an increase in pressure ratio shows an increase in efficiency on this type of plot. While it is evident that this does in fact occur for higher values of U_T/C_0' at low efficiencies, the exact opposite trend is seen for low U_T/C_0' at high efficiencies. Thus it is clear that based on present experimental results the turbine performs better at low speeds and high loads.

An explanation of this phenomenon may be found by examining the velocity triangles which represent an increase in blade tip speed at constant pressure ratio (and hence constant absolute gas speed). Figure 24a compares the inlet conditions at low tip speed with the conditions at a somewhat higher tip speed. It can be seen that the angle of incidence between the blade tips and the relative gas path is decreased, and thus incidence losses can be expected to decrease. This would tend to increase the overall efficiency of the turbine. Figure 24b shows the outlet conditions corresponding to the previous inlet

47.
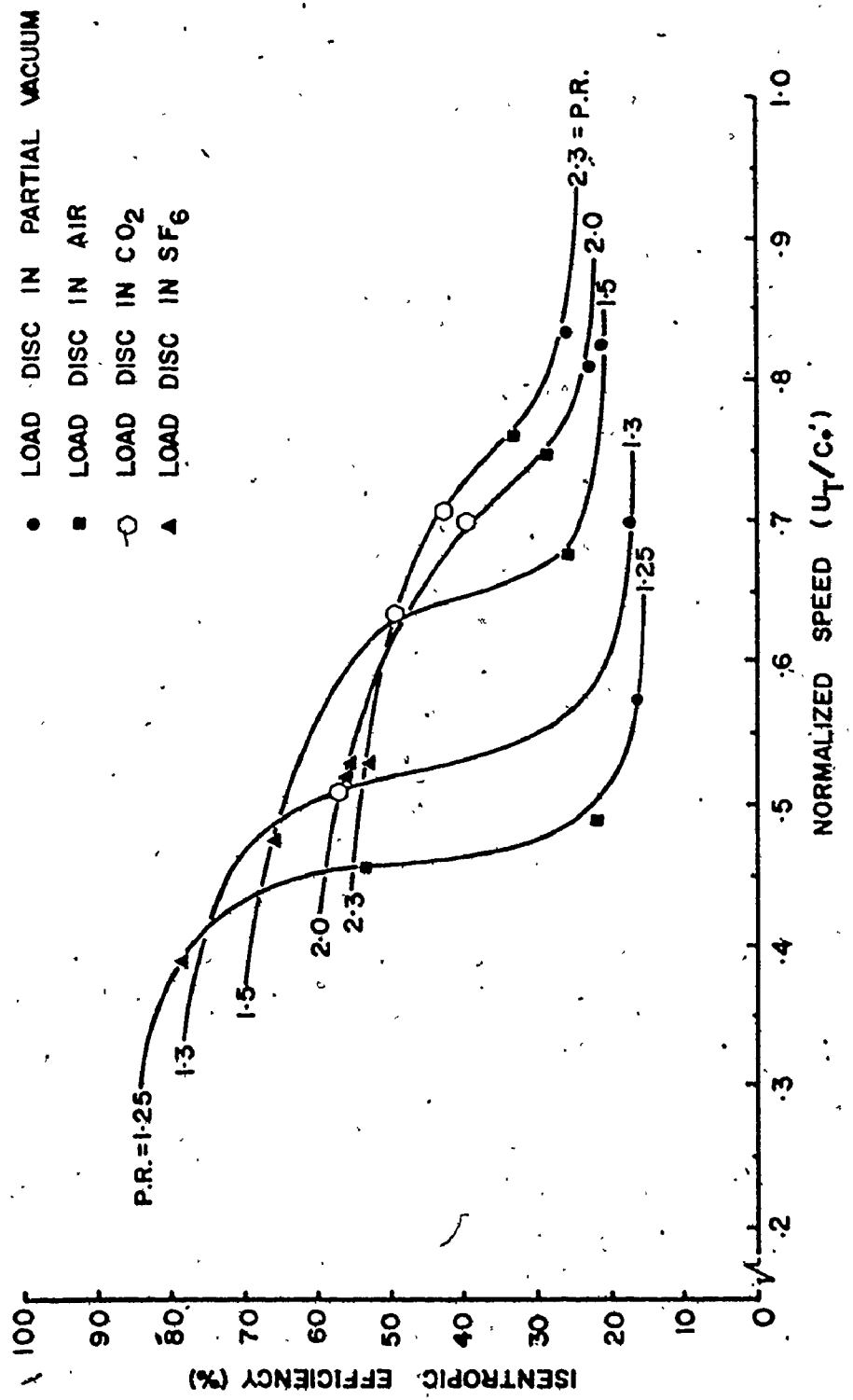
Figure 23   Graph of Isentropic Efficiency vs. Normalized
Speed Showing Lines of Constant Pressure Ratio
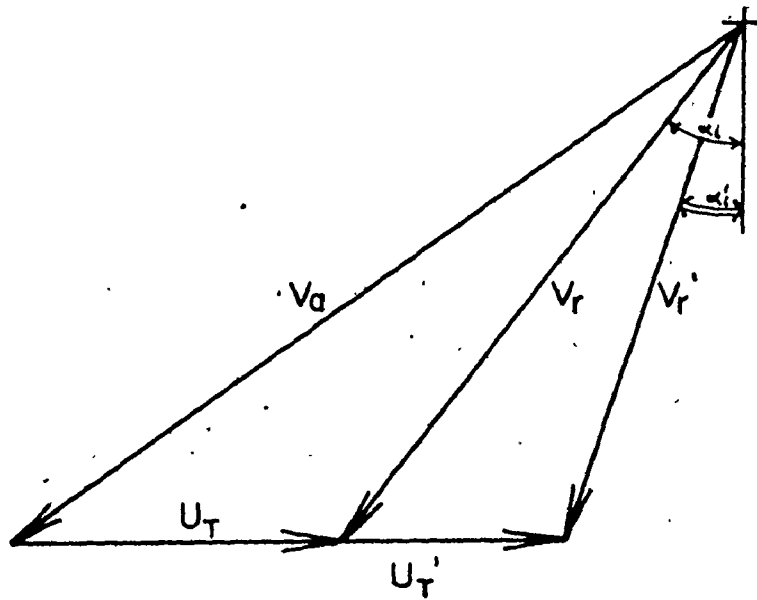
(a)   Inlet Velocity Triangles

(b)   Outlet Velocity Triangles
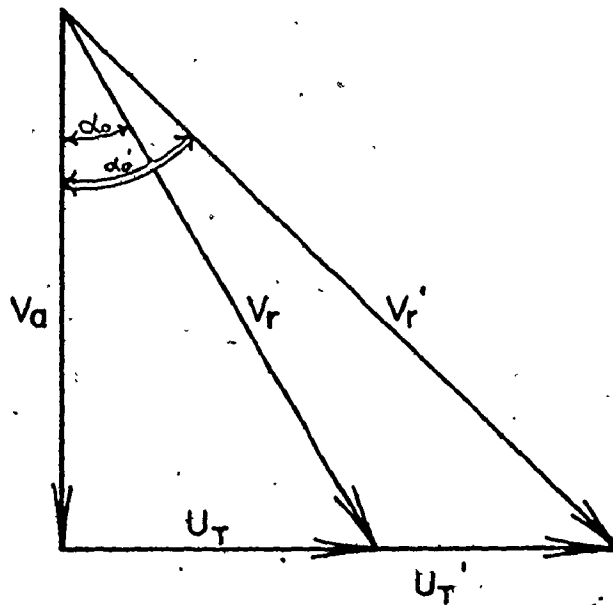
Figure 24   Inlet and Outlet Velocity Triangles for
Change in Blade Tip Speed at Constant
Pressure Ratio

conditions. The increase in blade tip speed is accompanied
by an increase in exit swirl, which would cause a decrease
in turbine efficiency. Since the observed result of such
a tip speed increase is, in fact, a reduction in the
isentropic efficiency of the turbine, it is evident that the
exit swirl plays a greater role in efficiency reduction than
do inlet losses. This suggests that the design deficiency
lies in the diffusion process rather than in the turbine per
se. Such a conclusion would explain the reason that high
efficiencies are reached under conditions of high load and
low speed: in such a case, the exit swirl is very low and
the diffuser is able to cope with the resultant flow.

Figure 25 shows lines of constant speed ($N/\sqrt{T_0}$) on
an efficiency vs. pressure ratio graph. For a standard
IFR turbine these lines would be shaped like a series of
inverted parabolae with the maxima occurring at approximately
the same value of efficiency, and as a function of pressure
ratio. Although no maxima occurred in the $N/\sqrt{T_0}$ lines
over the range of pressure ratios examined, the trend of
these lines (i.e., increasing peak efficiencies at lower
speeds) indicates once again that the turbine performs
better at lower speeds.

The very steep slopes in the lowest lines of constant
$N/\sqrt{T_0}$ offer an explanation for the turbine's sensitivity
to fluctuating loads (eg., viscous or bearing drag varia-
tion, etc.). Such fluctuations would allow a change in
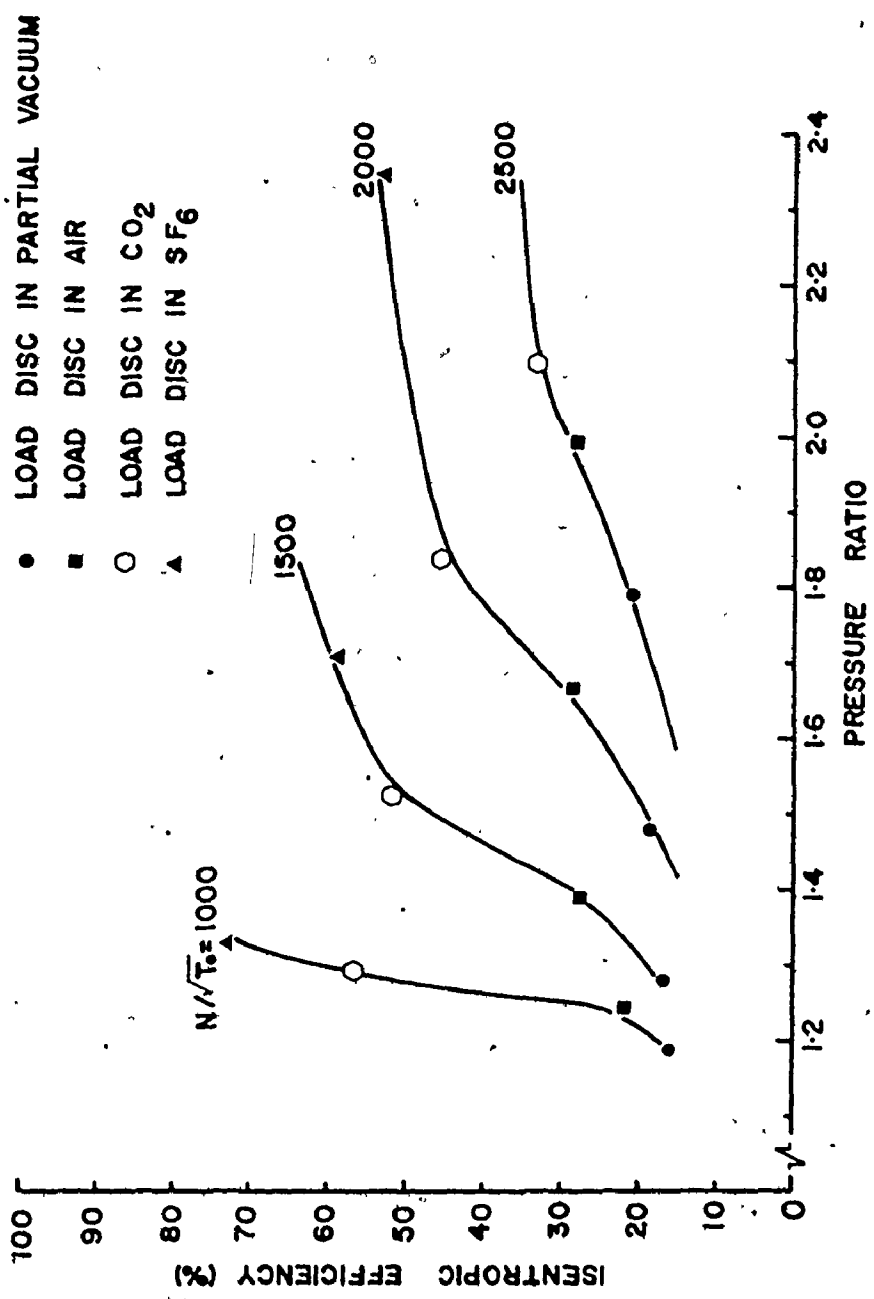
Figure 25 Graph of Isentropic Efficiency vs. Pressure
Ratio Showing Lines of Constant Normalized Speed

51.
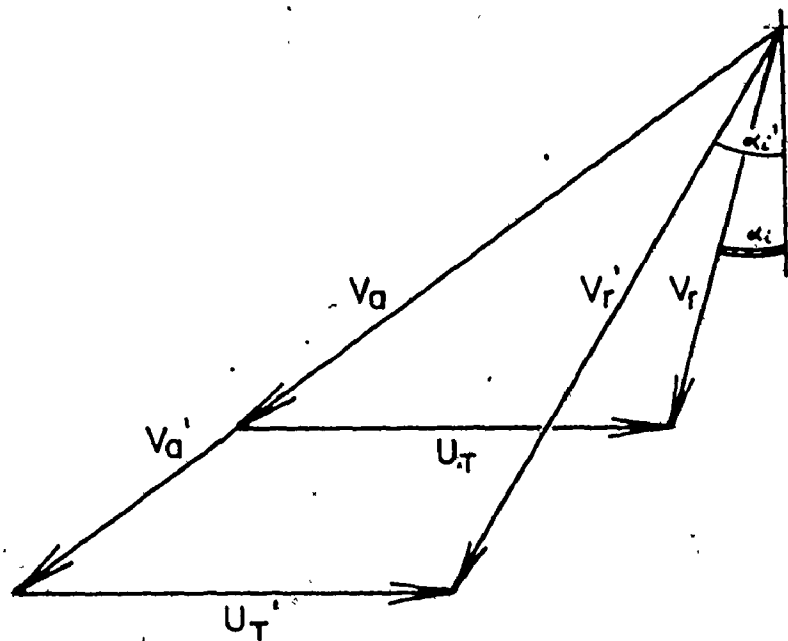
(a) Inlet Velocity Triangles

(b) Outlet Velocity Triangles
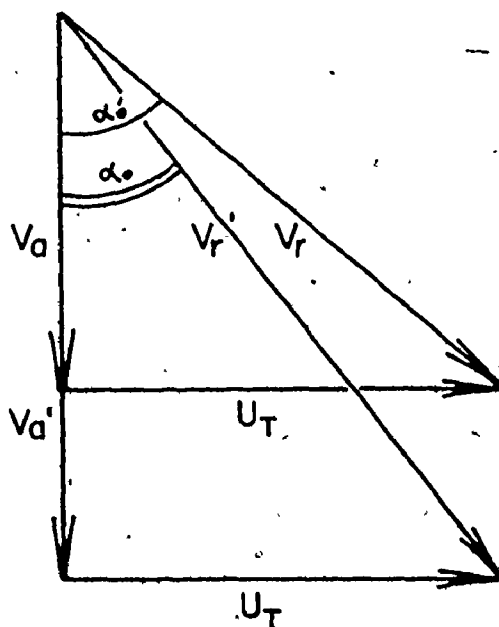
Figure 26 Inlet and Outlet Velocity Triangles for
Change in Pressure Ratio at Constant Blade
Tip Speed

pressure ratio to occur for a constant speed. Due to the steep slope, a very small change in pressure ratio yields quite an appreciable change in the isentropic efficiency of the turbine. Thus significant scatter in the efficiency values at low speeds is almost unavoidable.

At constant $N/\sqrt{T_0}$ (and hence constant blade tip speed), increasing the pressure ratio increases the absolute gas speed V_a, which increases the incidence angle at the inlet to the blades and reduces exit swirl (see Figures 26a and b). Since the efficiency increases for such an operation, the conclusion that exit swirl predominates the turbine efficiency is once again reached.

The constant pressure ratio lines on the graph of η vs. $N/\sqrt{T_0}$ (Figure 27) serve to re-emphasize the previous points. The steep slopes of the low pressure ratio lines show that small changes in speed can yield large variations in efficiency. At constant pressure ratio, increasing $N/\sqrt{T_0}$ reduces incidence losses and increases exit swirl (the velocity triangles being identical to those in Figures 24a and b). Since this process is accompanied by a decrease in η, the exit swirl must govern the turbine efficiency.
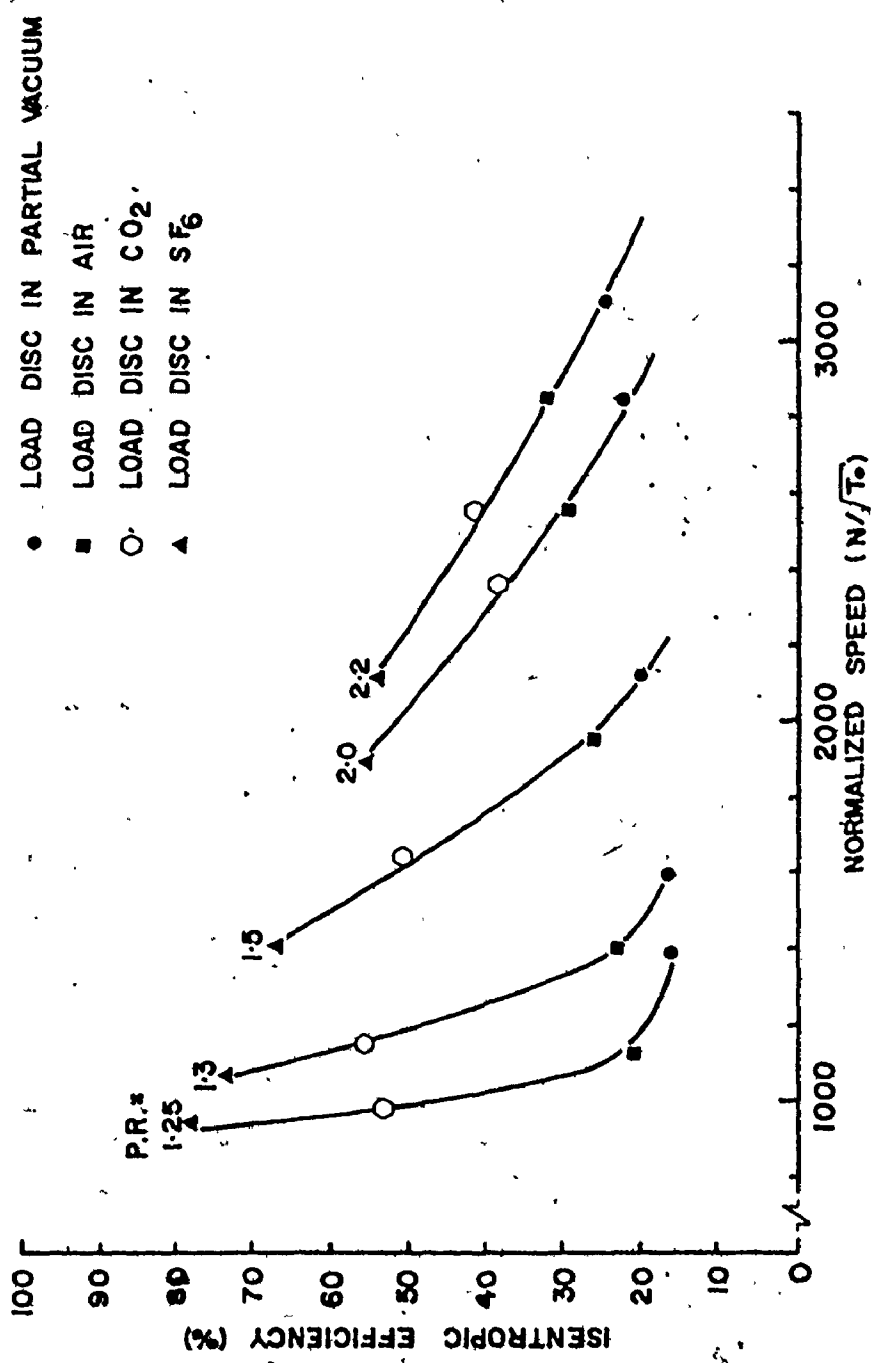
Figure 27 Graph of Isentropic Efficiency vs. Normalized
Speed Showing Lines of Constant Pressure Ratio

CHAPTER 6

DISCUSSION OF ERRORS IN EXPERIMENTAL WORK

6.1 Temperature Measurement

The errors associated with measuring the air inlet and outlet temperatures come from three sources. The thermocouples themselves have an inherent error of approximately $\pm$ 1°F in 300°F. The cold junction was considered to be in error by $\pm$ .2°F. The potentiometer could be accurately read to $\pm$ .002 millivolts, corresponding to $\pm$ .1°F.

Two copper-constantan thermocouple junctions	$\pm$ 2.°F
Cold junction temperature	$\pm$ 0.2°F
Potentiometer error	$\pm$ 0.1°F
Total	$\pm$ 2.3°F

6.2 Pressure Measurement

The inlet pressures could be read accurately to $\pm$ 0.01 inch of mercury. Pressure fluctuations were in the order of $\pm$ 0.05 inch of mercury per reading. The barometric pressure could be read to within $\pm$ 0.005 inch of mercury.

Inlet pressure measurement	$\pm$ 0.01 "Hg
Pressure fluctuations	$\pm$ 0.05 "Hg

Barometric pressure $\pm$ 0.005 "Hg

$$\text{Total} \quad \pm\ 0.065 \text{ "Hg}$$

6.3 Rotameter Measurement

The supply air rotameter could be read accurately to within $\pm$ .2 mm, corresponding to .001 lbm/sec. The leakage losses were measured by the loss rotameter to be approximately constant at 4 mm. This corresponds to .0009 lbm/sec. by which the supply mass flowrate is further in error:

Rotameter reading   .001 lbm/sec.

Leakage loss   .0009 lbm/sec.

$$\text{Total} \quad .0019 \text{ lbm/sec.}$$

6.4 Speed Measurement

The frequency counter can be read accurately to within $\pm$ 50 RPM. Speed fluctuations were in the order of $\pm$ 100 RPM per reading.

Frequency measurements $\pm$ 50 RPM

Speed fluctuations $\pm$ 100 RPM

$$\text{Total} \quad \pm\ 150 \text{ RPM}$$

6.5 Efficiency Calculations

Since the calculated values of the isentropic efficiency showed the greatest fluctuations for all the parameters, it was necessary to establish confidence limits for these values in each of the four experiments. Since

distribution must be assumed normal and the sample size is small (between 3 and 6), such limits are not wholly accurate. However, by computing the mean of the standard deviations for each data set, the approximate order of accuracy to be expected in the efficiency graphs may be shown.

For the first experiment, the average standard deviation is $1.69\%^2$, for the second $1.45\%^2$, for the third $2.03\%^2$, and $3.49\%^2$ for the fourth. Thus it may be stated with a 90% confidence level (1.65σ) that the values of efficiency lie within ± 2.79 units of the mean η for the first experiment, ± 2.39 units for the second, ± 3.35 units for the third, and ± 5.76 units for the fourth experiment.

CHAPTER 7

CONCLUSIONS AND
RECOMMENDATIONS

A review of the experimental results presented in Chapter 5 indicated that several conclusions could be drawn with regard to the performance of the combined turbine and diffuser system. By varying the pressure ratios across the system from 1.2 to 2.4, a series of parameters was investigated at turbine speeds up to 75,000 RPM. At constant pressure ratios, the turbine speed was found to increase with decreasing load. At constant mass flow parameters, the pressure ratio tended to increase with decreasing load. The efficiency of the system reached the design target of 80% for high loads at low turbine speeds; increasing the speed caused a decrease in efficiency. The efficiency was also found to be extremely sensitive to minor fluctuations in pressure ratio (or load) at turbine speeds below 20,000 RPM.

A study of the velocity triangles representing the flow conditions at the inlet and outlet to the turbine, showed that the large exit swirl into the diffuser introduced unexpectedly high losses responsible for the poor performance of the system. This confirmed one of the three initial explanations

proposed by the design engineers at Pratt & Whitney of Canada. It also implied that improvements could be made to overall design without changing the entire configuration of the system. The two major possibilities which suggested themselves were a change in blade design, or a modification of the diffuser section.

An exducer portion on the blades would reduce exit swirl and hence increase efficiency. This would, however, also defeat the initial purpose of the turbine which was the ability to be spun under power equally well in a clockwise or counter-clockwise direction. This indicates diffuser modification would be the best solution in line with the initial turbine design concept. Whether a diffuser could be designed to accept such a high degree of exit swirl remains a topic for future study.

REFERENCES

1. H. Cohen, G. F. C. Rogers, H.I.H. Saravanamuttoo, "Gas Turbine Theory", John Wiley & Sons, 1973.

2. U. Okapuu to J. H. T. Wade, Communication, 3 January, 1975.

3. F. J. Wallace, "Theoretical Assessment of the Performance Characteristics of Inward Radial Flow Turbines", Proceedings of the Institution of Mechanical Engineers, Number 33, Volume 172, 1958.

4. A. Dadone and M. Pandolfi, "A Method for Evaluating the Off-Design Performance of a Radial Inflow Turbine and Comparison with Experiments", International Journal of Mechanical Science, Volume 11, 1969.

5. M. Pandolfi, Quaderno, Number 14, A.T.A., 1967.

6. R. S. Berson, "A Review of Methods for Assessing Loss Coefficients in Radial Gas Turbines", International Journal of Mechanical Science, Volume, 12, 1970.

7. U. Okapuu and G. S. Calvert, "An Experimental Cooled Radial Turbine", UACL Report.

8. U. Okapuu and G. S. Calvert, "Cooled Radial Turbine for High Power-to-Weight Applications", AIAA Fifth Propulsion Joint Specalist Conference, Number 69-524, 1969.

9. A. V. Kovats and G. Desmur, "Pumps Fans and Compressors", Blackie, 1958.

10. L. F. Scheel, "Gas Machinery", Gulf, 1972.

11. A. Ferland to R. R. Marshall, Private Communication, 1 March, 1977.

12. R. A. F. Bennettt, "Primary Development of a Propane Air Combustor", M.Eng. Thesis, Dept. of Mech. Eng., McMaster Univ., 1967.

13. "Guide to Rotameter Application", Brooks Technical Bulletin T-022.

14. Turbine Design Computer Program Output, Pratt & Whitney Aircraft of Canada.

15. K. J. Enners to J. P. Lavoie, memo #223163, Pratt & Whitney Aircraft of Canada Ltd.

16. Drawing Number XPS-446, Pratt & Whitney of Canada Ltd.

17. G. J. Brown to J. P. Lavoie, memo #223176, Pratt & Whitney Aircraft of Canada Ltd.

18. K. V. Patel to U. Okapuu, memo, Pratt & Whitney Aircraft of Canada Ltd., 1 June, 1973.

19. W. Zemler to U. Okapuu, memo, Pratt & Whitney Aircraft of Canada Ltd., 17 July, 1974.

20. A. Ferland to R. R. Marshall, Communication, 1 Sept., 1976.

21. F. P. Beer and E. R. Johnston, "Vector Mechanics for Engineers: Dynamics", McGraw Hill, 1972.

22. W. C. Reynolds and H. C. Perkins, "Engineering Thermodynamics", McGraw Hill, 1970.

23. P. L. Meyer, "Introductory Probability and Statistical Applications", Addison Wesley, 1970.

24. J. R. Benjamin and C. A. Cornell, "Probability, Statistics and Decision for Civil Engineers", McGraw Hill, 1970.

25. J. H. T. Wade and H. S. Fowler, "An Introductory Note on Diffuser Design and Performance", ME-73-TF-1, McMaster University, 1973.

APPENDIX A

TURBINE DESIGN PARAMETERS
[14, 15, 17]

Mass Flow Rate,	m	0.330 lbm/sec
Total Temperature	T_O	535.0°R
Total Pressure	P_O	75.00 p.s.i.a.
Speed	N	75,000 RPM
Normalized Speed	$N/\sqrt{T_O}$	3242.53 RPM °R$^{1/2}$
Mass Flow Parameter	$m\sqrt{T_O}/P_O$	0.102 lbm °R$^{1/2}$ in lbf^{-1}sec^{-1}
Pressure Ratio	P.R.	4.29
Power		16.32 Hp
Torque	M	1.143 ft lbf

Z(in)	HUB-R (in)	SHROUD-R (in)
0	.900	
.050	.808	
.100	.740	
.150	.682	1.422
.200	.632	1.232
.250	.590	1.102
.300	.553	1.009
.350	.523	.943
.400	.496	.890
.450	.472	.849
.500	.453	.818
.550	.436	.798
.600	.423	.782
.650	.413	.770
.700	.406	.762
.750	.402	.758
.800	.400	.755

15 BLADES

R=.892"

RADIAL DISTANCE R(in)

AXIAL DISTANCE Z (in.)
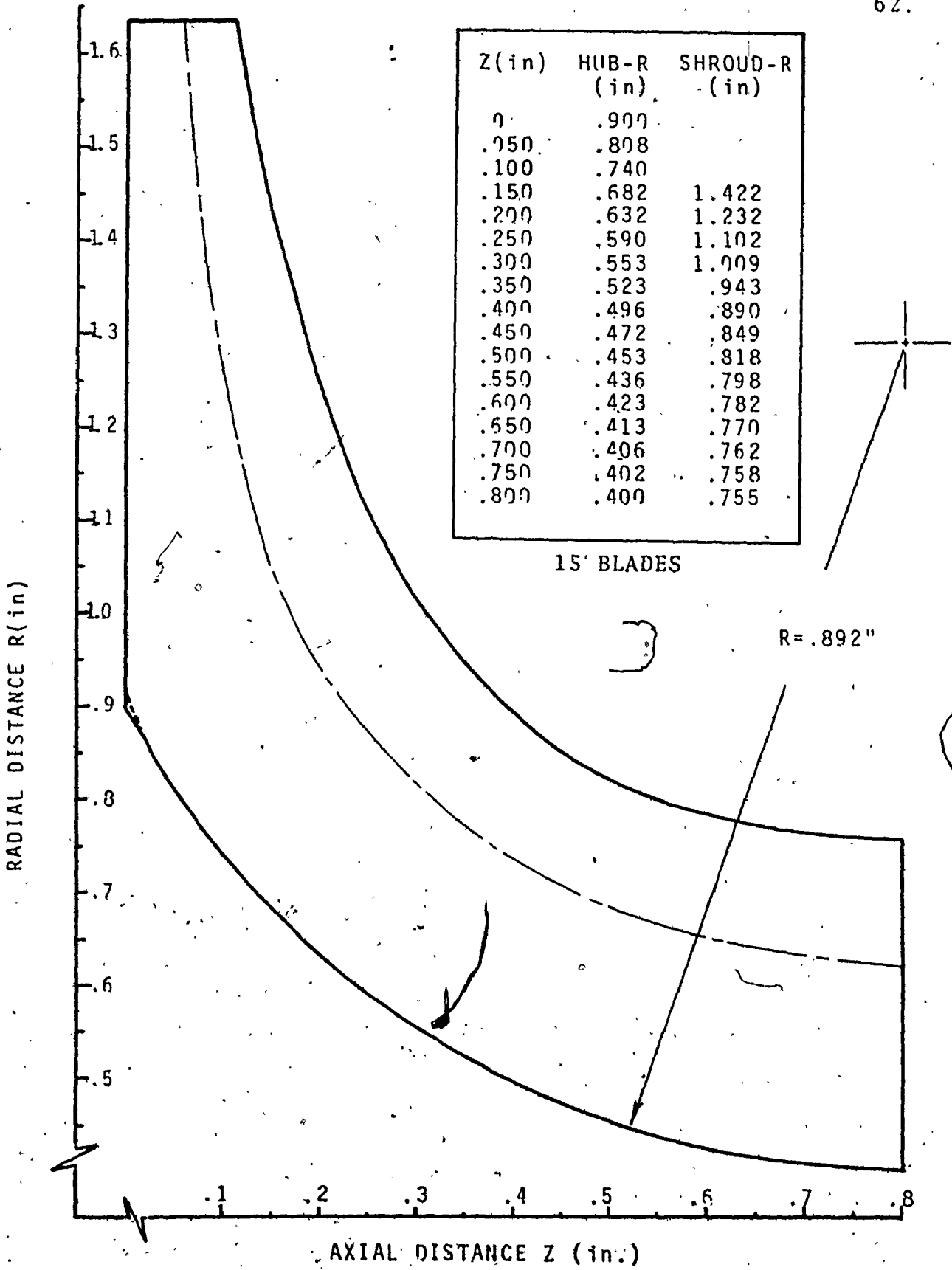
Figure A1 Spin Pit Turbine Aerodynamic Rotor
Definition

X	Y LOWER	Y UPPER
0.00	1.770	1.780
.050	1.775	1.792
.100	1.778	1.802
.150	1.782	1.810
.200	1.784	1.817
.250	1.785	1.823
.300	1.786	1.830
.350	1.785	1.836
.400	1.783	1.842
.450	1.783	1.848
.500	1.779	1.855
.550	1.775	1.862
.600	1.770	1.868
.650	1.764	1.874
.700	1.758	1.885
.750	1.752	1.899

X	Y LOWER	Y UPPER
.775	1.750	1.908
.800	1.752	1.913
.825	1.758	1.930
.850	1.770	1.943
.875	1.791	1.956
.885	1.804	1.956
.895	1.827	1.952
.905	1.856	1.944
.910	1.885	1.925
.912	1.905	1.905

32 VANES

VANE

VANE

SHROUD

ROTOR TIP

BACK-FACE

UPPER SIDE

LOWER SIDE

.115"

X (in)

Y (in)

Figure A2 Spin Pit Turbine Nozzle Definition

APPENDIX B

PARTS LIST: SUPPLIED
TURBINE HARDWARE [19]

Title	Qty	Remarks
Body & Shroud-Sub Assy	1	EFD 36732
Housing-Brg-Sub Assy	1	EFD 36773
Shroud-Exhaust	1	EFD 36721
Cap-Containment	1	EFD 36718
Rotor	1	EFD 36710
Nozzle Ring	1	EFD 36715
Plate-Sealing	1	EFD 36722
Spacer Bearing	1	EFD 36725
Collar-Sealing	1	EFD 36726
Spool-Oil	1	EFD 36724
Ring-RPM Pick Up	1	EFD 36730
Block-Junction	1	EFD 36729
Shim-Shroud-Exhaust	2	EFD 36728
Oil Sealing Assy	1	EFD 36318 (Items 4 thru 10)
Drive Spindle	1	EFD 37379
Exhaust Adaptor	1	EFD 36800
Damper Housing Mod	1	EFD 36996
Damping Spacer	1	BARBOUR STOCKWELL #2434
Damping Ring Assy	1	BARBOUR STOCKWELL #2530
Damping Spring	1	BARBOUR STOCKWELL #2443
Damping Disc Assy	1	BARBOUR STOCKWELL #2526
Damper Housing Gasket	2	BARBOUR STOCKWELL #2424
Nut Hex		BARBOUR STOCKWELL #2534
Screw	4	BARBOUR STOCKWELL #2449
Nut-Lock Rotor	1	BARBOUR STOCKWELL #2808 OR WHITTET HIGGINS #8MM-0
O-Ring	2	PRECISION #049-11647 OR MS9388-049
O-Ring	2	PRECISION #029-17107 OR MS9388-029
O-Ring	1	PRECISION #012-8187 OR MS9388-012 OR 3014222
O-Ring	1	PRECISION #010-8187 OR MS9388-010 OR 3014228
Bearing	2	XES 446
Wave Spring Washer	1	EFD 37146
Fitting	5	SWAGELOCK 200-1-2
O-Ring	1	MS9388-017 OR EQ
Plain End-Quick Con	1	AEROQUIP MOD No. 5602-8-10S
Magnetic Pick Up	1	
Screw Hex Head	4	.375-28NF x .75 LG
Screw Hex Head	6	.250-28NF x .75 LG
Screw Hex Head	10	.250-28NF x 1.00 LG
Screw Socket Head	2	#10-32NF x 1.38 LG
Screw Socket Head	3	#10-32NF x .50 LG
Screw Socket Head	3	#10-32NF x 1.75

EFD 36620 - ASSEMBLY RADIAL AIR TURBINE

Title	Qty	Remarks
Washer	3	.190 Dia Plain MS9320-09
Washer-Lock	16	.250 Dia
Washer-Lock	8	.375 Dia
Nut-Hex	4	.250-28NF
Thermocouple (Shield Types)		
Male Connector	1	EFD 37093
Strainer	1	EFD 37094
Insert	1	EFD 37095-1
Insert	1	EFD 37095-2
Tool Holder & Socket		EFD 37645
Oil Glass Sight	1	
Shim		EFD 36227
Collar Sealing	1	

EFD 38944

Title	Qty	Remarks
Static Probe	3	XPI 5499
Total Temp. Probe	3	XPI 5489-1
Total Pressure Probe	2	XPI 5501
Male Connector	1	SWAGELOK #400-1-4
Male Connector	13	SWAGELOK #200-1-2
Seal Blank	2	EFD 32114-1
Seal Blank	2	EFD 32114-2
Total Temp. Probe	3	XPI 5489-2
Cobra Probe	1	XPI 5500
Bracket	1	ERD 38963
Venturi (Outlet)	1	EFD 38965
Adapter-Venturi	1	EFD 38966
Bolt Hex Hd	6	¼"-20 NC x 1 1/8" LG
Nut	6	¼"-20 NC
Screw-Socket Head Cap	2	#4-40 NC x ¼" LG
Reducer	1	EFD 38974
Reducer 1" to 3/4"	1	PIPE FITTING
Dowel	3	.250 Dia x ½" LG

APPENDIX C

CALIBRATION CURVES: BROOKS ROTAMETERS
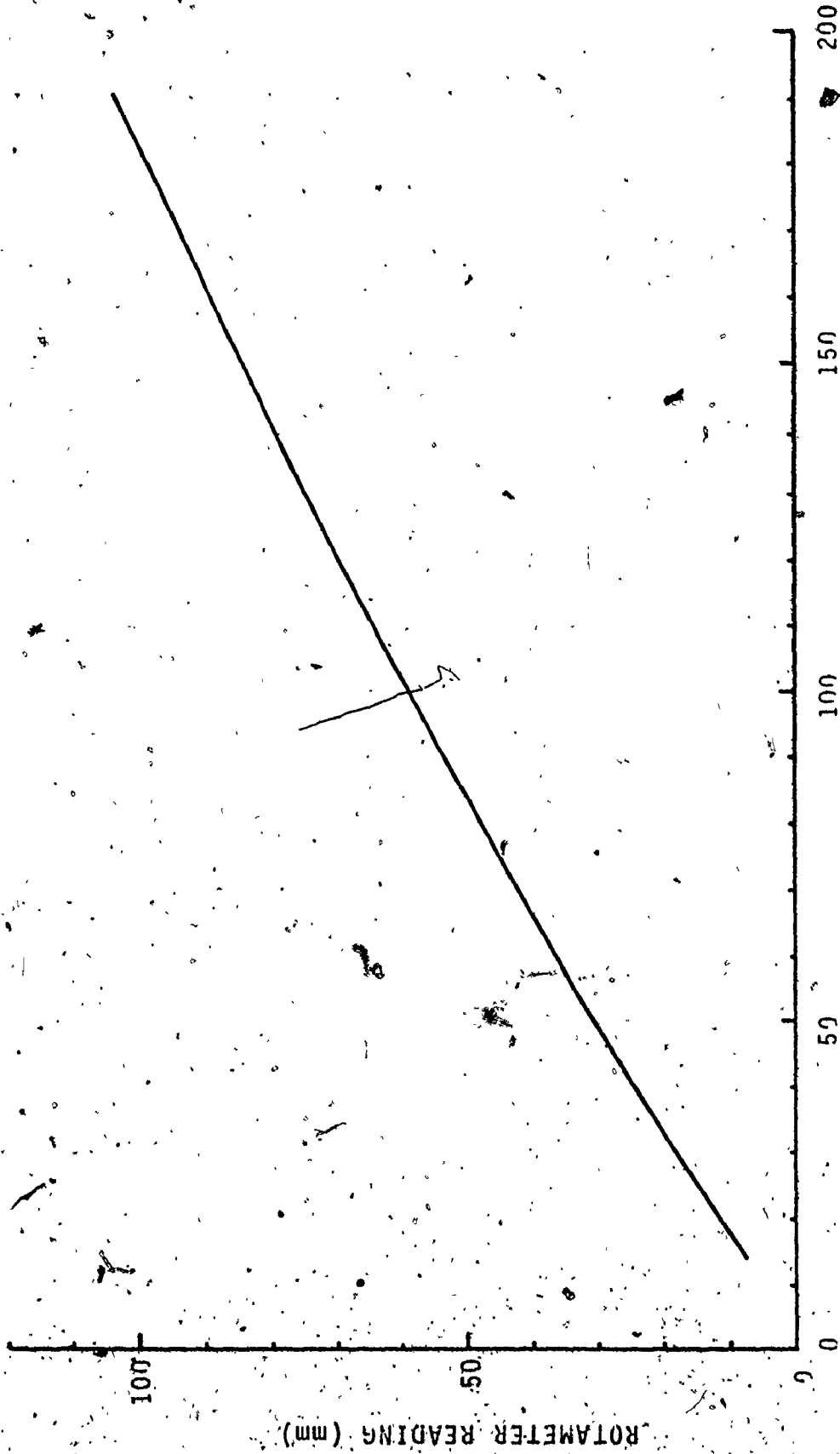
Figure A3   Calibration Curve for Brooks Rotameter Model AR-MET 12-3623-1118

SCFM AIR AT 70 F & 100 psig

ROTAMETER READING (mm)

68.
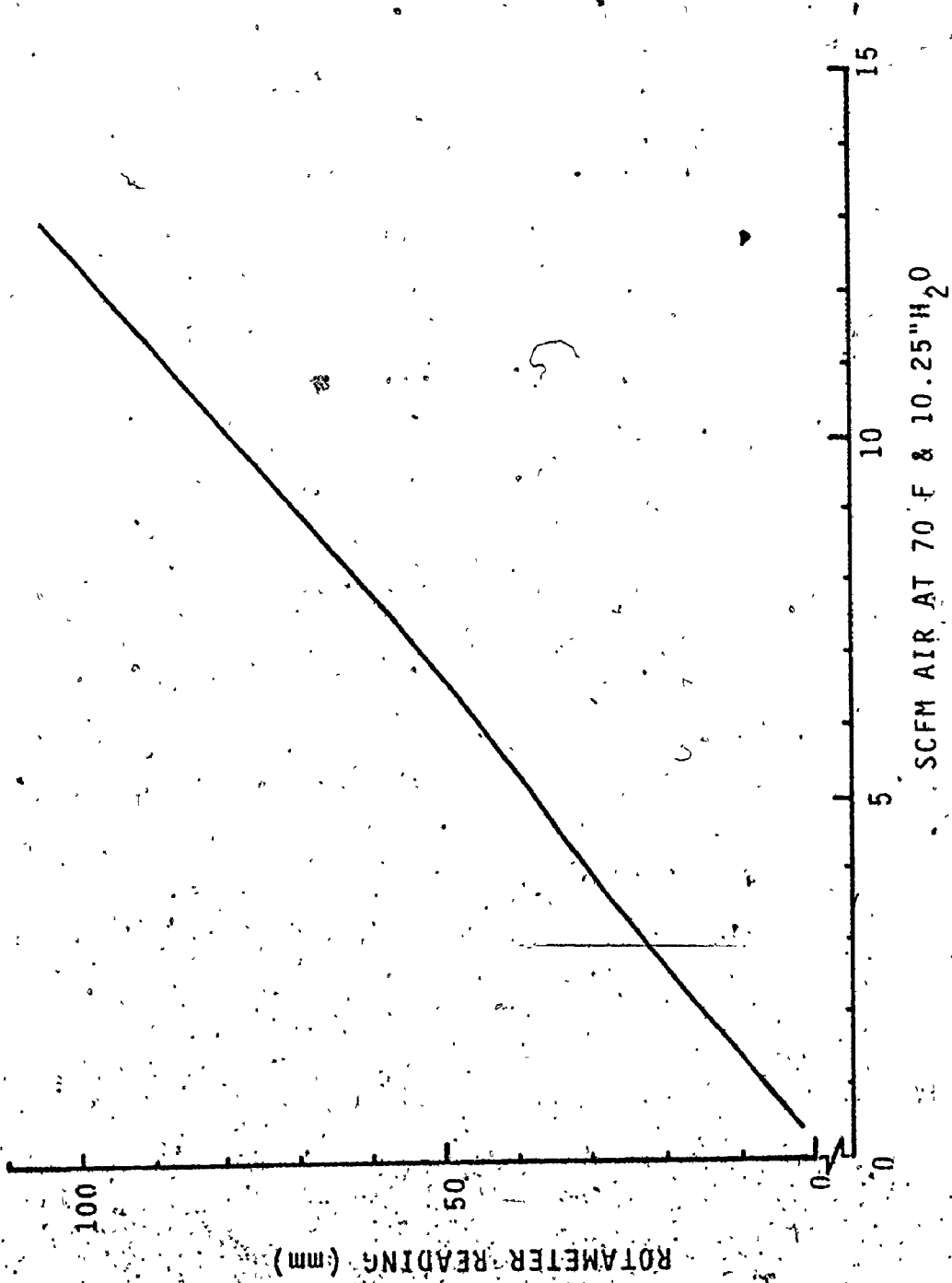
Figure A4 Calibration Curve for Brooks Rotameter Model 1307-12B

69.

APPENDIX D

DERIVATION OF ISENTROPIC AND
MECHANICAL EFFICIENCIES

A. Isentropic Efficiency

If the expansion in the turbine is considered to be
adiabatic, the turbine work is given by

$$w = c_p (T_{01} - T_{02}) \tag{A1}$$

for a perfect gas, where c_p is the specific heat at constant
pressure, and T_{01}, T_{02} are respectively the total tempera-
tures of the initial and final states of the gas. The maxi-
mum amount of work that can be obtained from the turbine would
occur if the expansion process were also isentropic (path "a",
Figure A5). The isentropic efficiency of the turbine is
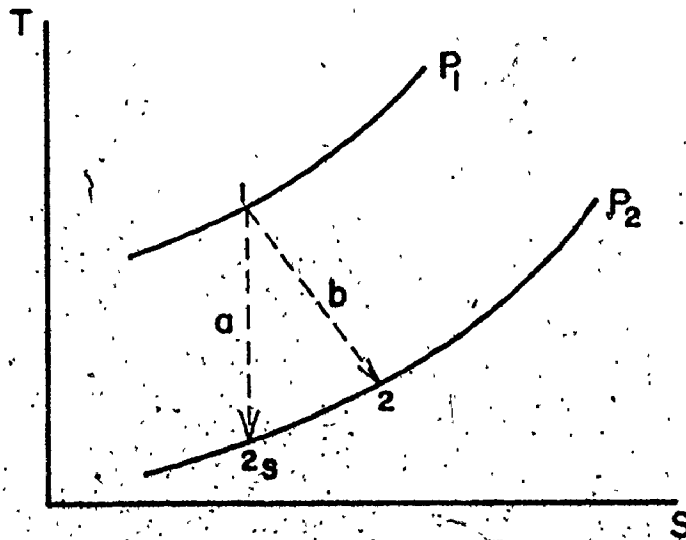
Figure A5: Temperature-entropy Diagram Showing Isentropic
Expansion (a) and Actual Expansion (b) from
States 1 to 2.

given by the ratio of the actual work, w, to the isentropic work, w_s. Thus

$$\eta = w/w_s \tag{A2}$$

so $\quad \eta = \dfrac{(T_{o1}-T_{o2})}{(T_{o1}-T_{o2s})} \tag{A3}$

$$= \dfrac{(T_{o1}-T_{o2})}{T_{o1}(1-\dfrac{T_{o2s}}{T_{o1}})} \tag{A4}$$

for an ideal gas. From isentropic flow equations, it can be shown that

$$\dfrac{T_{o2}}{T_{o1}} = (\dfrac{P_{o2}}{P_{o1}})^{\frac{\gamma-1}{\gamma}} \tag{A5}$$

Thus, designating the pressure ratio, P_1/P_2, by P.R, equation (A4) becomes

$$\eta = \dfrac{(T_{o1}-T_{o2})/(T_{o1})}{1-(1/P.R.)^{\frac{\gamma-1}{\gamma}}} \tag{A6}$$

B. Mechanical Efficiency

Representing the rate of change of angular velocity with respect to time (angular acceleration) by α, the moment of inertia about the centroid by I, and the moment or torque about the centre of rotation by M, it can be shown that

$$M = I\,\alpha \tag{A7}$$

for a rotating rigid body. An increment of work for this body is given by

$$dw = Md\theta \qquad\qquad (A8)$$

where w is work, and θ is the angle through the body has been rotated by the couple M.

Power may be defined as the rate of change of work with respect to time. Thus

$$\text{Power} = \frac{dw}{dt} \qquad\qquad (A9)$$

$$= \frac{d}{dt} Md\theta \qquad\qquad (A10)$$

$$= \frac{dM}{dt} d\theta + M \frac{d\theta}{dt} \qquad\qquad (A11)$$

For any short period of time, the angular acceleration of the turbine may be considered constant. This means that

$$\text{Power} = M \frac{d\theta}{dt} \qquad\qquad (A12)$$

$$= M w \qquad\qquad (A13)$$

and hence

$$\text{Power} = (I\alpha)w \qquad\qquad (A14)$$

The energy available to the turbine can be calculated from the total energy equation

$$E = KE + PE + U \qquad\qquad (A15)$$

where E is total energy, KE is kinetic energy, PE is potential energy, and U is internal energy. For the turbine in question the potential energy portion of the equation may be neglected. Kinetic energy is computed from the mass flow and the velocity of the air at the inlet to the turbine from

$$KE = 1/2 \ M \ V^2 \tag{A16}$$

The value of the internal energy may be calculated if the flow conditions (temperature, pressure, mass flow rate) are known at the inlet to the turbine, using

$$U = h - Pv \tag{A17}$$

where h is the specific enthalpy and v the specific volume of the gas.

The mechanical efficiency of the turbine is given by the ratio of the power absorbed by the unit to the available energy. Thus,

$$\eta = \frac{M \ w}{(\frac{1}{2} \ M \ V^2 + h - Pv)} \tag{A18}$$

APPENDIX E

EXPERIMENTAL RESULTS

TESTS OF APRIL 7, 1977   LOAD DISC SPUN IN PARTIAL VACUUM

N	PR	P_atm	P_atm	Prota-meter	Flow Rota-meter	Loss Rota-meter	T_inlet	T_outlet	TO	P_atm	P_plenum	P_plenum	V_c	m	N/√θ	P.R. $\frac{P_{pl}}{P_{atm}}$	U_tip/C₀	(%)
(RPM)	("Hg gage)	("Hg) gage)	("Hg gage)	("Hg gage)	meter (mm)	meter (mm)	(°F)	(°F)	(-T_inlet, °R)	("Hg)	("Hg gage)	("Hg abs)		lbm/sec				
73,450	42.99	29.58	54.0	70.0	3.5	129.18	97.45	589.18	29.58	39.4	69.18	119.0	.202	3025.5	2.34	.829	26.6
73,250	44.0		55.3	70.0	3.5	126.62	96.27	586.62		39.2	68.78	118.5	.201	3024.3	2.33	.824	25.5
72,950	43.25		56.5	69.8	4.0	124.83	91.33	634.83		40.5	70.08	120.0	.204	3057.9	2.37	.637	27.0
75,150	43.50		54.5	69.0	3.5	122.30	92.42	562.00		42.3	71.88	122.0	.207	3115.1	2.41	.851	27.9
73,550	41.42	29.58	53.5	67.5	4.0	121.50	92.12	581.50	29.58	36.7	69.28	118.8	.195	3050.0	2.34	.845	24.7
72,750	40.58		51.5	68.0	4.0	121.67	89.82	581.67		38.5	68.08	117.7	.193	3016.4	2.30	.841	27.1
74,550	38.4		51.0	66.5	4.0	114.78	90.62	574.71		36.9	66.48	115.5	.188	2984.6	2.25	.839	21.2
69,320	36.50	29.57	45.6	65.0	4.5	116.68	89.00	576.68	29.57	34.1	63.67	118.8	.172	2887.9	2.15	.831	22.6
68,950	36.01		45.1	64.5	4.5	112.71	89.00	572.71		33.6	63.17	111.0	.171	2881.1	2.14	.832	22.1
69,550	36.50		45.4	65.0	4.5	113.25	89.32	573.25		34.3	63.87	112.1	.172	2904.9	2.16	.836	22.1
68,850	36.05		45.4	65.0	4.5	114.46	88.91	574.46		33.4	62.97	110.9	.170	2872.6	2.13	.830	24.0
66,000	33.14	29.57	43.6	62.5	4.0	113.38	90.83	573.38	29.57	30.0	59.2	106.0	.156	2756.3	2.02	.617	22.0
66,000	33.0		42.0	62.5	4.0	110.56	88.18	570.54		30.0	59.7	106.0	.156	2763.1	2.02	.820	22.5
62,650	28.58	29.57	37.2	60.0	4.0	110.00	88.77	570.00	29.57	26.4	55.37	100.1	.139	2624.1	1.89	.807	23.2
62,350	29.25		37.5	60.0	4.5	110.00	89.66	570.00		26.0	55.57	99.8	.138	2611.6	1.88	.806	22.2
61,950	30.03		37.5	60.0	4.5	109.38	90.42	569.38		25.6	55.17	99.0	.137	2596.2	1.87	.794	21.1
63,650	30.63		37.6	61.0	4.0	110.21	88.64	570.21		27.4	56.97	102.0	.141	2665.5	1.93	.810	23.0
59,750	26.38	29.56	34.0	57.5	4.5	106.62	88.16	566.42	29.56	23.5	53.02	95.5	.125	2510.5	1.79	.800	21.0
60,000	26.55		34.0	57.5	4.5	106.62	88.1b	566.42		23.7	53.27	95.2	.125	2521.1	1.80	.805	20.3
58,350	23.85	29.56	31.0	55.0	4.5	104.50	85.41	564.5	29.56	22.3	51.86	92.7	.116	2455.9	1.75	.812	23.6
57,550	23.80		31.0	55.0	4.5	106.71	88.09	566.71		21.6	51.16	91.4	.114	2417.5	1.73	.80v	23.4
57,550	23.70		31.0	55.0	4.5	107.00	89.77	567.00		21.6	51.16	91.3	.114	2416.9	1.71	.601	22.0
57,350	23.60		30.5	54.0	4.5	107.00	89.32	567.00		21.4	50.96	102.0	.114	2408.5	1.72	.799	22.3
54,850	21.42	29.56	34.0	52.5	4.5	105.71	88.64	565.71	29.55	19.3	48.85	86.8	.102	2306.1	1.65	.791	23.3
53,150	19.00		34.0	50.0	4.5	100.12	88.41	560.12		17.7	47.25	85.9	.101	2245.8	1.60	.805	17.0
51,200	17.60	29.55	23.0	47.5	4.5	98.54	82.00	558.554	29.55	16.4	45.95	80.5	.088	2164.4	1.55	.833	17.8
51,050	17.60		23.0	47.5	4.5	99.36	87.18	559.36		16.3	45.65	80.1	.088	2158.5	1.55	.830	16.8
50,950	17.50		22.8	47.5		99.54	85.23	559.54		16.2	45.75	79.9	.087	2151.9	1.55	.828	22.3
41,900	15.75	29.55	20.8	45.3		99.36	86.41	559.36	29.54	14.1	43.64	75.5	.079	2025.3	1.48	.824	22.5
47,850	15.75		20.8	45.3		98.14	86.14	558.14		14.0	43.54	75.5	.079	2035.4	1.47	.829	20.5
47,650	15.75		20.8	45.3		98.14	85.59	558.14		14.0	43.54	75.5	.079	2023.4	1.47	.828	21.9
43,550	13.6	29.54	17.4	42.5		96.82	86.32	556.82	29.53	11.7	41.23	69.9	.069	1843.6	1.40	.796	17.0
43,550	13.4		17.2	42.5		97.05	86.09	557.09		11.7	41.23	69.9	.069	1845.1	1.40	.796	22.2
43,550	13.45		16.0	42.5		97.14	86.54	557.14		11.7	41.23	69.9	.069	1842.0	1.40	.796	21.3
40,450	11.75	29.53	15.8	40.0		96.53	89.14	556.59	29.53	10.2	39.73	66.6	.063	1714.6	1.35	.740	16.7
40,550	11.75		15.8	40.0		96.36	89.14	556.36		10.3	39.83	66.7	.063	1719.2	1.35	.741	16.0
40,450	11.75		15.8	40.0		96.95	88.91	556.95		10.2	39.73	66.6	.063	1714.0	1.35	.740	16.0
35,750	9.75	29.53	13.1	37.5		94.73	88.64	554.73	29.53	8.5	38.03	63.0	.056	1517.9	1.29	.707	15.9
35,450	9.70		13.2	37.5		95.45	88.77	555.45		8.3	37.83	62.5	.056	1504.2	1.28	.702	17.6
35,250	9.70		11.2	37.5		95.41	88.77	555.41		8.2	37.31	62.5	.056	1495.7	1.28	.698	17.9
25,950	7.4	29.51	10.8	35.5	45	92.57	87.09	552.67	29.53	5.9	35.41	57.1	.048	1103.8	1.15	.528	20.1
25,850	7.4		10.8	35.5		93.17	89.54	553.17		5.8	35.33	57.0	.048	1099.1	1.20	.576	13.2
16,150	5.5	29.54	8.1	32.5	45	91.58	90.82	551.58	29.54	4.4	33.94	57.1	.042	765.3	1.15	.457	20.1
16,050	5.5		8.1	32.5		96.33	92.36	556.33		4.1	33.94	53.7	.042	265.1	1.15	.457	16.5

TESTS OF APRIL 11, 1977   LOAD DISC SPUN IN AIR

N (RPM)	PA ("Hg gage)	P atm ("Hg gage)	P rota-meter ("Hg gage)	Flow Rota-meter (mm)	Loss Rota-meter (mm)	T inlet (°F)	T outlet (°F)	TO (=T inlet °R)	P atm ("Hg)	P plenum ("Hg gage)	P plenum ("Hg abs)	Vc	w (lbm/sec)	N/√TO	P.R. (P pl / P atm)	N tip/co	(-)
74,100	50.40	29.76	59.7	77.0	4	134.17	90.83	594.17	29.76	42.6	72.36	136.1	.242	3039.9	2.60	.798	33.0
72,950	49.17	.	58.0	76.0	.	130.21	90.42	590.21	.	46.2	75.96	134.0	.238	3002.8	2.56	.794	30.6
72,450	48.50	.	57.4	75.8	.	129.92	86.54	589.92	.	45.5	75.26	133.1	.236	2982.9	2.53	.791	34.1
71,950	47.83	.	56.7	75.4	.	129.08	86.73	589.08	.	44.9	74.66	132.1	.234	2964.4	2.51	.790	33.5
71,550	46.70	29.77	56.1	73.0	35	126.88	85.04	586.88	29.77	44.1	71.87	131.5	.223	2953.5	2.49	.792	32.0
70,500	45.60	.	54.7	73.0	.	129.75	85.91	589.75	.	42.9	72.67	129.5	.220	2903.1	2.45	.784	34.8
69,250	44.00	.	52.9	73.0	.	125.21	87.27	585.21	.	41.3	71.07	127.5	.217	2862.6	2.39	.781	31.5
66,650	41.50	29.77	47.8	70.0	4	122.33	83.75	582.33	29.77	37.2	66.97	121.2	.192	2730.5	2.25	.755	35.2
65,750	35.91	.	48.0	69.5	.	119.88	84.42	579.88	.	37.2	67.47	121.3	.192	2730.4	2.27	.766	31.3
65,550	35.80	.	47.7	69.5	.	122.50	84.71	582.50	.	37.1	66.87	121.0	.192	2716.4	2.25	.763	31.6
62,550	36.72	29.76	43.7	67.7	45	119.08	84.29	579.08	29.76	33.5	63.26	115.6	.174	2599.3	2.12	.751	33.0
62,250	36.00	.	43.3	67.5	.	116.36	84.38	576.36	.	33.1	62.86	114.9	.173	2589.0	2.11	.750	30.6
62,550	36.30	.	43.7	67.3	.	117.91	83.08	577.91	.	33.5	63.26	115.6	.174	2602.0	2.12	.751	33.1
59,450	32.40	29.77	39.8	64.9	4	113.0	83.83	573.0	29.77	30.5	60.26	110.0	.155	2483.6	2.02	.743	29.4
58,750	31.95	.	39.0	64.5	.	112.75	81.67	572.75	.	29.7	59.46	108.9	.154	2454.4	2.00	.554	28.5
58,250	31.50	.	36.4	64.4	.	111.88	84.88	571.88	.	29.1	58.86	107.9	.152	2435.6	1.98	.736	28.0
56,050	29.30	29.76	35.8	62.5	45	110.42	84.42	570.42	29.76	27.0	56.76	104.0	.140	2346.8	1.91	.726	28.4
56,000	28.95	.	35.7	62.5	.	111.71	84.71	571.71	.	27.0	56.76	104.0	.140	2342.1	1.91	.727	29.4
55,650	28.40	.	36.5	62.0	.	111.71	84.09	571.71	.	27.5	57.26	105.0	.141	2327.4	1.92	.727	29.9
53,300	25.72	29.76	31.8	60.0	45	107.33	85.88	567.33	29.76	24.4	54.16	99.1	.128	2237.7	1.82	.722	25.6
52,950	25.45	.	32.0	59.6	.	107.33	81.67	567.33	.	24.0	53.76	98.5	.127	2223.0	1.81	.720	30.5
54,650	27.90	.	34.5	61.0	.	110.96	82.42	570.96	.	25.7	55.46	101.5	.131	2295.5	1.86	.721	32.3
50,950	23.32	29.76	30.1	57.5	45	106.17	83.92	566.17	29.76	22.1	51.86	95.0	.117	2141.3	1.74	.715	27.9
50,750	23.19	.	30.0	57.5	.	106.46	82.88	566.46	.	22.0	51.76	94.8	.117	2132.3	1.74	.713	29.2
50,750	21.60	.	30.0	57.5	.	106.42	82.88	566.42	.	22.0	51.76	94.8	.117	2132.4	1.74	.709	29.1
50,000	21.10	29.76	29.3	55.0	45	105.42	83.29	565.42	29.76	21.4	51.16	93.4	.114	2102.7	1.72	.727	28.4
49,950	21.00	.	29.2	54.6	.	103.96	83.29	563.96	.	21.4	51.16	93.3	.114	2103.3	1.72	.729	28.5
49,300	20.90	.	29.1	54.6	.	104.12	82.25	564.12	.	21.3	51.06	93.0	.115	2096.6	1.72	.726	28.3
48,300	19.50	29.76	27.1	52.5	45	102.33	85.41	562.33	29.76	20.0	49.76	90.5	.108	2036.8	1.67	.725	22.7
48,050	19.50	.	27.0	52.5	.	102.50	81.96	562.50	.	19.8	49.56	89.9	.107	2025.0	1.67	.721	20.0
46,050	19.41	.	27.0	52.5	.	102.84	81.96	562.84	.	19.6	49.56	89.9	.107	2025.1	1.67	.722	20.6
43,900	17.85	29.76	24.1	50.0	3	100.88	83.58	560.88	29.76	16.9	46.66	82.0	.091	1853.7	1.57	.682	20.4
43,650	16.30	.	23.9	50.0	.	101.58	83.96	561.58	.	16.6	46.36	81.5	.091	1842.0	1.56	.671	27.2
43,650	16.00	.	24.0	50.0	.	102.50	85.09	562.50	.	16.8	46.56	81.8	.091	1848.9	1.57	.678	20.0
36,350	13.90	29.74	18.6	47.5	45	100.81	83.88	560.81	29.74	12.6	42.34	78.3	.078	1534.9	1.42	.620	32.5
36,150	12.90	.	18.5	47.2	.	103.25	83.92	561.25	.	12.5	42.24	78.0	.078	1525.9	1.42	.618	31.4
33,200	12.22	29.75	17.2	45.0	45	99.00	85.5	559.00	29.75	11.5	41.25	75.0	.073	1425.4	1.39	.607	27.0
30,850	10.60	29.74	15.7	42.5	45	97.82	87.45	557.82	29.74	10.3	40.04	71.6	.068	1306.2	1.35	.590	23.3
30,750	10.58	.	15.6	42.5	.	92.64	87.59	557.64	.	10.2	39.94	71.5	.068	1302.2	1.34	.589	22.3
23,250	8.54	29.73	12.3	40	4	91.58	84.04	551.58	29.73	7.5	37.23	64.0	.056	990.0	1.25	.489	22.1
23,250	8.54	.	12.3	40	.	91.71	84.54	551.71	.	7.5	37.23	64.0	.056	989.8	1.25	.488	21.2
19,450	7.28	29.72	11.8	37.5	45	88.45	84.0	548.45	29.72	6.4	36.10	61.0	.053	830.5	1.21	.439	19.1
19,350	7.25	.	11.7	37.5	.	90.00	84.0	550.00	.	6.4	36.10	61.0	.053	825.1	1.21	.437	20.4

TESTS OF APRIL 15, 1977 · LOAD DISC SPUN IN SULFUR HEXAFLUORIDE

N (RPM)	PA gage ("Hg)	P_ATM ("Hg) gage	P_rota-meter ("Hg gage)	Flow Rota-meter (mm)	T_inlet (°F)	T_outlet (°F)	T_o (=T_{inlet}, °R)	P_{atm} ("Hg)	P_plenum ("Hg gage)	P_plenum (plenum "Hg abs)	V_c	ṁ (lbm/sec)	$N/\sqrt{T_o}$	P.R. (P_{pl}/P_{atm})	U_{tip}/C_o	η (%)
49,300	41.51	29.54	64.0	78.0	143.69	83.92	601.69	29.54	40.3	69.84	137.0	.256	2006.5	2.36	.534	50.4
49,450	47.40	-	61.8	79.0	143.31	83.54	603.31	-	40.5	70.04	137.6	.258	2013.2	2.37	.536	50.3
49,800	46.80	-	62.5	78.5	143.35	79.54	603.25	-	39.7	69.24	136.0	.255	1994.9	2.34	.527	54.8
49,900	52.11	-	62.5	79.2	145.62	79.50	605.62	-	39.7	69.24	136.0	.255	2027.7	2.34	.526	56.8
45,050	37.50	29.54	50.0	71.0	137.83	79.91	597.83	29.54	32.1	61.64	122.0	.198	1842.5	2.09	.526	56.6
45,000	39.01	-	52.3	72.0	138.58	75.91	598.58	-	33.8	63.34	125.0	.202	1880.0	2.14	.530	55.5
45,350	36.20	-	50.1	72.0	136.67	80.67	596.67	-	32.7	62.24	123.0	.199	1856.6	2.11	.535	54.0
41,500	29.80	29.54	41.0	65.0	125.94	80.79	589.96	29.54	26.4	55.94	112.1	.160	1708.6	1.89	.524	54.6
41,450	30.10	-	40.9	45.0	130.50	75.00	590.50	-	26.4	55.94	112.0	.160	1705.7	1.89	.521	57.3
41,750	31.10	-	41.6	66.0	130.50	79.09	590.50	-	26.7	56.24	112.8	.161	1718.1	1.90	.520	56.8
37,450	23.98	29.54	33.0	60.5	124.83	79.45	584.83	29.54	21.0	50.54	102.5	.130	1548.6	1.71	.511	59.2
37,700	23.84	-	33.3	60.5	125.00	79.45	585.00	-	21.3	50.84	103.3	.131	1558.7	1.72	.516	58.6
37,750	23.60	-	33.4	60.0	124.54	80.92	584.54	-	21.3	50.84	103.4	.131	1561.4	1.72	.518	56.2
30,550	16.00	29.54	23.0	55.0	117.64	79.36	577.64	29.54	13.8	43.34	90.1	.098	1271.1	1.47	.465	64.5
31,350	16.18	-	23.5	55.0	117.45	79.45	577.45	-	14.5	44.04	91.6	.099	1304.6	1.49	.476	65.4
31,700	18.03	-	24.2	55.0	117.41	79.36	577.41	-	15.0	44.54	92.2	.100	1319.2	1.51	.482	63.8
22,250	14.20	29.54	19.5	50.0	112.71	79.71	572.71	29.54	11.4	40.94	85.0	.089	1138.7	1.39	.456	69.1
22,250	14.18	-	19.4	50.0	112.71	80.21	572.71	-	11.4	40.94	85.0	.089	1138.7	1.39	.456	67.6
22,250	14.00	-	19.5	50.0	113.12	80.33	573.12	-	11.4	40.94	85.0	.089	1138.3	1.39	.458	68.2
20,150	10.00	29.54	13.7	45.0	107.29	81.04	567.29	29.54	7.7	37.24	73.3	.065	846.0	1.26	.390	75.8
20,350	9.97	-	13.8	45.0	107.33	81.04	567.33	-	7.8	37.34	73.6	.066	854.37	1.26	.394	75.1
19,950	9.92	-	13.6	44.5	106.67	78.77	566.67	-	7.6	37.14	73.0	.065	838.1	1.26	.388	81.8
19,950	9.90	-	13.5	44.5	105.92	78.32	565.92	-	7.6	37.14	73.0	.065	838.6	1.26	.388	81.0

TESTS OF MAY 2, 1977, LOAD DISC SPUN IN CARBON DIOXIDE

N (RPM)	P_plenum ("Hg gage)	P_A ("Hg gage)	P_ATM ("Hg gage)	P_roto-meter ("Hg gage)	Flow Roto-meter (cm)	T_inlet (°F)	T_outlet (°F)	T_0 I-T inlet (°R)	P_atm ("Hg)	P_plenum ("Hg gage)	P_plenum ("Hg abs)	V_c	m (lbm/sec)	N/√T0	P.R. [p_p1/p_atm]	U_tip/C0	
60,750	37.75	42.41	29.72	58.0	77.0	142.35	90.5	602.35	29.72	37.75	67.47	132.6	.233	2472.3	2.27	.700	42.12
60,650	38.00	42.30	"	58.0	76.0	140.31	91.08	600.31	"	38.00	57.72	132.5	.233	2472.4	2.27	.700	42.02
61,050	37.75	42.00	"	57.8	75.8	139.17	93.08	599.17	"	37.75	67.47	131.1	.231	2451.2	2.27	.711	39.93
54,750	29.70	33.10	29.72	45.0	70.0	122.41	88.68	582.41	29.72	29.70	59.62	120.9	.183	2260.7	2.00	.698	44.25
54,850	29.91	33.56	"	45.0	70.0	125.58	90.79	585.58	"	29.91	59.63	120.6	.183	2260.6	2.01	.695	35.04
54,750	29.96	33.56	"	45.1	70.0	126.17	87.18	586.17	"	30.00	59.72	121.0	.184	2265.6	2.01	.696	39.46
54,850	29.85	33.40	"	45.0	70.0	125.42	81.42	585.42	"	29.85	59.57	120.8	.183	2267.0	2.00	.697	45.31
54,850	29.73	33.31	"	45.0	70.0	127.33	85.14	587.33	"	29.73	59.45	120.8	.183	2261.3	2.00	.696	41.09
50,100	25.05	28.22	29.72	37.2	65.8	122.96	80.46	582.96	29.72	25.05	54.77	111.8	.152	2075.0	1.84	.676	47.82
50,000	24.50	27.60	"	37.1	65.0	121.12	80.79	581.12	"	24.50	54.22	111.7	.152	2074.1	1.83	.682	46.02
49,500	24.55	27.20	"	37.0	65.0	121.33	80.38	581.33	"	24.55	54.27	111.6	.152	2066.1	1.83	.676	47.80
49,950	24.40	27.57	"	37.1	65.0	121.04	82.34	581.04	"	24.40	54.10	111.6	.152	2072.2	1.82	.661	45.31
49,550	24.35	27.51	"	37.1	65.0	122.50	84.31	582.50	"	24.35	54.05	111.6	.152	2069.6	1.82	.680	44.64
45,050	20.15	22.80	29.73	31.0	59.0	117.09	81.33	577.09	29.73	20.15	49.86	101.9	.127	1875.1	1.68	.659	49.09
45,200	20.25	22.90	"	31.0	59.0	116.50	81.92	576.50	"	20.25	49.98	102.1	.127	1882.5	1.68	.661	43.45
45,050	20.20	22.78	"	30.8	59.0	113.29	81.92	573.29	"	20.20	49.93	101.9	.127	1887.8	1.68	.663	42.07
45,050	20.20	22.78	"	30.8	59.0	115.5	81.92	575.50	"	20.28	49.93	101.9	.127	1872.9	1.68	.659	42.18
45,050	20.35	22.90	"	31.0	59.0	113.88	83.04	573.88	"	20.35	49.98	101.9	.127	1880.5	1.68	.660	41.20
39,950	16.28	18.53	29.73	25.5	55.0	107.04	75.00	567.04	29.73	16.28	46.01	91.9	.104	1677.7	1.55	.637	53.11
39,950	16.25	18.45	"	25.3	55.0	111.50	76.95	571.50	"	16.25	45.98	91.9	.104	1671.1	1.55	.635	47.93
39,850	16.31	18.56	"	25.4	55.0	111.33	81.79	571.33	"	16.31	46.04	91.8	.104	1667.2	1.55	.633	36.52
40,150	16.55	18.90	"	26.0	55.0	109.96	80.29	569.96	"	16.55	46.28	92.1	.105	1681.8	1.56	.635	55.26
35,050	13.41	15.38	29.73	21.5	51.8	107.63	78.95	567.63	29.72	13.41	43.14	85.1	.090	1470.9	1.45	.604	56.07
35,000	13.45	15.40	"	21.5	51.8	107.25	76.09	565.25	"	13.45	43.16	85.0	.090	1472.1	1.45	.605	53.21
35,000	13.45	15.39	"	21.5	51.8	108.25	77.54	568.25	"	13.45	43.18	85.0	.090	1464.2	1.45	.603	64.16
34,950	13.45	15.39	"	21.5	51.8	106.88	76.73	568.88	"	13.45	41.18	84.4	.090	1465.3	1.45	.602	57.72
29,850	10.63	12.40	29.72	17.6	48.0	103.33	74.82	563.33	29.72	10.63	40.55	79.1	.078	1257.7	1.36	.565	55.59
30,150	10.95	12.54	"	18.0	48.0	108.00	82.33	568.99	"	10.95	40.62	79.3	.078	1267.1	1.37	.562	55.26
30,150	10.90	12.50	"	17.8	48.0	106.08	78.59	586.08	"	10.90	40.60	79.1	.078	1267.2	1.37	.563	59.61
29,950	11.00	12.60	"	18.0	48.0	106.67	80.42	586.67	"	11.00	40.72	79.2	.078	1298.1	1.37	.519	56.49
25,000	8.88	10.21	29.725	15.0	44.7	103.38	81.54	563.38	29.72	8.88	38.00	73.5	.068	1053.1	1.30	.511	55.07
25,150	8.80	10.15	"	14.8	44.7	103.62	82.62	563.62	"	8.80	38.52	73.6	.068	1059.6	1.30	.514	53.71
24,950	8.82	10.16	"	14.7	44.7	103.67	80.42	563.67	"	8.82	38.54	73.4	.064	1050.9	1.30	.510	60.16
24,950	8.85	10.20	"	14.9	44.7	102.79	80.42	562.67	"	8.85	38.57	73.4	.068	1051.8	1.30	.510	57.72
20,050	7.00	8.10	29.725	12.0	41.0	98.54	80.44	558.54	29.72	7.00	36.72	67.9	.059	848.4	1.24	.453	55.72
20,050	6.95	8.02	"	12.0	41.0	99.45	82.63	558.45	"	6.95	36.67	67.9	.059	847.7	1.23	.461	53.31
20,000	6.96	8.01	"	12.0	41.0	98.69	83.75	558.64	"	6.96	36.68	67.9	.059	846.2	1.23	.460	49.33
20,050	6.92	8.01	"	12.0	41.0	99.64	80.46	559.64	"	6.92	36.64	67.9	.059	847.5	1.23	.461	46.97
14,950	5.72	6.64	29.72	10.0	38.6	95.45	83.71	555.45	29.72	5.72	35.44	61.9	.051	634.3	1.19	.375	44.19
14,950	5.70	6.62	"	10.2	38.6	96.18	81.42	554.18	"	5.70	35.42	61.9	.051	633.9	1.19	.335	55.35
15,050	5.72	6.68	"	10.2	38.8	92.29	79.41	552.29	"	5.72	35.44	62.0	.051	640.4	1.19	.379	48.17
15,100	5.72	6.63	"	10.3	38.4	95.36	80.84	555.36	"	5.72	35.44	62.1	.051	640.8	1.19	.379	54.77
10,000	4.80	5.40	29.72	8.5	35.0	90.71	84.46	550.71	29.72	4.80	34.32	56.3	.045	426.1	1.15	.281	34.51
10,150	4.75	5.60	"	8.6	35.0	92.62	85.09	552.62	"	4.75	34.47	56.5	.045	431.1	1.16	.270	31.25
10,050	4.60	5.42	"	8.5	35.0	92.83	81.33	552.83	"	4.60	34.32	56.4	.045	527.4	1.15	.282	41.43
10,050	4.62	5.42	"	8.6	35.0	91.25	80.54	551.25	"	4.92	34.34	56.4	.045	426.0	1.16	.279	42.02
5,150	3.30	3.90	29.72	6.4	30.0	86.54	84.21	546.54	29.72	3.30	33.02	50.8	.038	220.1	1.11	.168	14.42
5,150	3.25	3.82	"	6.0	36.0	85.23	79.18	545.23	"	3.25	32.97	50.6	.038	220.6	1.11	.168	33.42

APPENDIX F

SAMPLE CALCULATIONS

A. Temperature

The temperatures were calculated by linear inter-polation from National Bureau of Standards values. The example cited here is from the tests of April 7, 1977 with the load disc operating in a partial vacuum.

$$N = 73,450 \text{ RPM} \qquad \text{EMF inlet} = 1.265 \text{ mv}$$

from the tables:

T	EMF
125°F	1.16 mv
130°F	1.28 mv

thus
$$\frac{1.265-1.16}{1.28-1.16} = \frac{T-125}{130-125}$$

from which
$$T = 129.4^\circ\text{F}$$

B. Inlet Plenum Pressure

The inlet plenum pressure was only recorded for the tests of May 2, 1977 with the load disc spun in CO_2. As these values are the closest to the actual turbine inlet conditions, it was decided to calculate inlet plenum pressures from the existing rotameter pressure and inlet line pressure data. Figure A6 shows a plot of inlet plenum pressure against inlet line pressure for the tests of May 2. The resultant curve shows linear variation between these two pressures. Figure A7
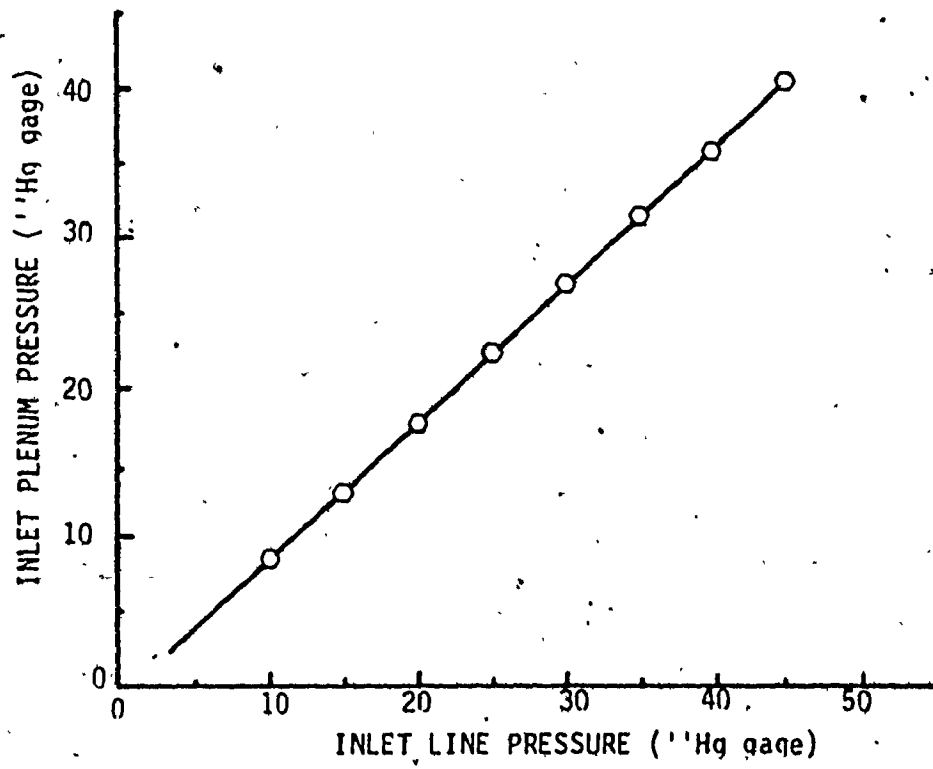
Figure A6   Graph of Inlet Plenum Pressure vs.
Inlet Line Pressure
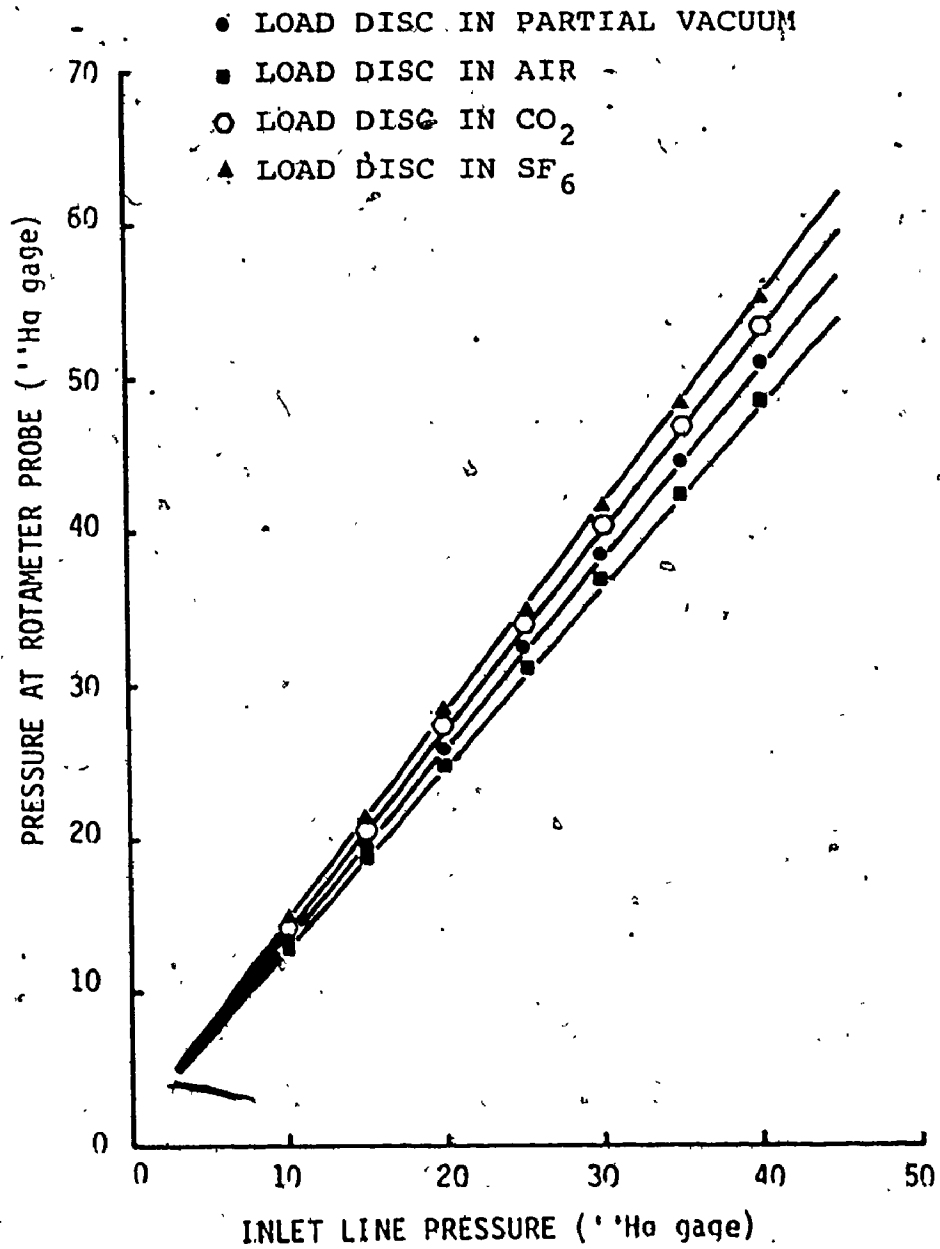
Figure A7   Graph of Rotameter Pressures
vs. Inlet Line Pressures

shows a plot of rotameter pressure against inlet line pressure. These two pressures are also seen to be linearly related. Thus, considering Figures A8 to A11, for

$$\Delta_1 = Pr - P_1 \tag{A19}$$

and $\quad \Delta_2 = P_1 - P_2 \tag{A20}$

it can be seen that, for example,

$$\frac{\Delta_1 \ CO_2}{\Delta_1 \ air} = \frac{\Delta_2 \ CO_2}{\Delta_2 \ air} \tag{A21}$$

where Pr = rotameter pressure

P_1 = inlet line pressure

P_2 = inlet plenum pressure

subscripts denote load gas.

Thus $\quad \Delta_2 \ air = \dfrac{(\Delta_2 CO_2)(\Delta_1 \ air)}{(\Delta_1 \ CO_2)} \tag{A22}$

and hence

$$P_2 = P_1 - [\frac{\Delta_2 \ CO_2)(\Delta_1 \ air)}{(\Delta_1 \ CO_2)}] \tag{A23}$$

Figures A8 to A11 show graphs of inlet line pressures vs RPM for various probe locations including the calculated values of P_2, the inlet plenum pressures.

C. Mass Flow

Figures A12 to A15 show curves of rotameter reading vs RPM and the corresponding values of calibrated air volumetric
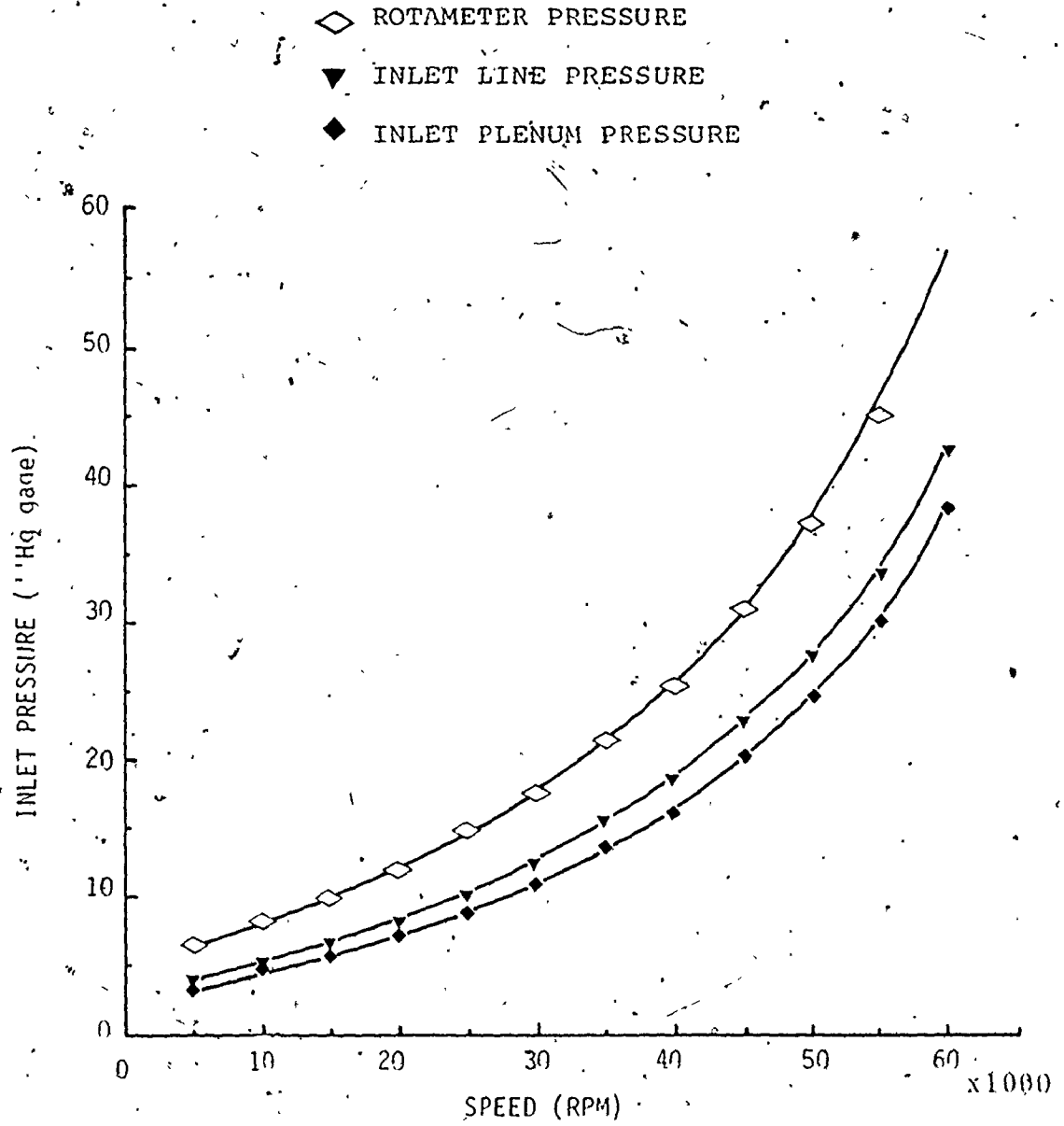
Figure A8   Graph of Inlet Pressures vs. RPM for
Load Disc Spun in Carbon Dioxide

◇ ROTAMETER PRESSURE

▼ INLET LINE PRESSURE

— INLET PLENUM PRESSURE
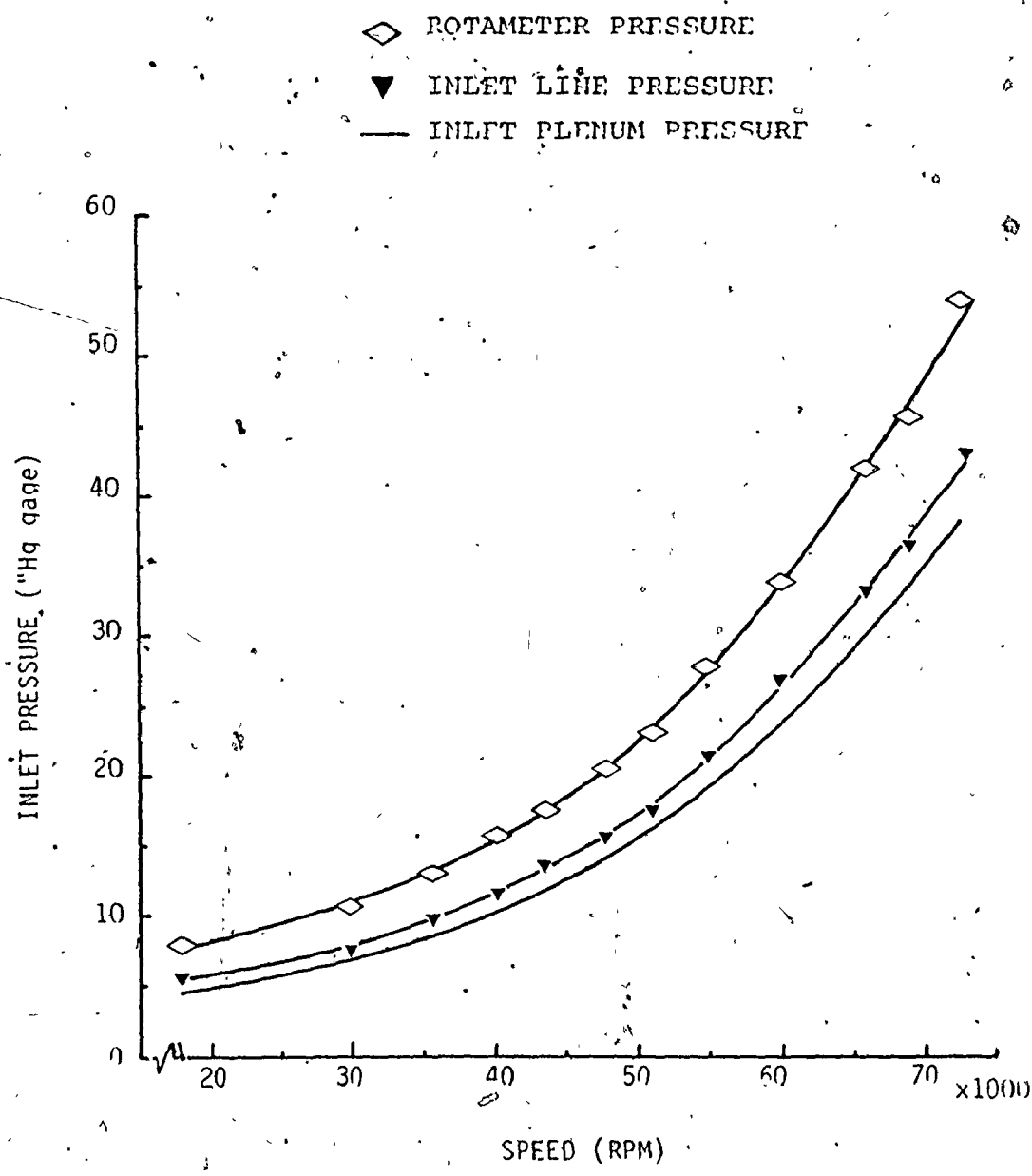
Figure A9   Inlet Pressures vs RPM for Load Disc
Spun in Partial Vacuum.
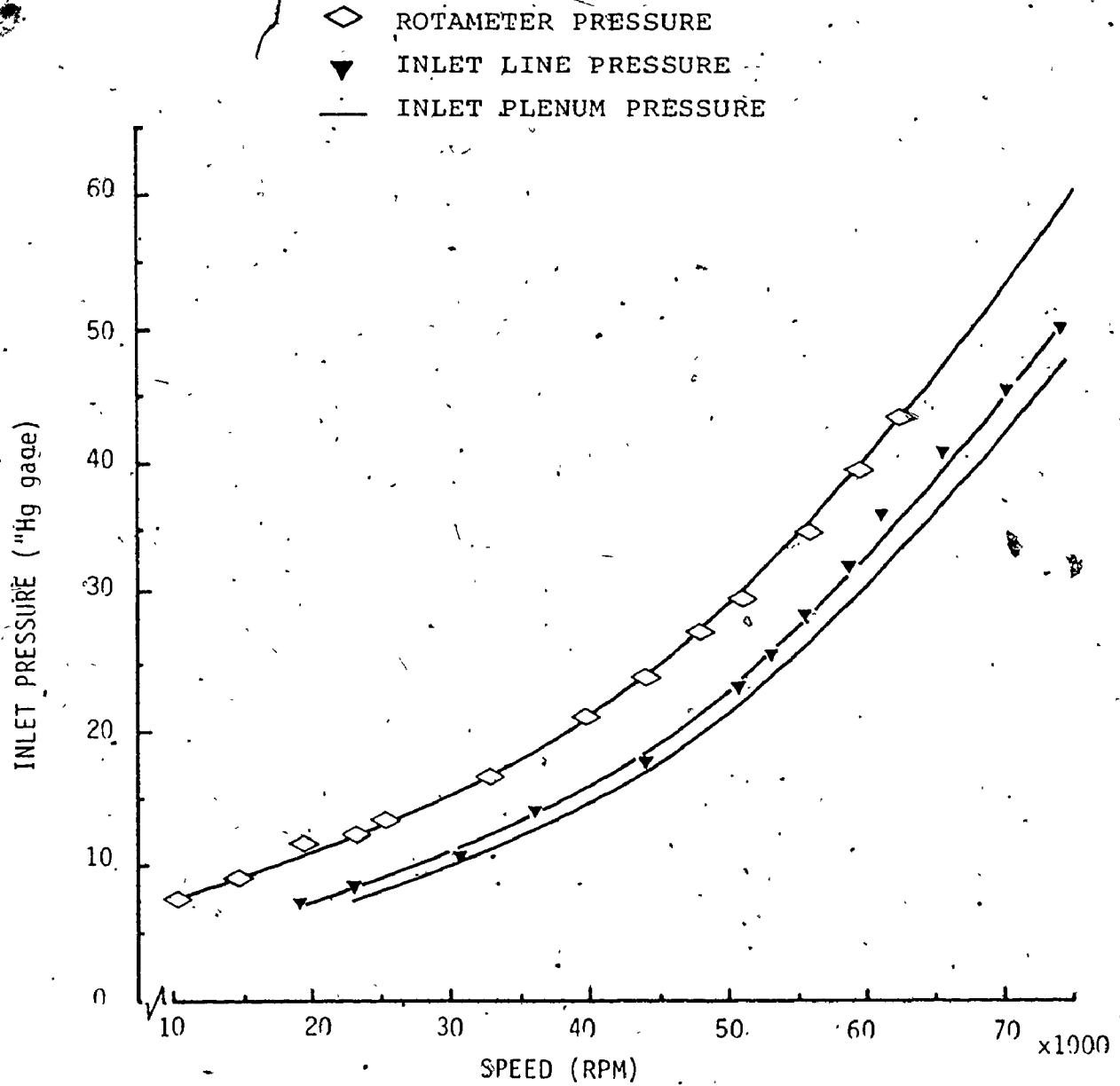
Figure A10 Graph of Inlet Pressures vs. RPM for Load Disc Spun in Air
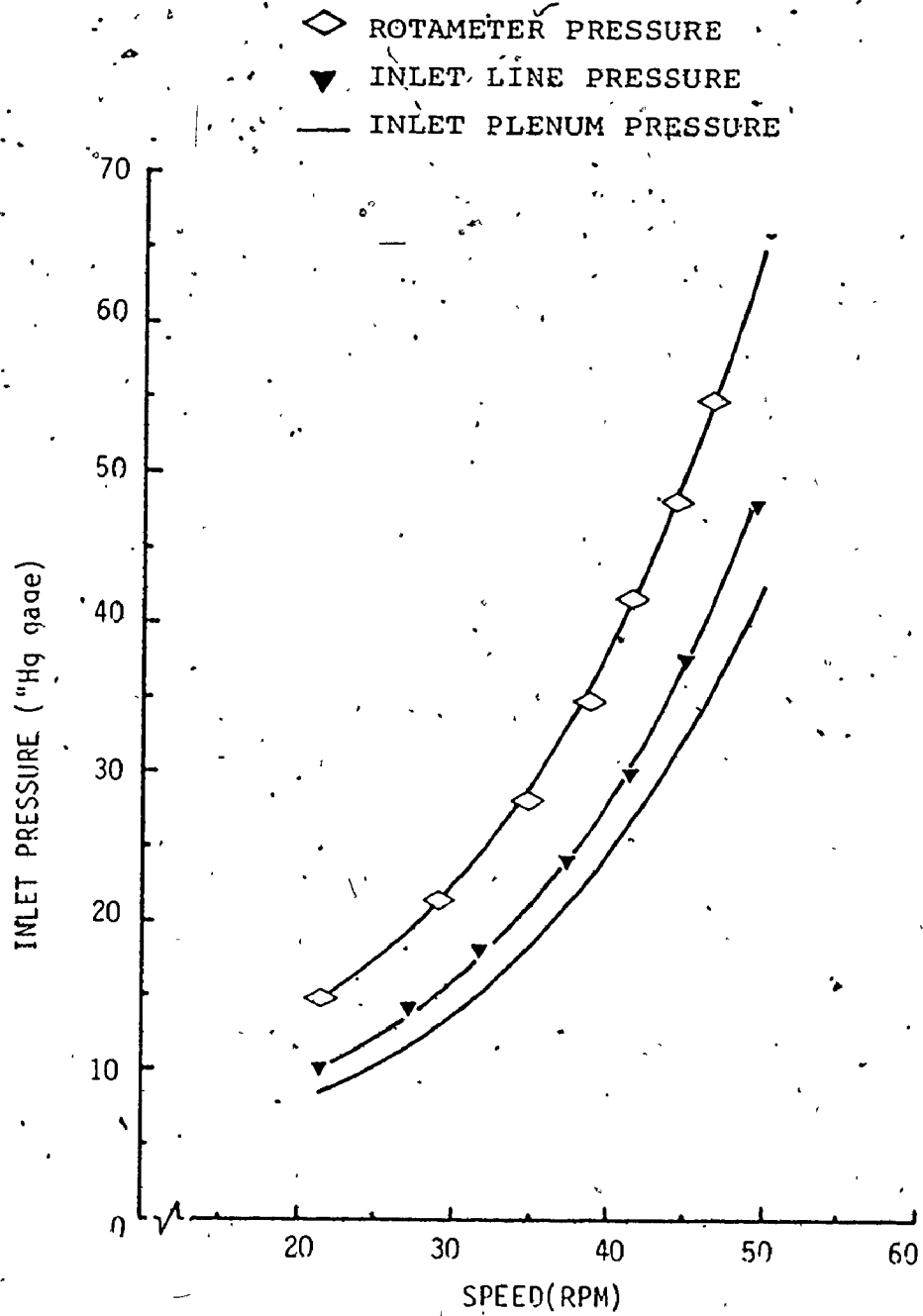
Figure A11 Inlet Pressures vs. RPM for Load
Disc Spun in Sulfur Hexafluoride
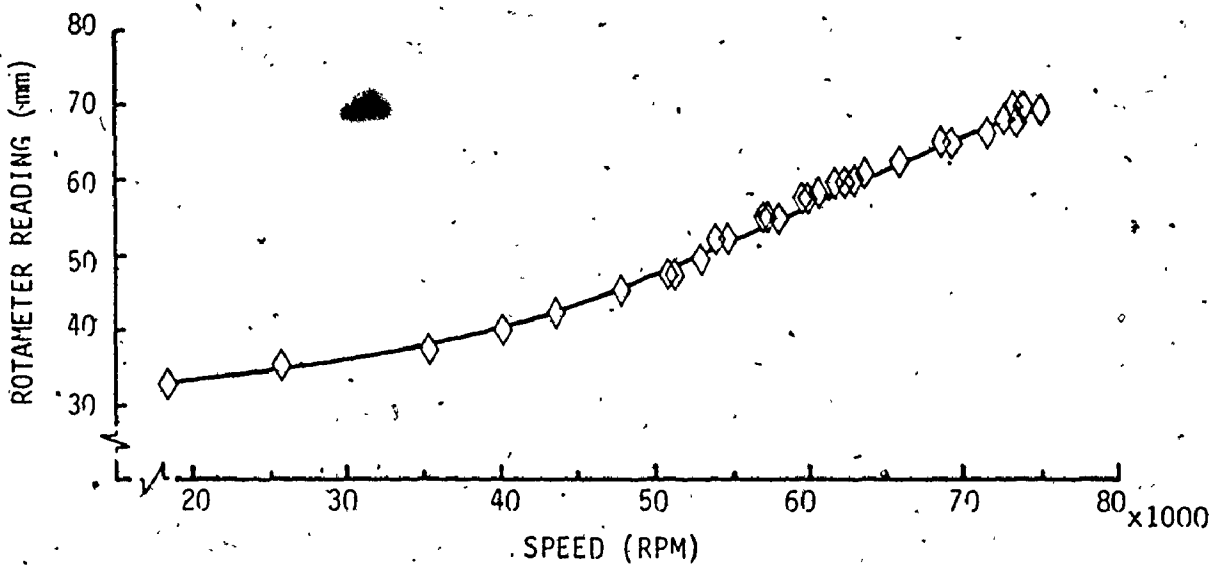
a) Rotameter Reading vs. RPM
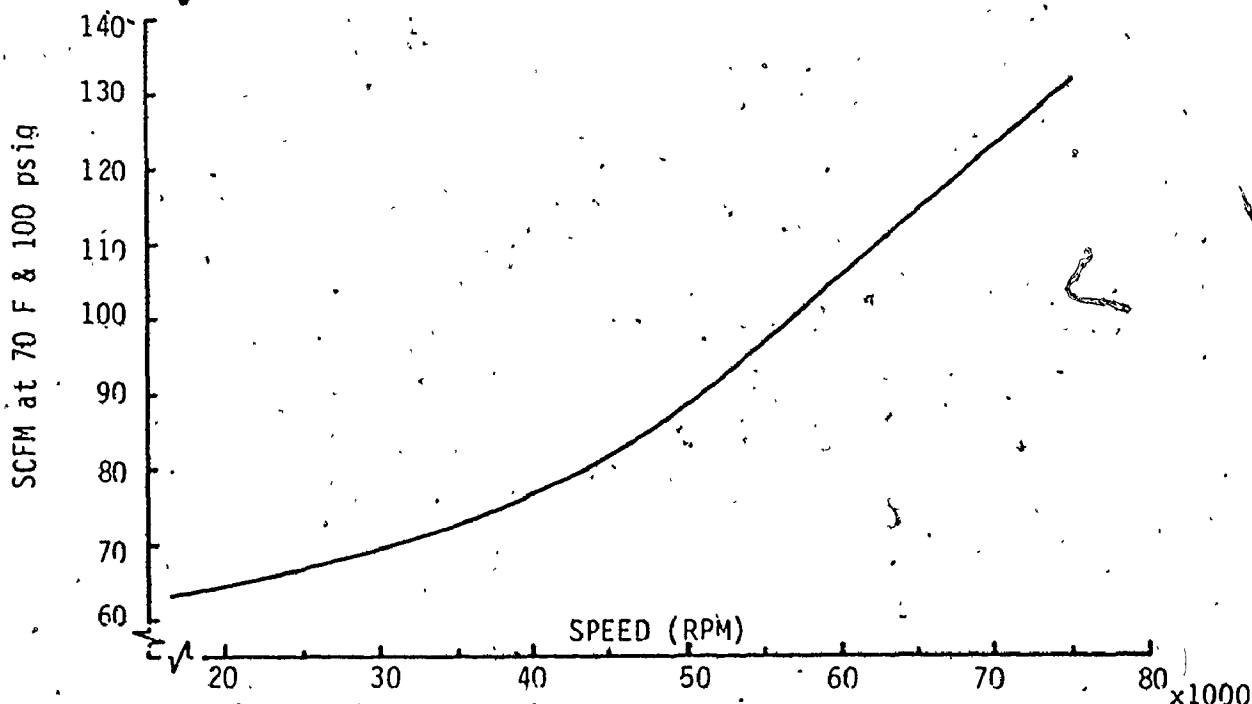
b) Calibrated Air Flowrate, V_c vs. RPM

Figure A12 Graph of Rotameter Reading vs. RPM and Corresponding Values of Calibrated Air Flowrate for Load Disc Spun in Partial Vacuum
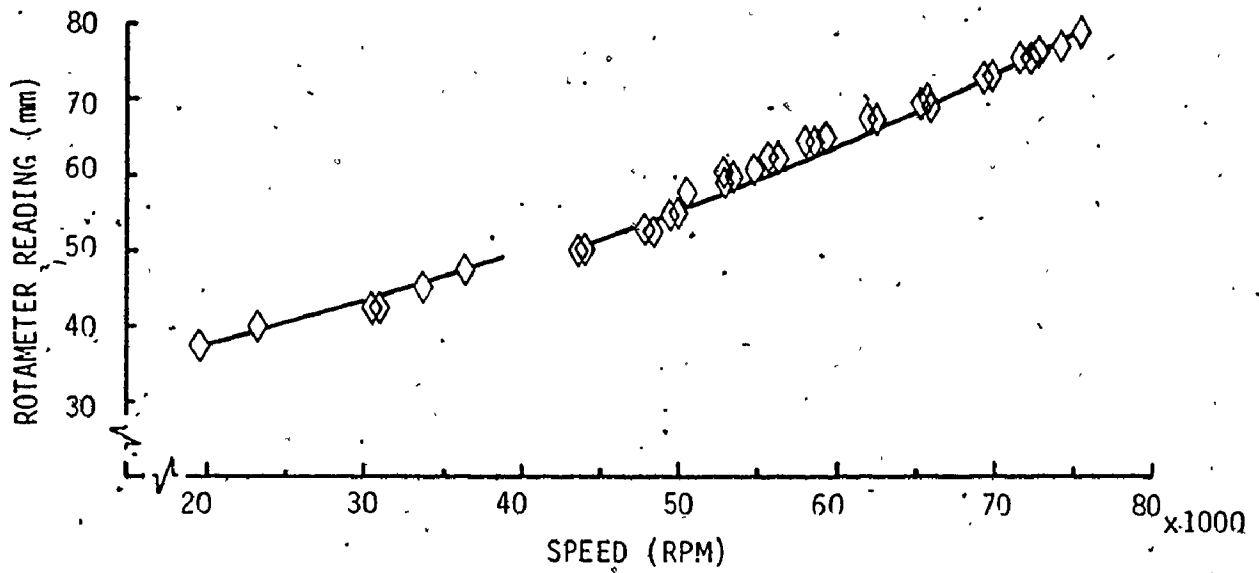
a) Rotameter Reading vs. RPM
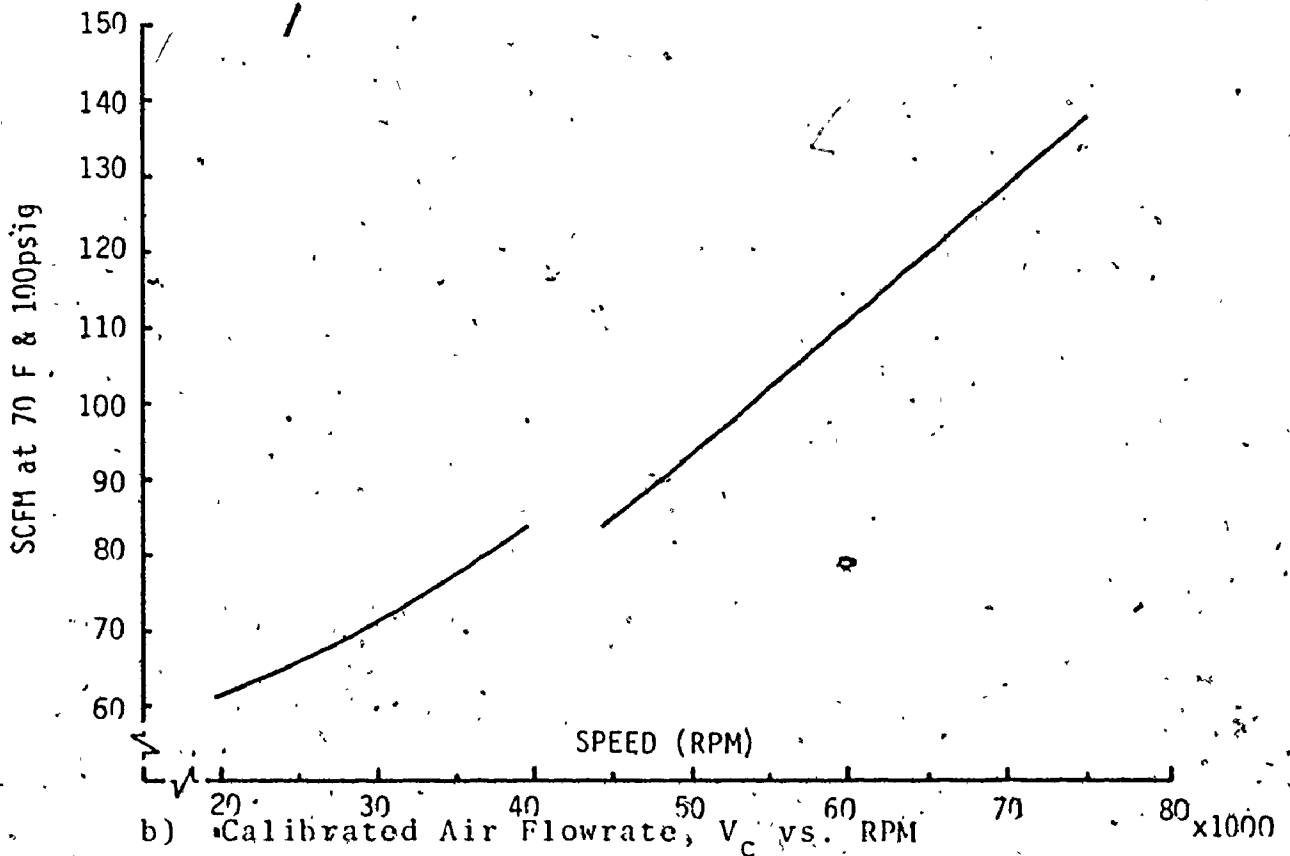
b) Calibrated Air Flowrate, V_c vs. RPM

Figure A13   Graph of Rotameter Reading vs. RPM and Corres-
              ponding Values of Calibrated Air Flowrate for
              Load Disc Spun in Air
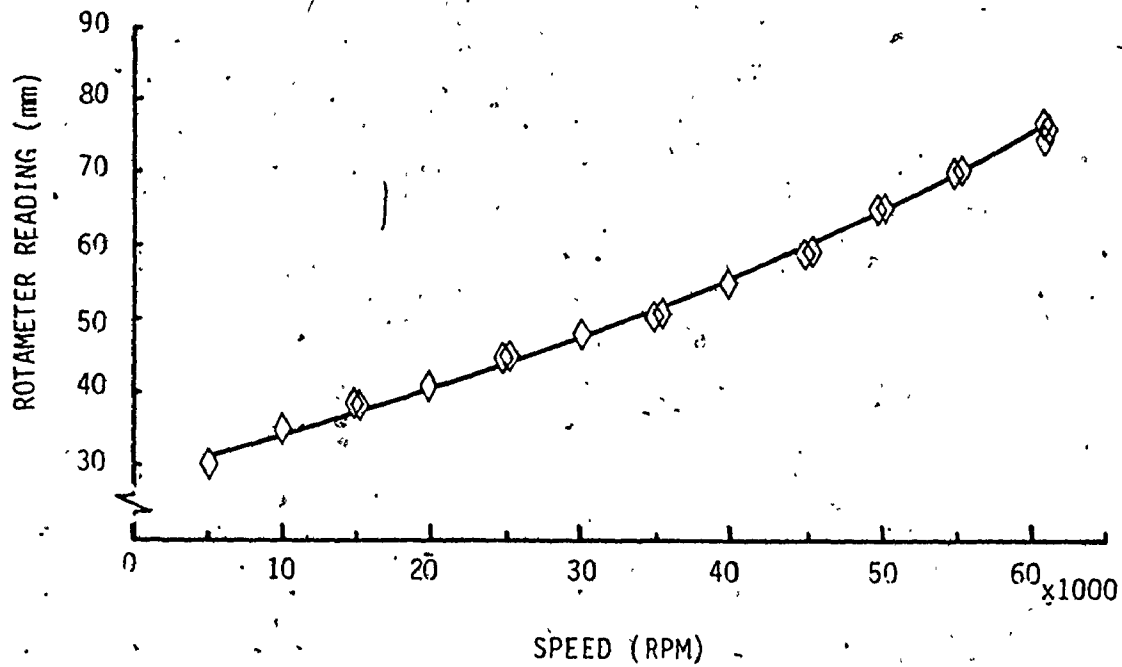
a) Rotameter Reading vs. RPM
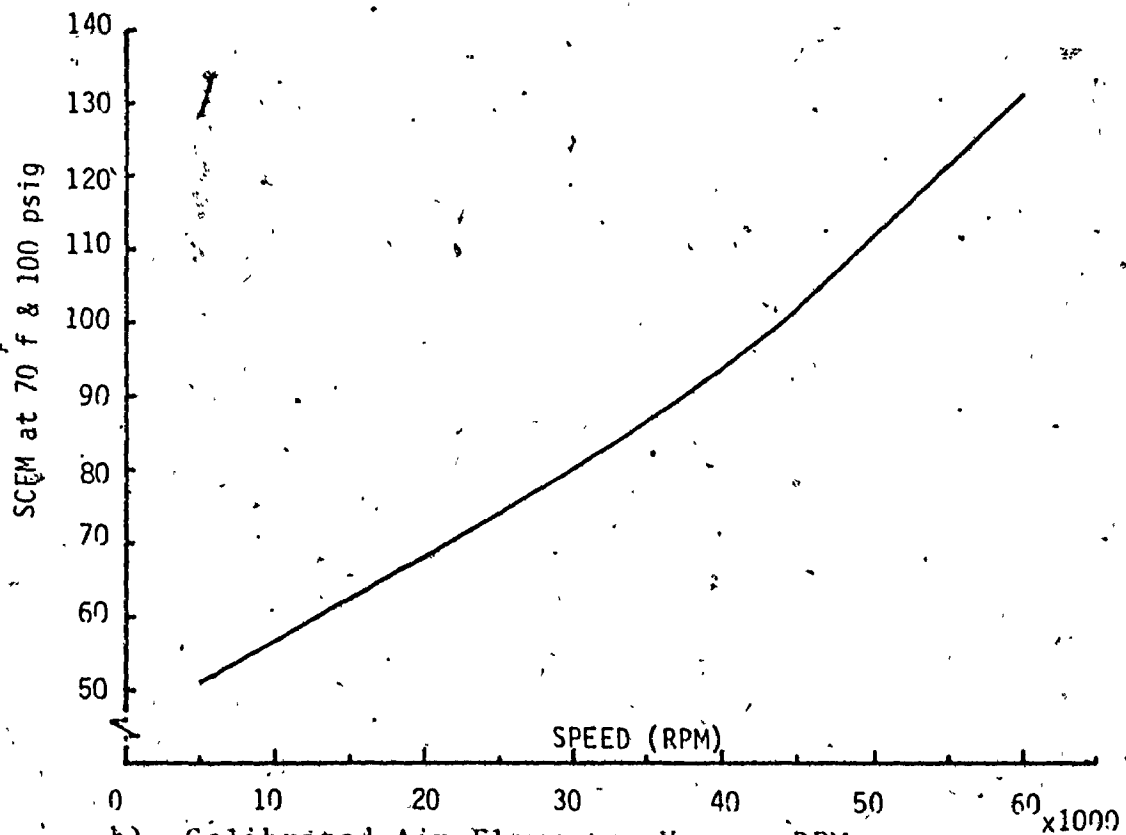
b). Calibrated Air Flowrate, V_c vs. RPM

Figure A14   Graph of Rotameter Reading vs. RPM and Corres-
ponding Values of Calibrated Air Flowrate for
Load Disc Spun in Sulfur Hexafluoride
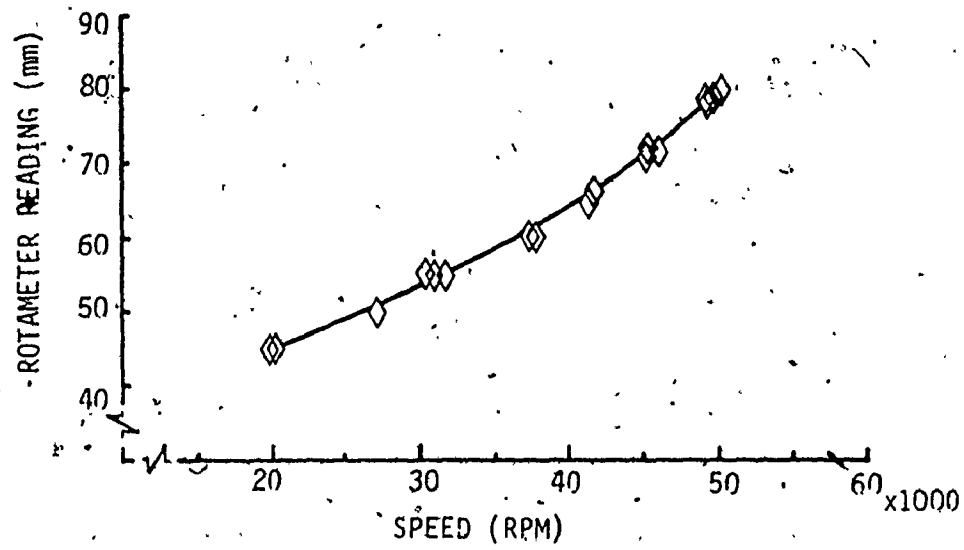
a) Rotameter Reading vs. RPM
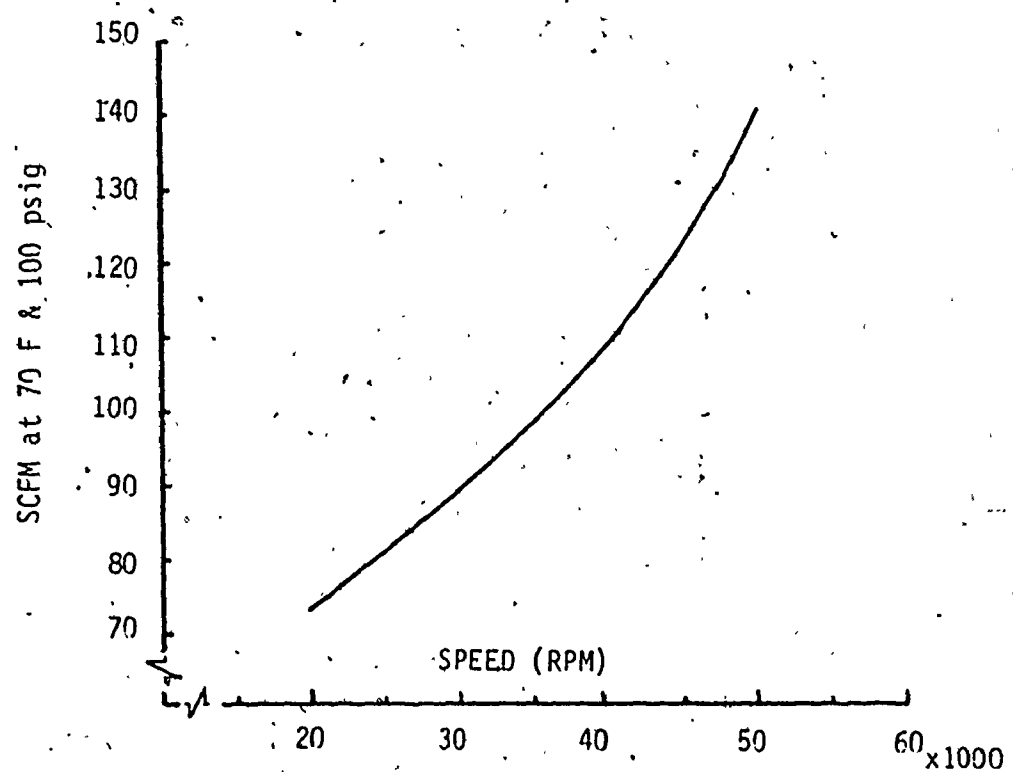
b) Calibrated Air Flowrate, V_c vs. RPM

Figure A15 Graph of Rotameter Reading vs. RPM and Corresponding Values of Calibrated Air Flowrate for Load Disc Spun in Carbon Dioxide

flow rate, V_c, vs. RPM. Again, using the results from April 7, with the load disc spun in a vacuum:

$N = 73,450$ RPM   Rotameter reading = 70.0, $P_2 = 69.18$ "Hg$_{abs}$.

$P_O = 29.58$ "Hg

$T = 589.38^O$R

Thus $m = (7.502 \times 10^{-3}) \dfrac{V_c \sqrt{\dfrac{P_2}{100+Po}}}{\sqrt{\dfrac{T_2}{P_2}}}$

for m in lbm/sec, T in ^{O}R and P in p.s.i.a. Converting pressure to inches of mercury,

$$m = \dfrac{(7.502 \times 10^{-3})\, V_c \sqrt{\dfrac{P_2}{203.6+Po}}}{\sqrt{\dfrac{T_2}{P_2}}}$$

so $m = \dfrac{(7.502 \times 10^{-3})(119.0) \sqrt{\dfrac{69.18}{233.18}}}{\sqrt{\dfrac{589.38}{69.18}}}$

$= .202$ lbm/sec.

D. $U_T/C_o{}'$

As shown in Chapter 5, the equation for the non-dimensional velocity $U_T/C_o{}'$ is given by

$$U_T/C_o{}' = \sqrt{\dfrac{0.0143N}{12,025\, T_o [1-(\dfrac{1}{P.R.})^{\frac{\gamma-1}{\gamma}}]}} \qquad (6)$$

This is derived from

$$U_T = \frac{2\pi}{60} \times N \times r \qquad \text{(A24)}$$

where r is the radius of the blade tip which is 1.625 inches and

$$C_o' = \sqrt{2gH} \qquad \text{(A25)}$$

where H is the adiabatic head equivalent velocity given by

$$H = J \, c_p \, T_o' \, [1-(\frac{1}{P.R.})^{\frac{\gamma-1}{\gamma}}] \qquad \text{(A26)}$$

In this equation, J is equal to 778 ft. lb/BTU and c_p is the ratio of specific heats. For the case in which the load disc was spun in a partial vacuum, with

$N = 73,450$ RPM, $\quad T_o = T_{inlet} = 589.38^{\circ}R$, $\quad$ P.R. $= 2.34$

gives

$$U_T/C_o' = \sqrt{\frac{(0.0143)(73,450)}{(12,025)(589.38)[1-2.34^{(\frac{0.4}{1.4})}]}}$$

$$= .829$$

E. __Isentropic Efficiency__

The isentropic efficiency has been defined in Appendix D, equation (A6) as

$$\eta = \frac{\Delta T/T_o}{[1-(\frac{1}{P.R.})^{\frac{\gamma-1}{\gamma}}]}$$

Again, considering the experimental results used in the previous

examples

$$N = 73,450 \text{ RPM}$$

$$T_o = T_{inlet} = 589.38^\circ R$$

$$\Delta T = T_{inlet} - T_{outlet} = 589.38 - 557.95^\circ R = 31.93^\circ R$$

$$P.R. = 2.34$$

gives

$$\eta = \frac{31.93/589.38}{[1-(\frac{1}{2.34})^{\frac{0.4}{1.4}}]}$$

$$= 26.6\%$$

APPENDIX G

BEARING FAILURE ANALYSIS

As indicated in Chapter 5, experiments with the turbine were terminated prematurely due to a failure of the upper bearing. An examination of the components of the bearing showed severe wear on the thrust surface of the outer ring ball race. The balls themselves were worn in a band approximately 0.1 inch wide. This band circled the entire ball (see Figure A16). High temperature discoloration was evident in all parts of the bearing except on the band of wear across the balls.

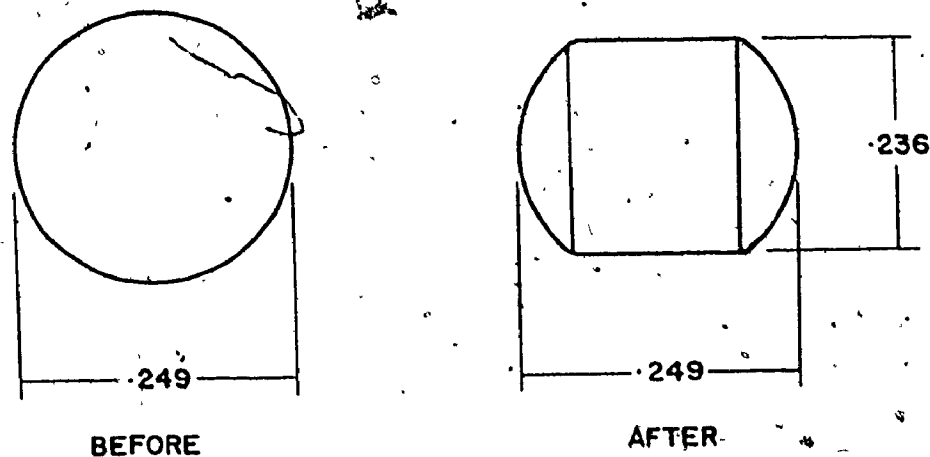BEFORE   AFTER

·249   ·249   ·236

Figure A16 Illustration of Ball Bearings Before and After Failure

A comparison between the balls taken from an unworn bearing and those from the failed specimen showed that the overall ball diameter was reduced from an average of 0.2494 inch to 0.2491 inch; across the worn band the ball diameter was reduced to 0.2361 inch.

An examination of the above observations indicates that the bearing failure per se was due to insufficient lubrication. Factors contributing to this condition wear

(a) high thrust loads and

(b) the failure of the upper bearing thermocouple monitor lead.

Because of the poor lubrication, a wear process between the balls and the thrust surface was initiated. This process ultimately led to high temperatures and failure of the bearing. It is evident that the bearing was subjected to unexpectedly high thrust loads. In all probability these loads were due to aerodynamic lift caused by spinning the load disc in media other than a partial vacuum. Combined with the high loads the lack of temperature monitoring lead allowed the wear to go unnoticed until failure finally occurred.